"CFD Based Design Optimization, Fabrication and Testing of A Micro Hydro Pelton Turbine "

A dissertation Submitted for the Partial Fulfillment of Degree of Doctor of Philosophy (PhD) in Mechanical Engineering (Thermal and Energy Conversion) , in Addis Ababa University, Addis Ababa Institute of Technology (AAiT)

By:

Tilahun Nigussie Gemechu

Supervisors:

1. ***Dr.-Ing. Edessa*** **Dribssa (Associate Professor)**

   Addis Ababa Institute of Technology, Addis Ababa, Ethiopia.

2. **Prof. Abraham Engeda**

   Mechanical Engineering Department, Michigan State University, USA.

In collaboration with Ministry of Water, irrigation and Energy of Ethiopia.

December 8, 2018

Addis Ababa, Ethiopia

Addis Ababa University

Addis Ababa Institute of Technology

School of Mechanical and Industrial Engineering

Thermal Engineering Stream

Addis Ababa, Ethiopia

This is to certify that the thesis prepared by Tilahun Nigussie, entitled: ***CFD Based Design Optimization, Fabrication and Testing of a Micro Hydro Pelton Turbine*** *submitted in fulfillment of the requirements for the Degree of Doctor of Philosophy in Mechanical Engineering (Thermal Engineering) complies with the regulations of the University and meets the accepted standards with respect to originality and quality.*

By

Tilahun Nigussie

Signed by the Examining Committee:

School Dean_____Signature_____Date_____

Internal Examiner_____ Signature_____ Date_____

External Examiner_____Signature_____Date_____

Supervisor_____ Signature_____ Date_____

Co- Supervisor_____Signature_____Date_____

ABSTRACT

In areas where the supply of grid power is very difficult, utilisation of Micro hydro-power as renewable energy source is of great concern now a-days to eliminate extreme poverty around the world. These schemes can provide environmentally sustainable electricity and mechanical power to rural communities. For this purpose, selected types of micro hydro turbines need to be designed and developed depending up on the site locations.

Thus, considering the potential of hydropower generation in Ethiopia, this research addresses the design, optimization, local manufacturing, and experimental test of a model of micro hydro Pelton turbine for one of the selected potential site (Indris River) in South West Shewa of Ethiopia to meet the requirements of the energy demands of the nearby village as a case study.

Initially, the geometries to be compared (baseline design of the turbine) were done with the design guide lines and tested by developing numerical model using commercial CFD. Considerations are taken in designing the turbine with an effective post life recycling scheme in mind so that there will be minimum wastage of resources once the turbine is made redundant.

CFD simulations using ANSYS-CFX were conducted, to optimize further the bucket shape in order to get a cost effective runner design. Additionally, consequences of variation in each design parameter were evaluated from the baseline design. The result of the study proposes some modifications in the baseline design. Through the analysis, a weight reduction of around 7.6% is achieved due to the modified runner design. Moreover, CFD was predicting a 3.9 % improvement of hydraulic efficiency. The optimization of number of buckets, length, depth and shape of the lip curve are the main design parameters for the achieved improvement in efficiency. It is then checked for structural safety with a more accurate method using ANSYS. At a later stage, the model was experimentally tested at the AAIT Lab to have a tangible confirmation of efficiency at variable operational conditions. The experimental results confirmed a 2.8% improvement in efficiency. This prediction was validated for the modified runner design used in the simulation using the same head and flow rate conditions as for the baseline design.

Overall, the comparative results with CFD were satisfactory and in line with the theory, and verifying the turbine model design effectiveness which will be useful for implementation of rural electrification projects.

Keywords: *Rural Electrification, bucket geometry, hydro turbine, Pelton Turbine, Numerical Modeling, Computational Fluid Dynamics, optimized, Experimental Testing.*

ACKNOWLEDGMENT

First I would like to offer my deepest appreciation to my supervisors, home and abroad, Dr. Ing. Edessa Dribssa, and Professor Abraham Engeda for their kind and generous guidance throughout this program. Their guidance and support, helped me immensely towards the completion of this research. In addition, their professionalism has given me much stimulation that is helpful for my continuing career development. Their expertise and constructive comments on the research helped me further dig into the depth of the flow mechanisms. I want also to thank Dr. Bjørn Winther Solemslie from Norwegian University of Science and Technology Faculty of Engineering Science and Technology, Department of Energy and Process Engineering, for his great enthusiasm for his field and will to give some documentations on Pelton research.

I am also thankful for all the help given during laboratory work, by Sema Baye, Kassa and Anteneh deserves special thanks. Without their patience and sense of perfectionism, the implementation of experimental test would not have been made possible.

I was very lucky to know as a friend and be able to collaborate with Mekuannint Mesfin from the Michigan State University. Working with him and my supervisor Professor Abraham Engeda has broadened my knowledge and was a wonderful experience which I have been for three months in Michigan state University. I would also like to acknowledge and thank all those whom have made contributions to my research and the writing of this research. It has been a pleasure working with everyone in the thermal sciences group at Addis Ababa University.

I am very grateful for the sponsorship of my PhD provided by Addis Ababa Institute of Technology and Ministry of Education. I am also very grateful to Ministry of water ,irrigation and electricity of Ethiopia for their Financial support of the Research Grant Scheme.

Lastly and most importantly I am thankful to my family. Many thanks for your love, support, guidance and inspiration. Nothing would have happened without you.

ACADEMIC ACHIEVEMENTS

1. Master Thesis Co-advised:-
   i. Improving the Performance of Cross-Flow Water Turbine Manufactured by Selam Technical and Vocational College using CFD.
   ii. Feasibility study for power generation using off-grid energy system from micro hydro-PV-diesel generator-battery for rural area of Ethiopia: The case of Melkey Hera village, Western Ethiopia.
   iii. Performance Analysis of Centrifugal Pump Operating as Turbine for identified Micro Hydro Site in Ethiopia.
   iv. Design and CFD Analysis of a Micro Kaplan Turbine Runner.
   v. Performance Improvement of Distributor and Nozzle for a Micro hydro Pelton Turbine.
   vi. Manufacturing and Experimental Performance Analysis of a Micro Hydro Pelton Turbine.
2. Final Year Project advised: Design and CFD Analysis of Axial compressor and 3 others thermal Projects.
3. Participate on Research grant Award on title ‘’Local Capacity Building of Micro Hydro Power’’ by Ministry of Water, Irrigation and Energy of Ethiopia.
4. Participate on the development of micro hydropower implementation project by MWIE.
5. Second Place Certificate award for excellent performance in 2018 First PhD student Research Poster exhibition competition day which held in AAIT which was also part of this research.
6. Certificate of achievement for the successful completion of GE Hydro Technical Training on Hydro discovery tour, Turbine and governing system and generator and excitation system.

LIST OF JOURNAL PUBLICATIONS

1. Performance Analysis of Centrifugal Pump Operating as Turbine for identified Micro Hydro Site in Ethiopia. *International Journal of Engineering Research and General Science Volume 3*, Issue 3, May-June, 2015 ISSN 2091-2730 668 www.ijergs.org.
2. Design and CFD Analysis of Centrifugal Pump *International Journal of Engineering Research and General Science* Volume 3, Issue 3, May-June, 2015 ISSN 2091-2730 .
3. Feasibility study for power generation using off- grid energy system from micro hydro-PV-diesel generator-battery for rural area of Ethiopia: *The case of Melkey Hera village, Western Ethiopia, AIMS Energy*,5(4):652-674.DOI:10.3934/energy.2017.4.652,Received: 10 April 2017, Accepted: 10 July 2017, Published: 18 July 2017.
4. Design, modeling and CFD analysis of a micro hydro Pelton turbine runner: for the case of selected site in Ethiopia, *International Journal of Rotating Machinery*, 2017, 3030217. This articles include the research presented in this research. The candidate is the main and corresponding author respectively for the publication.

CONTRIBUTION TO KNOWLEDGE AND PRACTICE

i. The technology will be beneficial to local manufacturing industries and will thus ensure availability of the turbines locally at low cost and will further, ensure the support services in terms of spare parts and maintenance.

ii. It provides information to various stakeholders and contributes knowledge to hydro power research.

iii. The results of the research will ensure availability of prototype and documented procedures for designing, fabricating and testing of micro hydro turbine in Ethiopia.

Most importantly, a general awareness and technical understanding of successful Micro-hydro turbine technology can be developed and fostered at the local and regional levels so that rural electrification projects can be implemented effectively.

List of Abbreviations, Symbols, and Nomenclature

d_{jet}	Jet or nozzle diameter (m)
K	Nozzle (jet) discharge coefficient
D_{pn}	Diameter of penstock connected to the nozzle
D_{pt}	Diameter of penstock connected to the turbine
PCD	Runner (wheel) circle diameter
F_d	Deflector force
F_{dr}	Required deflector force
H_g	Gross head
H_n	Net head
L_n	Nozzle length
L_{pt}	Length of penstock between intake and turbine
Z	Number of buckets
n_j	Number of turbine nozzles
N_r	Turbine run-away speed
η	Efficiency

Greek symbols

β	Nozzle tapper angle (degrees)

ACRONYMS

MWIE	Ministry of Water, irrigation and Energy
AAIT	Addis Ababa Institute of Technology
CFD	Computational Fluid Dynamics
VOF	Volume of Fluid
MHP	Micro Hydro Power
MHT	Micro Hydro Turbine
SST	Shear Stress Transport
CFX	CFD code by ANSYS
BEF	Best efficiency point
IEC	International Electrical Commission

Contents

List of Tables

List of Figures

CHAPTER 1
INTRODUCTION

The presented case study is on one of an ideal Micro hydropower plant for exploiting the unused micro hydro potentials in Ethiopia by developing turbine technology. Ethiopia's Micro hydro power capacity was a key driver for this research. However, technology developed during this research is not limited and can be used in any different hydro potential sites in the world. Furthermore, the expected outcomes and contribution will be explained, as well as the way of approaching the research is also briefly overviewed.

1.1. Background and Significant of Study

Flowing water has hydraulic energy that can be transformed into electrical energy. Access to modern forms of this energy can have a tremendous impact on the lives of impoverished people living in developing countries by reducing manual labor, encouraging economic activity, improving health conditions, and reducing the overall cost of energy. The mechanical power produced can be utilized for vital industrial and agricultural processes such as milling grain, running water pumps for irrigation, and powering refrigeration cycles, to name a few applications. The electricity produced can also serve a number of useful purposes, namely home lighting. Electrical lighting can increase the productive hours in the day, thereby allowing more time for education and economic productivity.

Although, many rural communities have good access to plenty of water resources, the most serious problem faced by a country like Ethiopia is that of rural electrification. Generation of electricity for these local areas remains a challenge in power industry. In general, one of the most important and achievable method to produce electricity and reduce the difficulties involved in local generation of electricity is, to introduce a standalone electric power generation, using renewable resources. More recently, Rural Electrification Fund (REF), which is operating under the Ministry of Water, Irrigation and Energy (MWIE), is working to control this energy crisis in the country. In its effort, it has identified some potential micro hydro sites in the Country. These potential for small-scale hydro power is estimated to be 10 % of the total potential (1,500 - 3,000 MW). So far, out of the total potential for Micro Hydro Potentials (MHPs) in the country (over 1000 MW) only a minute portion of it (less than 1%) is developed [S.Melessaw, 2009]. If these water resources (Fig.1) are properly harnessed, they will help Ethiopia to meet its power demand and maintain her economic growth for the next decade.

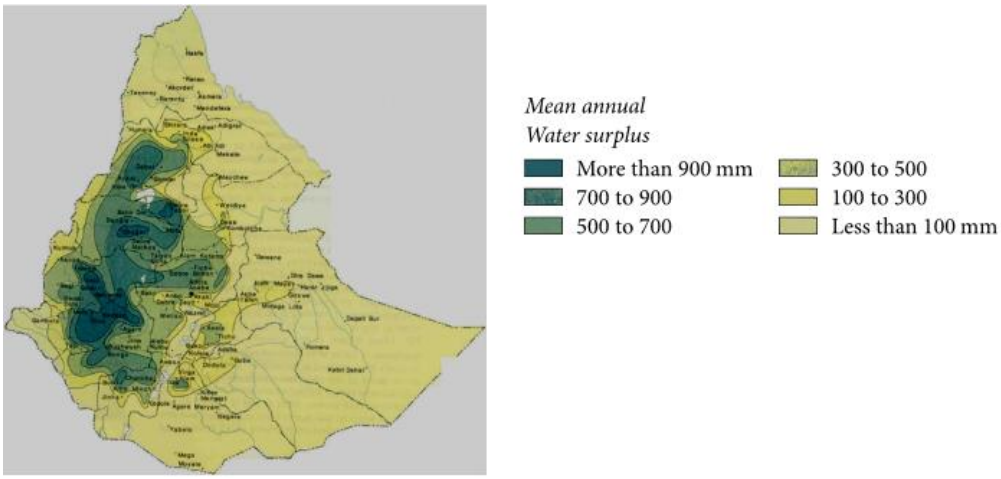

Figure 1.1: Distribution of MHP Potential Sites in Ethiopia [S.Melessaw, 2009].

Fig.1.1 above shows some MHP areas. These areas are mainly in the Western and South-Western part of the country and they are characterized by high mean annual rainfall ranging from 300 mm to over 900 mm. Consequently, there have been feasibility studies for Pelton turbine to harness this high head water resources [Tilahun et.al, 2017].

For many of these sites, a Pelton turbine is the only option. This is due to higher mountains providing higher heads and seasonal variation in flow rates makes appropriate the choice of Pelton turbines for hydro power projects in the country [Barstad, 2012].

Depending on water flow and design, Pelton wheels operate best with heads from 15 meters to 1,800 meters, although there is no theoretical limit. In this turbine, water is brought down through the penstock pipe to a nozzle, and it comes out into the turbine casing. The jet is then directed at a wheel, or runner, which has a number of buckets around its edge. The force of the jet on this wheel makes it turn, and gives the output power [Jeremy, 2000].

Micro hydro Pelton turbines refer to turbines with capacity ranging from 5kW which is just enough to provide domestic lighting to a group of houses through a battery charging to100 kW which can be used for small factories and to supply an independent local micro-grid.

In general, micro hydro does not need dams and a reservoir as water is diverted and then conducted in a penstock to a lower elevation and the water turbine. Generally placed within a rural electrification context, using these turbines for power generation is more cost-effective than using diesel/gasoline generators, wind turbines, or solar photovoltaic systems. Except their power rating, these turbines are not different from small or large hydro turbines. For example, the principles of operation, types of material units, and the mathematical equations

used in the selection and design of turbines are essentially the same as large hydro turbines. Moreover, Pelton turbines offer high operating efficiency over a wide range of flow conditions, are widely available, and are fairly inexpensive to manufacture making them a common choice for high head micro hydro applications [Jeremy, 2000].

Besides, investigation reveals that, there is no company engaged in supplying this Micro Pelton turbines locally in the country. As a result, the necessity and the possibilities to design and manufacture Pelton turbines using locally available materials and with local manufacturing capability has been identified for those sites which have been evaluated and proved to be viable, the aim being to cut the equipment cost which is imported from various countries from Europe and Asia [S.Melessaw, 2009].

Building local design and manufacturing capabilities in power generation and distribution technologies (especially MHP), will provoke an increase in local content of power generation, transmission and distribution projects. More often the material and the skilled labour as well as technical staff are available but what is missing is the information and know–how.

Thus, this motivated us to focus on ensuring availability of prototype and documented procedures for designing, fabricating and testing of micro hydro Pelton turbine in Ethiopia.

It is also vital to adopt indigenous design and development of hydropower components, since it makes sense to start such a research by building up experience gradually.

1.1.1. Losses of Micro Hydro Turbines

A pressure pipe, known as a penstock, conveys water from the forebay (reservoir) to the turbine. The turbine drives an alternator or a generator to generate electricity. The energy losses that occur within a turbine are attributable to volumetric, mechanical, and hydraulic losses.

The volumetric loss arises from the slight leakage (from the high pressure side to the low pressure side) in the small clearances that must be provided between the rotating element and the casing.

The mechanical loss is a result of power loss due to mechanical friction at bearings and fluid shear in the clearances.

The hydraulic loss arises from head loss in the flow passages due to friction and eddies. The diagram shown in Fig 1.2 gives Pelton turbine losses in various components.

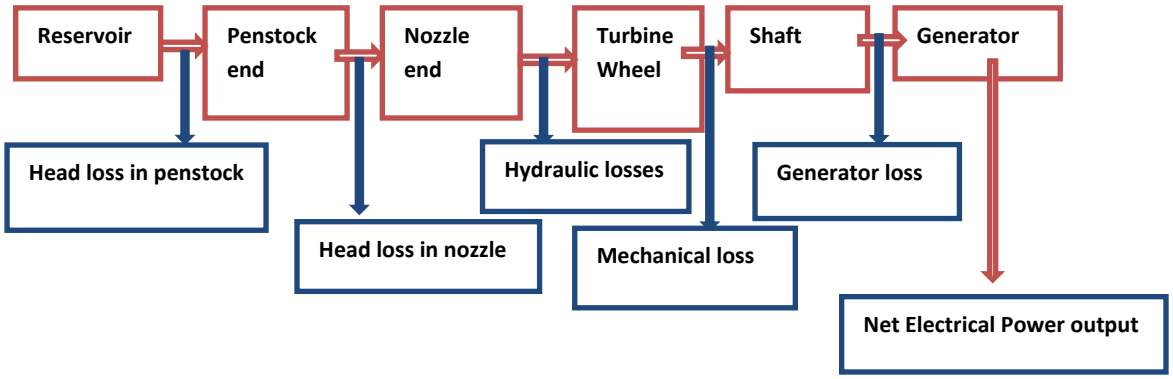

Figure 1.2: Impulse turbine losses [Zhengji Zhang, 2016].

1.1.2 Efficiencies and Applications of CFD in the Design of MHT

Turbine efficiency can be considered separately as hydraulic efficiency, mechanical efficiency, volumetric efficiency and overall efficiency.

Hydraulic efficiency is defined at the ratio of power given by water to the runner of a turbine to the power supplied by the water at the inlet of the turbine.

The ratio of the power available at the shaft of the turbine to the power delivered to the runner is defined as *mechanical efficiency*.

The volume of the water striking the runner of a turbine is slightly less than the volume of water supplied to the turbine. Some of the volume of the water is discharged to the tail race without striking the runner of the turbine.

Thus the ratio of the volume of the water actually striking the runner to the volume of water supplied to the turbine is defined as *volumetric efficiency.*

Overall Efficiency is the ratio of power available at the shaft of the turbine to the power supplied by the water at the inlet of the turbine.

For most schemes, head and flow, Water-to-wire efficiency (Overall efficiency) is quite low on most of the installations, ranging from 7% up to 59%. The expected efficiency should be closer to 50-60% [Z.Zheng, 2016; Jeremy, 2000]. However, the growth and competition in the energy market, necessitates more production of electricity with less cost, leading to an improvement in the hydropower plant equipment. It is therefore important to increase the efficiency of hydropower plants, namely the efficiency of the turbines. More precisely, in the new context where harvesting small hydro potentials can become economically viable, there is also a need to provide solutions to reduce the design cycle time and cost for Pelton runners. On the other hand, it is known that, with increasing demand, the performance analysis of turbine such as efficiency and dynamic behavior is also an important aspect to analyze its suitability under different operating conditions [Z.Zhang, 2016]. Additionally, it is used by the turbine producer to guarantee the hydraulic performance of a turbine to the customer.

However, it is known that, design of Pelton turbine is mainly conducted from know-how and extensive experimental testing, which provide an empirical understanding of factors that are important to turbine design. But, in today's highly competitive market of turbine, the performance is often difficult to determine in the short term with this traditional practice. Therefore, the incorporation of computational fluid dynamics (CFD) in the design of micro hydro turbines appears to be necessary in order to improve their efficiency and cost-effectiveness beyond the traditional design practices.

The main topic of investigations by the CFD method has focused on the interactions between the jet and the rotating buckets as well as the relative flows within the buckets. These are the flows that are so far not easily accessible by experimental measurements [Barstad, 2012; Z.Zhang, 2016].

CFD simulations are therefore likely considered as an available way for investigating complex flows in Pelton turbines, provided that, they are reliable and able to reveal the possibility of improving the system efficiency. It is based on governing equations of viscous flow that describe three fundamental principles of conservation: Conservation of mass (continuity), Conservation of momentum (Newton's 2nd law) and Conservation of Energy (1st law of thermodynamics).

Eqs.1.1, 1.2 and 1.3 represent Navier Stokes equations of conservation of mass, momentum and energy respectively. The fluid used is incompressible and there is not significant change in temperature. Eqs. 1.4 and 1.5 are the modification for incompressible fluid and by neglecting energy equation.

$$\frac{\partial \rho}{\partial t} + \rho \nabla . V = 0 \qquad [1.1]$$

$$\rho \frac{DV}{Dt} = \rho g + \nabla . \tau_{ij} - \nabla P \qquad [1.2]$$

$$\rho \frac{DV}{Dt} = \rho g + \nabla (k \nabla^2 T) + \emptyset \qquad [1.3]$$

$$\nabla . V = 0 \qquad [1.4]$$

$$\rho \frac{DV}{Dt} = \rho g + \mu \nabla^2 V - \nabla p \qquad [1.5]$$

There are many commercially available codes (CFX, Fluent, STAR-CD, etc.) where a solution can be calculated. The numerical analysis of CFD in micro hydro turbine consists of incompressible fluid flow. In addition, the temperature effect is negligible during the analysis. Therefore, conservation of energy is ignored during analysis.

In terms of multiphase modeling, CFX has two sub-models applicable for free surface simulations known as homogeneous and inhomogeneous indicating whether the velocity field of different phases is shared or separate respectively.

In the homogeneous flow model a common flow field is shared by all fluids (in this research water and air). In addition to the flow field, other relevant fields such as temperature or turbulence are also shared. Therefore, the multi-fluid model can be simplified [ANSYS Inc. 2013b].

In the inhomogeneous (or the inter-fluid transfer) model the interfacial transfer of momentum, heat and mass is directly dependent on the contact surface area between the two phases.

As introduced above, Turbine efficiency can be increased by an optimization process of the turbine geometry parameters. Successive tests are needed for the improvement of turbine efficiency. Therefore, Model testing and Computational Fluid Dynamics (CFD) are used in the design process to optimize the result. The aim is to increase the efficiency of the power plant by redesigning the turbine or reducing the manufacturing cost. In doing so, preliminary solid model dimensions of turbine are subject to CFD analysis for the evaluation of the hydraulic performance. Slight changes in the solid model of the turbine, especially in the runner, leads to an optimized geometry of the turbine with optimized efficiency. Optimized turbine geometry is checked for structural safety and is ready for manufacturing.

CFD simulation in this study is conducted by using ANSYS CFX using Shear stress transport Model. This model has widespread use for design, optimization and validation with the experimental data of the hydro turbine [Barstad, 2012; Perrig, A. et. al, 2006 and Perrig, A., 2007]. It is the combination of k-e and k- ω model. These two models are two equation turbulence models whose transport equations are solved along with mass and momentum equations.

Therefore, in the present work, the design of Pelton turbines needs to be developed by means of CFD simulations and model studies in order to optimize the turbine, which will be useful for implementation of rural electrification projects.

Consequently, this research will provide also the necessary information for the design, numerical analysis, local manufacturing and experimental testing to validate numerical simulations of this turbine for installing and running them successfully. Achieving such a goal, will lead to project cost reduction, availability of parts, adequate operation and maintenance personnel, more job creation and make power sustainability a reality, so that the benefits of this technology can be brought to rural populations.

1.2. Objectives of the Research

In order to accommodate the main concern and challenge introduced above, this research title *"***CFD Based Design Optimization, Fabrication and Testing of A Micro Hydro Pelton Turbine***"* is conceived. The main objectives of this research are, through CFD simulations and validation against experimental data:-To ensure availability of documented procedures for designing, constructing and performance testing of Pelton turbine. This will further support to cut the cost of installation using imported equipment by providing the necessary equipment locally and so, making the electricity affordable to our rural citizens.

The Specific Objectives of the Research are:

- Selecting one site from those already identified by MWIE as potential MHP sites.
- Identifying the type of turbine suitable for the selected site in this case Pelton Turbine.
- Optimizing the design of Pelton Turbine for best performance using CFD simulation.
- Design the methodology of production and fabricate the optimal model turbine locally.
- Test the performance characteristics of the model turbine and verify with the performance predicted by the CFD simulation.

More specifically, the research deals with the design, production, and performance testing of a micro-hydro turbine model. Such objectives commonly rely on the use of CFD simulation tools and optimization techniques to solve the turbine design problem. The simulation was performed on key part of the turbine which is the runner. Identifying the importance of the runner design parameters and their influence on performance was within the scope of this research. Therefore, the design problem addressed in this research can be informally described as finding the runner geometry providing the best performance. Consequently, the present study has also the ambition to reduce the size of the runner to have a cost effective runner design.

The design process starts with the design of initial dimensions for the runner based on different literatures (baseline design) and directed towards the modeling of the runner using a 3D CAD tool called CATIA V5. The performance of the runner has been analyzed in ANSYS CFX simulation tool (CFD) under given loading conditions of the turbine.

Through the process, the research aims at building the local capacity needed for affordable and sustainable development of the resources for the benefit of those citizens dwelling nearby the sites.

The constructed model turbine could be used as instructional material in training mechanical engineering students.

1.3. Research Methodology

The first step of this research after selecting potential site was collecting technical data (Head and flow rate) that are used for turbine design. Following this, the design approach combining theoretical expressions, extensive CFD simulation and experimental model were done. Initially, the geometries to be compared were designed by standard procedures and optimized and tested by CFD analyses. At a later stage, following the results obtained, a model turbine was tested at the Addis Ababa Institute of Technology's laboratory to have a tangible confirmation of efficiency with variable operational conditions. The results obtained from both approaches (CFD and Experimental) were analyzed, compared, and the momentum transfer in the bucket were discussed. A methodology is developed, as shown in Fig.1.3, to obtain optimized turbine design.

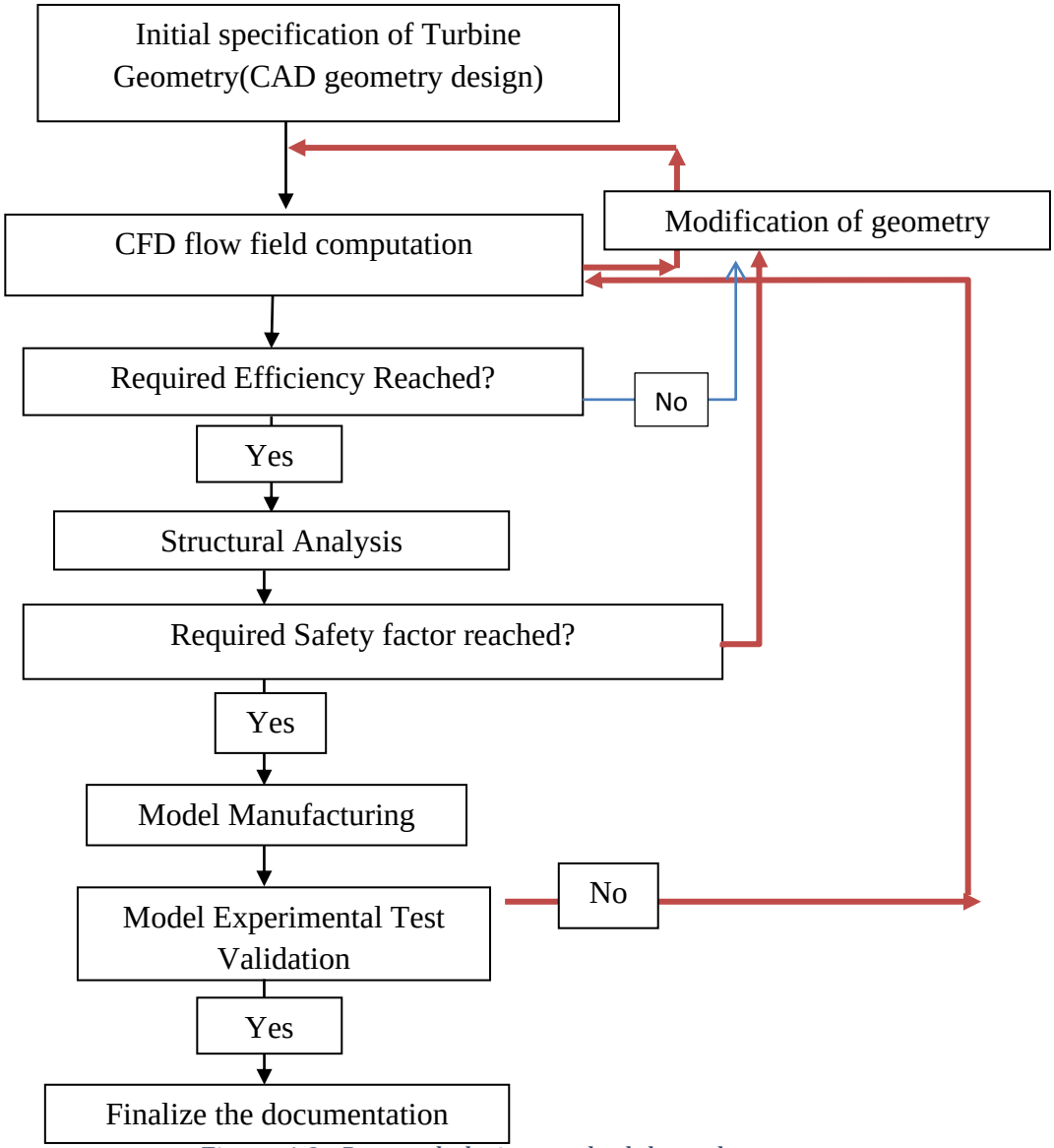

Figure 1.3: Research design methodology chart.

1.4. Dissertation Organization

This research is organized in eight chapters and it starts with a brief discussion of micro hydro turbines applications, functions, its contribution to rural electrification and the objective of the research in general. This is followed by a comprehensive and critical review of the literature as detailed in **Chapter 2**. In addition**,** the available design guidelines and review of research and developments in Pelton Turbine were also presented. The remaining chapters are organized as follows:

Chapter 3 deals with the design aspect of a Micro hydro turbine. It started from site selection and finally based on the site data, selection of a suitable turbine (Pelton turbine), and calculations of the design parameters were done.

Chapter 4 Performance Analysis of the Baseline Design Turbine By CFD: Process of geometric modeling, simulation of the baseline design turbine using ANSYS CFX is performed.

Chapter 5 Design Optimization Considering Manufacturability: Numerical simulation is playing a very essential role for optimization of Pelton turbine by varying shape and positioning of the turbine components, until the best model is found. In this phase, comparison with previous results guarantees that the model is in the optimal range. It is then checked for structural safety with a more accurate method using static structural analysis.

Chapter 6 Manufacturing of the Model Pelton Turbine: Preparing part, assembly and manufacturing drawings of the optimized design turbine model. Manufacturing Methodology of the turbine parts were also discussed.

Chapter 7 Validation of the CFD Model: Following computational analysis and design optimization, scale model testing was carried out in the lab to prove the validity of the current simulations.

Finally, in **Chapter 8 Conclusions and Recommendations:** the study presents the outcomes of the research, and reflects on the goals set and success in meeting them. Moreover, this chapter provides a list of recommendations for future work.

CHAPTER 2
LITERATURE REVIEW

This chapter is a review of the published relevant literature to the commonly used Pelton turbines' design guidelines and followed by previous research and development used to model, optimize and test the performance of Pelton turbine.

2.1. Available Design Guidelines

The most useful source for the design of Pelton turbines, based on analytical and experimental studies was the "Micro-Hydro Pelton Turbine Manual" by Jeremy Thake (2000). This manual covers the process of designing a Pelton turbine in fine detail. Extending past the design of the turbine, the author also describes the processes used to form the turbine and its associated housing and nozzle components. The theory of operation of a Pelton turbine is also covered in great detail.

Other more recent textbooks that include design guidelines for Pelton turbines are Water Power Development by E. Mosonyi (1991), MHPG Series: Harnessing Water Power on a Small Scale, Volume 9. In addition to these textbooks, there are some publications and textbooks that include design guidelines for Pelton turbines [Atthanayake 2009; Zh. Zhang 2016; Židonis A. 2015]. However, usually it is not known what kind of research these guidelines are based on as most of the experimental data is not available to the public and is kept as commercial secret by the turbine manufacturers [Solemslie and Dahlhaug 2012]. Nevertheless, some of the guidelines are based on theoretical calculations and assumptions and are usually in agreement with the commercial product designs of the leading turbine producers. The related practical experiences have thus always played a major role besides applying general design rules.

As mentioned in the literature [Židonis A 2015], even the number of bucket on a Pelton wheel, for instance, is determined only by experience or model tests without relying on any hydro mechanical background.

2.2. Research and Development of Pelton Turbines

The rapid development of flow simulation for water turbines has already led to substantial improvements in the design and performance of Kaplan, Cross flow and Francis turbines. This technology has not been extensively used in Pelton turbines, but has reached a stage of maturity where simulations of the flow in the distributor and the flow nozzles of Pelton turbines can be routinely carried out.

According to the literature by Zh. Zhang (2016), the flow in the jet and the moving buckets are more difficult to simulate, as they involve a jet flow with a free surface and the unsteady interaction of the jet with the buckets. Such simulations are now possible but, as the methods have not yet been widely validated, the simulation have to be considered to be an area of active research and development. Therefore, the purpose of the research and development work presented in this section was to propose and elaborate a practical methodology, in order to integrate additive design and numerical methods in product development cycle, for Pelton turbine.

The Pelton Turbine was invented by Lester Allan Pelton in the (1880s) (see Fig. 2.1). Over the years since it was first patented in 1880, improvements to Pelton's original design were made by many contributors, the final major one being made by Pelton Water Wheel Company's competitor, William Doble [Perrig et al. 2006 and Perrig 2007]. Doble noticed how the buckets in the Pelton design were worn down quickly due to the scouring of the sand of the water jet in turbulent flows hitting the buckets. Doble fixed this by essentially creating a double bucket design with the addition of a water splitter, which divides the jet of water in half and minimizes the turbulence and abrasion of the water in the buckets since previously the bucket were merely cups. Doble's revision of the design led to "a second stage in the development of Pelton turbines" [**"**Pelton Waterwheel Collection**,** 1898**"**].

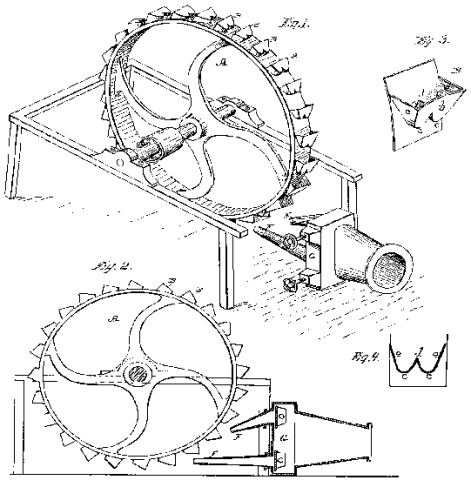

Figure 2.1: Pelton turbine original patent document [Perrig, A et.al., 2006].

The Layout of a typical modern Pelton turbine is provided in Fig. 2.2. It has a circular disk mounted on the rotating shaft or rotor. This circular disk has cup shaped blades, called as buckets, placed at equal spacing around its circumference.

For low output requirements, the horizontal shaft Pelton turbines with single or twin jets are used [Perrig et al. 2006 and Perrig 2007]. The force of water jet on buckets is tangential and

it produces torque on shaft due to which runner rotates. It can be seen that the bucket shape has evolved into much smoother round shape to reduce the flow losses. Moreover, the buckets have a cutout that ensures better transition as the jet goes from one bucket to another. In addition to that, the injector contains a nozzle and a spear valve to control the flow rate and maintain good quality of the jet.

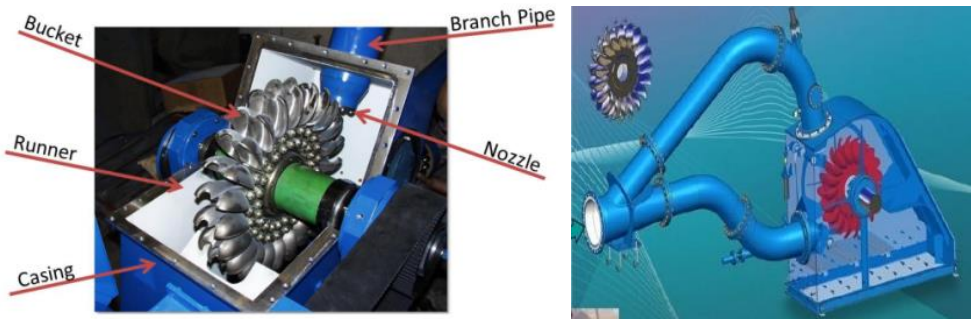

Figure 2.2: Typical layout of a modern Two injectors Pelton turbine [Židonis A 2015].

As stated in Zhengji Zhang (2016) book, vast amount of research was performed on the design of Pelton turbines throughout the years providing the hydro community with some guidelines or best practice recommendations. However, the reality of the knowledge within Pelton turbines is that, there are still areas within the physics that are still not understood completely. These gaps in the understanding of the flow within Pelton turbines have been given increasing interest by the research community within multiple fields. This is due to the increasing demand for energy on a global basis in addition to the growing focus on meeting the increasing demand by utilizing renewable energy resources

The researches on turbines consist mainly of analytical, numerical and experimental studies. In the past, Pelton turbines had been designed using more of a trial and error approach, where a prototype was constructed, tested, and improved upon in successive prototypes. At the end of the last century, the computational fluid-dynamics (CFD) started to be applied to Pelton turbines and the experimental investigations were mainly aimed at validating the numerical analyses carried out on simplified configurations. Mention should be made of investigations carried out, for instance, by Perrig, A.,(2007), Židonis A. (2015), Barstad, (2012) as well as Panthee, A.et.al (2014).

Over time, fairly high efficiency designs were built, though the mechanisms that made one design superior to another were not well understood. As mentioned in most of the above researches, CFD is also being used to aid the design of multi-jet Pelton turbine systems. More

jets, which allow for higher flow rates and thus greater power output, necessitate a better understanding of the flow through the turbine and how manifold design impacts water jets.

So far, few investigators have only reported diverse values of maximum efficiencies as shown in Table 2.1. Because of commerciality of the turbine, many of the investigators normalized their results in their publications. Most papers report that the shape of the efficiency curve is well captured, while actual differences between measured and numerically predicted efficiency remain unreported. Fewer still go deeper into the design and performance analysis of the turbine. An exception is listed in Table 2.1, the first two authors did their simulation on the same size of the runner at the Pich circle diameter (PCD) of 400mm, but for different head and flow rate conditons from best efficiency point (BEP).

Table 2.1: Some Pelton Turbine studies and maximum efficiency levels attained.

Investigators	Net Head(m)	Flow rate (m^3/sec)	Runner speed (rpm)	PCD (mm)	Maximum efficiency, %
Amod Panthee, 2014	53.9	0.05	600	400	82.5
Panagiotopoulos, 2015	100	135% of BEP	1000	400	86.7
Solemslie, B. 2012	70	-	-	513	77.75
Sanam Pudasaini, 2014	80.85	0.09218	600	490	87.71

Currently, CFD modeling and experiments are also being used, with the hope of raising turbine efficiency from the 50% range seen on the market (as of 2009) to above 80%, for developing new turbine designs [Zh. Zhang, 2016]. However, due to the irregular geometry of Pelton turbine bucket and rotation, visually observing the flow of water through the turbine is difficult. Recent advances in computer processor power have allowed for more accurate modeling of the flow [Zh. Zhang, 2016, Barstad, 2012]. Even though, this is a well-established turbine technology, there are many unanswered questions regarding design and optimization. Thus, further development is still relevant today. The above results still indicate room for further performance improvement in Pelton turbines that are readily manufactured. Until the fulfillment of these requirements, however, there is still a long way to go.

According to Zhang and Casey (2007), the main reasons for the noticeable lack of knowledge regarding basic hydromechanics of Pelton turbines are the complex flow conditions in both the high-speed jet and the unsteady interaction between the high-speed jet and the rotating Pelton buckets. Despite the importance and long history of Pelton turbines, nearly no advanced hydro mechanical applications can be found in this engineering design

specialty. At least physical flow processes in a Pelton turbine have not yet been as well understood as in other fluid machines such as pumps and Francis turbines [Zh. Zhang 2016].

Since the beginning of this century, measurements have been widely extended to the pressure distributions on the bucket surface in the model turbine. Corresponding pressure measurements in the rotating Pelton buckets were published, for example, by Kvicinsky et al. (2002), and Perrig et al. (2006). The pressure measurements in a Pelton bucket which is fixed on the ground of the laboratory were carried out by Zoppe´ et al. (2006).

Strictly speaking, the measurement result from a fixed bucket should not and cannot be applied to a rotating bucket, because the available volume forces that determine the flow in the bucket are not the same. It should also be mentioned here that most pressure measurements were carried out with the aim to validate the numerical simulation of the flow in the rotating bucket. The pressure distribution itself on the bucket surface is not of practical significance, except for the simulation of the abrasive particle motion in the flow towards the bucket surface.

In the years, experimental, numerical and theoretical investigations were carried to study more in depth the fluid-dynamics of the Pelton turbines. The first attempts to carry out a numerical simulation of the flow in a moving Pelton turbine bucket were made by Hana (1999); and Janetzky et al. (1998). However, the most detailed Computational Fluid Dynamics (CFD) analysis of rotating Pelton turbine was done by Perrig et al. (2006) and Perrig (2007), by considering five buckets (one-quarter of the runner) and the computed results were compared with experimental results at best efficiency point (BEP).

The good agreement obtained between numerical results and experimental data highlighted the importance of further investigation of the cutting process by a real jet. However, the first work succeeding in the numerical analysis of the effects of a real jet on the cutting process of a moving Pelton turbine was of Santolin et al. (2009). Turbulence was modeled using the k-ε model and the multi-phase flow was modeled using the Homogeneous model. The main findings of this research said that k-ε model had difficulties when modeling flow near the cutout region. Moreover, the simulations showed a presence of the Coanda Effect, that is, back of the bucket contributing to the torque as the passing jet is attracted to the surface. However, this observation could not be validated experimentally as the pressure was not measured on the backside of the bucket. Nevertheless, the error of the simulation was said to be around 5%, whereas the modeled backside contribution was around 7.5%.

Another research simulating a performance of a Pelton runner with a real jet was performed in University of Padova, Italy. The software used for simulations was CFX code. The chosen

turbulence model was the k-ω, SST. After the initial comparison of homogeneous and inhomogeneous models for multi-phase flow the Inhomogeneous model was chosen despite the slightly higher computation demands. Since the turbine model chosen was working in a plant in the north of Italy, the available experimental data of the test carried out at the installation time were exploited to validate the numerical analysis as explained by Santolin et al. (2009).

As reported by Santolin et al. (2009), the error in the calculation of the mechanical power was around 6 per cent, in line with the error orders of other numerical analyses carried out on Pelton turbines. The main reason of the discrepancy appears to be due to the mechanical losses that were not possible to evaluate experimentally and were not taken into account in the numerical simulation. This simplification involved an over prediction of the power at the shaft of the numerical model.

Similarly, Barstad, L. F. (2012), developed and validated a numerical model for the torque applied to a rotating Pelton bucket. The model was developed in CFX, homogenous model and based on a model turbine supplied by the turbine producer DynaVec. A comparison of experimental and simulated results showed a torque over-prediction of approximately 1.5 %.

Although, successful simulation of the whole system from the branch pipe to the casing is important but most probably not feasible to date because of such limiting factors like timescales or very high computational costs. That is why compromises are introduced to achieve an optimum effect within economically reasonable costs.

The main difficulties in simulating the performance of Pelton turbines are pressure losses, secondary flows, jets, film flow, free surfaces, spray formation, ventilation losses, unsteadiness and complex interaction between components [Keck, H. and M. Sick, 2008]. In addition to that, quasi-steady state approximations do not work for flows in Pelton buckets, requiring completely unsteady time dependent simulations with rotor-stator interaction to be used, hence significantly adding to the already high computational demands.

Numerical analysis of flow in a Pelton turbine is therefore, much more complex and time consuming. The difficulty to analyze the inner fluid-dynamics and to investigate the parameters affecting the performance of this type of turbines, prevented the development of well-consolidated design procedures, as those defined for the Francis and Kaplan turbines. As an example, a research project performed by Slovenia et al, (2010) produced results using CFX-12.1. A two-jet horizontal axis Pelton turbine was modeled at several operating points. The turbulence was modeled using the k-ω, SST model and the free surface was modeled using the two-phase homogeneous model. Half of the runner geometry was meshed and the

mesh consisted of 25.7 million elements and 11 million nodes. The time required for calculating performance of the turbine at one point was five days on a supercomputer with 2048 processor cores. Hence, the main limitation of the simulation was the computational cost. The results of the research show that accurate simulation of the jet and the mesh density was the main factors affecting the accuracy. Therefore, large computational cost of the simulations is also the main factor why there is a lack of publications on CFD usage for optimization of Pelton turbines [Solemslie and Dahlhaug 2012] in spite of some encouraging results**.**

Various authors made different simplifying assumptions in order to reduce this cost as much as possible and make Pelton optimization possible. All available CFD simulations reviewed in this section were assuming symmetry in the flow and therefore modeling only half of a runner or a bucket. Because of the periodic behavior assumption, the majority of simulations used only a fraction of a runner with the number of buckets in the section modeled being 2, 3, 5, 7 or even 10. Fairly large amounts of buckets such as 5, 7 or 10 were used so that a periodic torque on the runner could be achieved [Perrig, Avellan et al. 2006; Perrig 2007; Gupta, Prasad et al. 2014].

Other authors used only 3 consecutive buckets [Barstad 2012; Panthee, Neopane et al. 2014] where the torque was measured only on the bucket in the middle. This torque measured on a single bucket was then used to construct the torque on the runner assuming that every bucket would undergo identical loading. The first bucket was required to produce the back-splashing water that impacts the middle (or the second) bucket. The third bucket was required to realistically cut the jet when it is impacting the second bucket. Eventhough it was shown that it is possible to model the complete runner, this could be seen as unnecessary usage of computational resources. For instance, using the same computational resources and a reduced complexity simulation with only 3 buckets would allow simulations with better discretized grids (therefore improved accuracy) or analyzing more operating points or design variations and enable the optimization of Pelton turbine. As an example [Barstad 2012; Panthee, Neopane et al. 2014] highlighted CFD analysis using three-dimensional, unsteady, air-water, two-phase flow simulations in the rotating buckets by adopting the shear stress transport curvature correction turbulence model and homogenous model.

The suggestions of all the authors reviewed in this section were taken into account in the CFD analysis of the Pelton turbine for this research. The dimensions of the runner for the selected site in Ethiopia are in accordance with the minimum required values for model size and test parameters of IEC 60193 (1999).

CHAPTER 3

DESIGN ASPECT OF A MICRO-HYDRO PELTON TURBINE

Conceptual design involves the identification, data collection during field work on the proposed site for micro hydro power plant development. Planning for any small/micro hydro turbine design begins with the (near to) accurate estimation of head and flow available. The main aim behind these surveys was to check the data we received from Oromia Energy office is correct and select a suitable micro turbine for the site. Finally based on the site data, method of turbine selection (Pelton), calculation of basic design parameters and 2-D/3-D model of each component has to be made. In this chapter all the initial design parameters were calculated. These parameters included turbine power, runner diameter, runner speed, bucket dimensions, number of buckets, turbine specific speed.

3.1. Site Visit

In June 8, 2015, the first field visit was conducted by the research team with the principal objective of problem contextualization, confirmation and investigation of basic data for turbine development. Focus was placed on the West and Southwest regions of potential micro hydro sites as proposed by Oromia Energy bureau. Three Woreda's rural properties such as Ilfeta (Giche Keble), Toki Kutay (Melkay Herra Keble) and Ambo (Awaro Kore) with water resources capable of supporting small-scale hydroelectric generation in these regions were visited for initial survey and feasibility study. In all of these water resources with waterfalls, it is necessary and capable of developing the micro hydro power plant for rural electrification. One major challenge we faced in Phase I was selecting the target village to address economic and environmental considerations and then select a site from the three identified /proposed site by Oromia Energy office in which to build an ideal power plant.

After surveying three villages in the District, we narrowed our choices down to one: Melkey Herra Keble, which is one of the rural community Keble situated in West Shewa in the Oromia Region of Ethiopia (see Fig.3.1). Comparatively,this water resource is at favorable location and exhibit a great need for electricity and we came to the conclusion that this village was the ideal location for our first implementation as they had a more active population and showed great willingness to work with us. Once this village was chosen, we collected village data from two survey trips to design a micro-hydro turbine tailored to the needs and characteristics of the village.

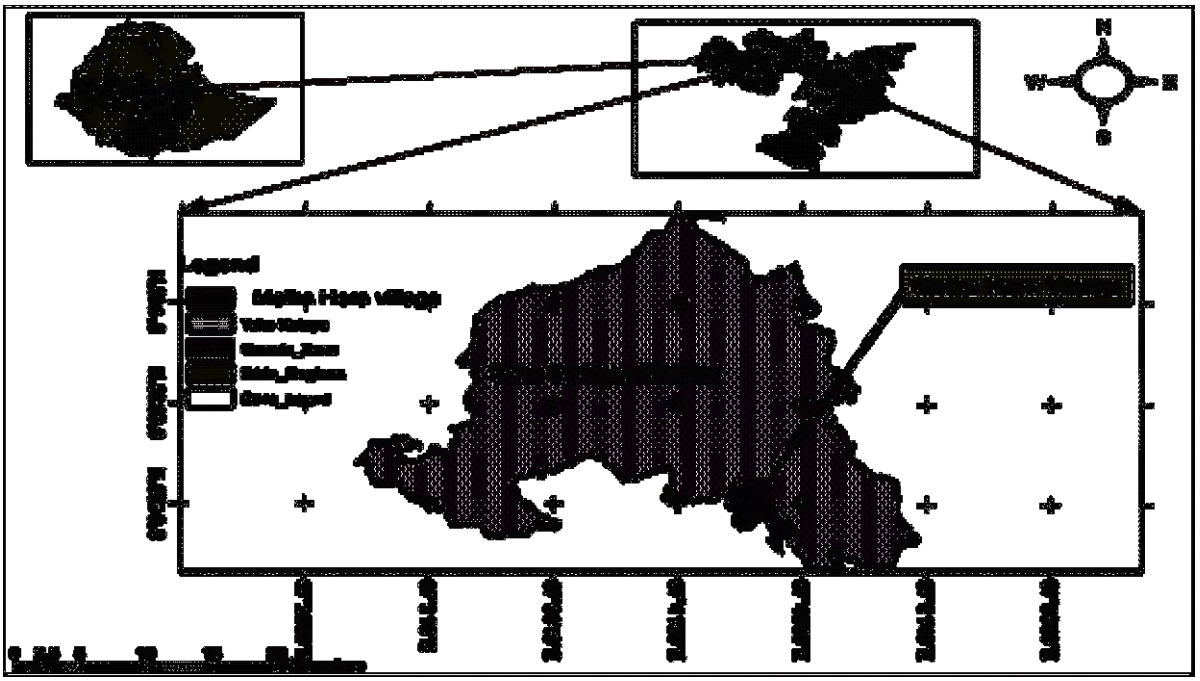

Figure 3.1: Map of the Study Area, From Arc GIS Software.

The selected water resource for hydroelectric generation is, "Indris River" for the communities living in the village called "Melkey Herra Keble", in "Toki Kutay Woreda. This village is located 15 minutes walking down from the nearest road, and it took 2 hours to go to the river from Addis Ababa, its geographical coordinates are 08° 51' 40" North, 37° 45' 10" East which is roughly 149 kilometers from Addis Ababa and is well renowned for tourism. The area doesn't have the access to electricity. Due to a small population (about 400 inhabitants) and inaccessible location around 27 km from Ambo, the village has received little assistance from the government with the development of the community.

In early 2007 E.C, the community lacked basic necessities, such as light, potable water, education, and reliable roads. As a cooperation, the Oromia Energy office under Ministry of Water, Irrigation, Energy established priorities for projects to be executed. The micro hydroelectric project is a main priority to the community. The next task is actually collecting important data like head and flow rate for turbine development.

The following methodologies were used for site survey:

Prepare necessary Goods for Site Survey:

- GPS (portable) and Altimeter
- Digital Camera, Checklist, Interview sheet and Field notebook

Investigation of potential capacity:

- Head measurement

Requirements for Structure Layout: the following main points were considered during the determination of suitable position for each component of the micro hydro power plant.

Selection of Intake Location: The top of the waterfall identified as a possible location on our first visit. This intake location is compared to the other location, the topography between the turbine and this intake location provides fewer challenges which include difficulties in transportation as well as challenges in how to provide infrastructure when laying the pipeline with this high head site. Approximate location with altimeter or portable GPS was taken by considering the above facts.

Figure 3.2: Possible location of the Intake, Weir.

Choice of Powerhouse Location: Finding a location for the surface powerhouse is dictated by topography–any suitable reasonably flat area is a candidate. The exact location for the power house at the site is selected which appears to be relatively safe from flood damage, Stable foundation, good accessibility for construction and Operation &Maintenance.

Choice of Forebay Location: A forebay tank is normally required at the transition between canal and penstock to handle transient flows due to changes in plant operation and also to facilitate plant control for plants operating in water level control mode. Top of the water fall is selected for the position of the forebay tank since this position is relatively stable, flat land and easy to install spillway from the forebay.

To sketch the layout plan and geographic condition, Photographs of the site was taken. From these on site observations, it is often possible to identify practical locations for Fore bay tank and powerhouse (turbine location).

Figure 3.3: Portable GPS equipment used in the field research.

After knowing the location of power house and forebay, the penstock routing was determined. Figure 3.4 shows topographic of the site and shows the pipeline route and point of interest. These locations, their elevations and co-ordinate were measured with portable GPS equipment and Altimeter. For this analysis the height and length estimates are shown in the diagram.

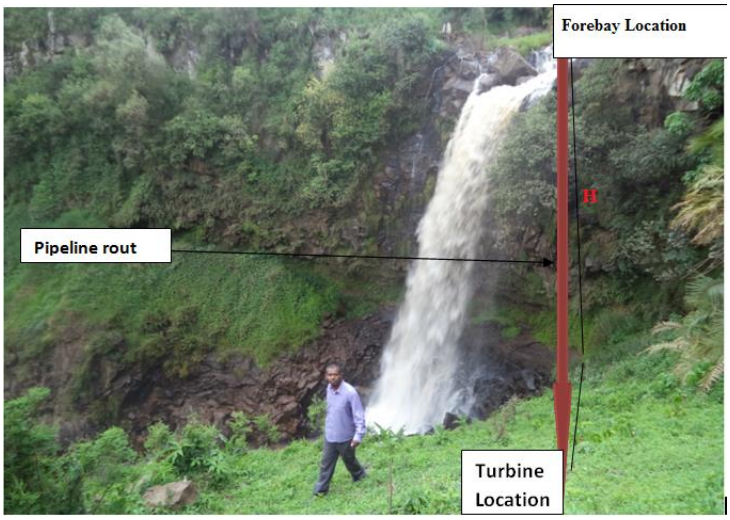

Figure 3.4: Photographs of the site with sketch of proposed penstock routing.

Head is the vertical distance that water falls from the forebay or intake to the turbine. The difference in elevation between the two points is determined by reading the altimeter at the two points and the difference of the two readings, with some atmospheric effect considered, gives gross head required. All that have been done at the site is to record one reading at the proposed forebay location and one at the site of the turbine in order to determine the head. The survey at a planned site proves that a gross head of 50 m and penstock length of 60m is available.

Secondary Data Collection: Secondary data are those collected by someone else (may be the researcher) for another purpose. For this research the secondary datum which also very important for turbine design is the flow rate and head of the rivers, taken from MWIE (Oromia Energy bureau) of Ethiopia. Sample of these data is placed in the following table.

Table 3.1: Proposed site for MHP development (Source: Oromia Energy bureau)

Region	Zone	Wereda	Keble	River Name	Head (m)	Flow rate (L/s)
Oromia	W/showa	Tokikutay	Melkey Hera	Indris	>50	140

Flow rate is the quantity of water available in a stream or river and may vary widely over the course of a day, week, month and year. When a site has been identified as topographically

suitable for hydropower, the first task is to investigate the availability of an adequate water supply. In order to adequately assess the minimum continuous power output to be expected from the micro-hydropower system, the minimum quantity of water available throughout the year must be determined. There are remnants of old irrigation canals close to the proposed site. These are not currently used for agriculture but have been in the past.

From Table 3.1, as the first estimate, electrical output power can be made from the gross head with total system efficiency values of 0.56 [Jeremy 2000].

$P=H_{gross}\times\rho_{water}\times g\times Q\times\eta_{total}$

$P=50\times1000\times9.81\times0.07\times0.56=19.2$ kW.

1 kW of electric power can light 10-12 rural households. This power is not thought to be enough for the small village, even though they only want a few lights. Further searching reveals, there are two waterfalls as shown in the Fig. 3.5 below which are only about 15 meters apart from each other and we proposed to combine the first water falls to the second using channel so that we can increase the flow rate of the site to 0.14m^3/s and the gross head remain the same. The flow of water in the selected river Indris is adequately high year round so that the theoretical limit of power production does not limit the proposed project and we assumed the design flow rate to be 0.14m^3/s for the driest season of the year. Assuming the total efficiency (56%) has not changed, the flow has increased twofold, so the power should increase likewise, to 2×19.2kW=38.4kW.

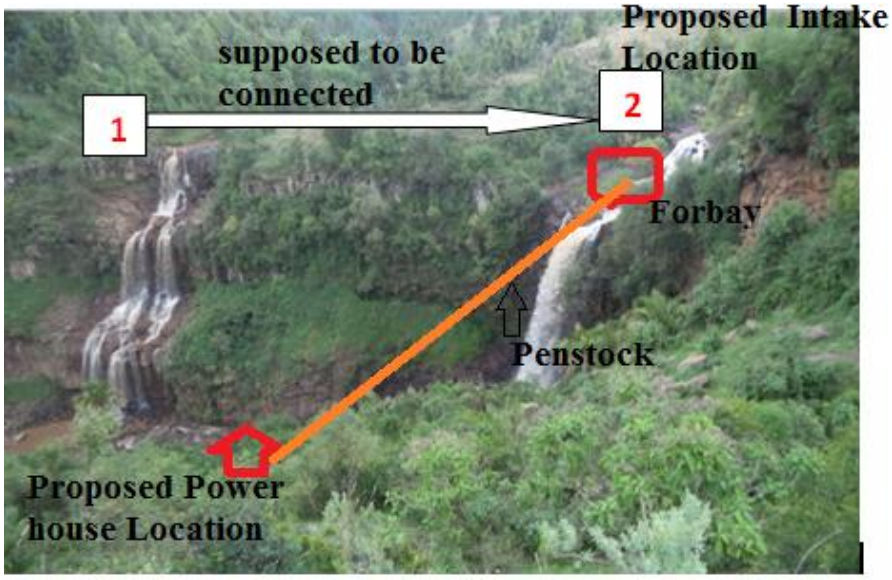

Figure 3.5: Photograph of two waterfalls at the proposed site.

Both secondary data obtained from MWIE as well as information gathered during field survey from interviewing the local people are used for this research.

A description is given in following section, on how to design the penstock and how to determine the net head.

3.2. Determination of Optimum Penstock Diameter

In this research, we used developed formula by Sarkaria's equation for economical determination of a penstock diameter as given below [European small Hydropower Association, 1998].

$$d = \sqrt{1.273\frac{Q}{V}} \qquad [3.1]$$

Where, V is the velocity of the water in the penstock and chosen to be 3m/s. Therefore, the diameter of the penstock pipe (d) is:

$$d = 1.13\sqrt{\frac{0.14}{3}} = 0.244m$$

3.3. Calculation of the Net Head (H_n)

Once the gross head is known, the net head at the nozzle exits can be expressed by the following formula [Jeremy, 2000].

$$H_n = H_g - H_l \qquad [3.2]$$

Where, H_g=the gross head and H_l=total head losses due to the open channel, trash rack, intake, penstock and gate or valve. These losses are approximately equal to 5% of gross head. This makes the net head available at the end of penstock as 50m-2.5m =47.5 m.

3.4. Selection of Turbine

Selecting the type of turbine that best suit a project is a detailed process. This involves technical, environmental, financial, and other considerations. The most inexpensive turbine may not be the best solution to the available head and flow [Jeremy 2000]. For the proposed site data head, 50m and flow rate, 140 l/s combination, principally a choice was necessary between Pelton and Cross flow situations as shown in Fig. 3.6. The figure shows the approximate application ranges of turbines for micro-hydro. Therefore, this chart can be used for selection of the turbine type.

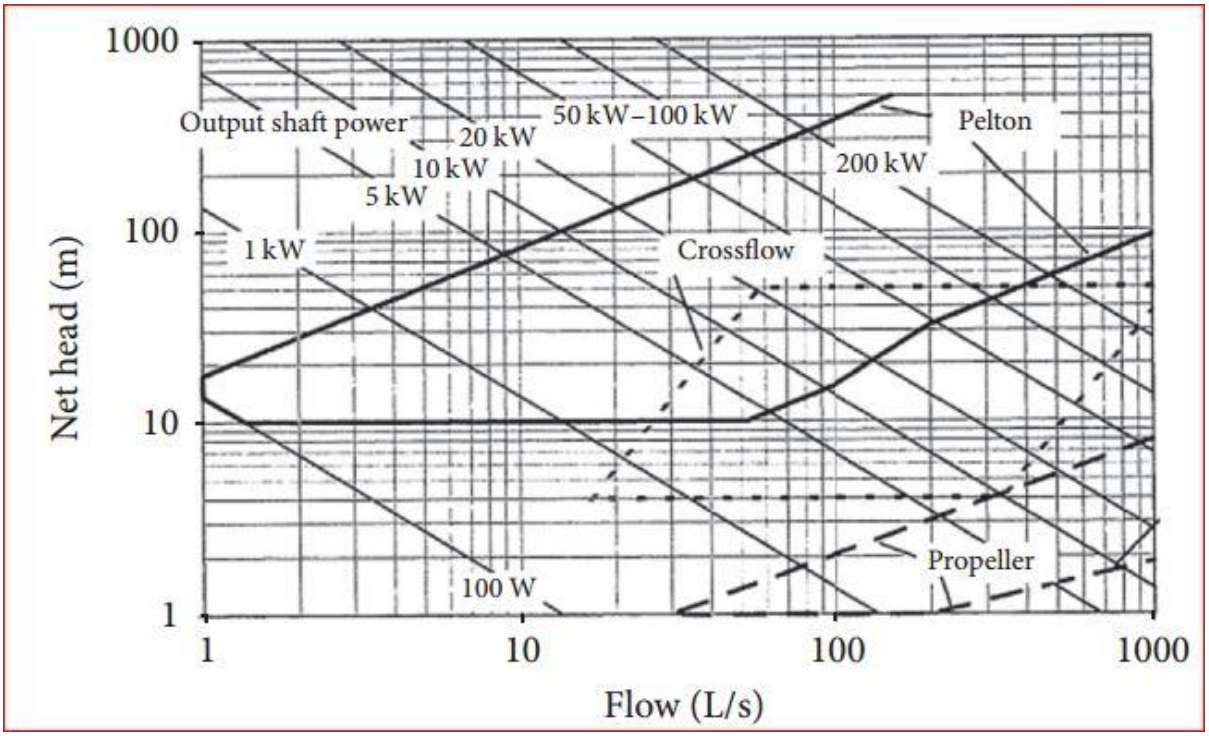

Figure 3.6: Application ranges for different types of turbine [Jeremy 2000].

A Pelton turbine design was chosen:

- due to its improved efficiency in high head, high flow situations characteristic of the site,
- To stand our design apart from those already in existence cross flow turbine design
- And with the objective of creating local capacity needed for developing this turbine.
- Ability to deliver power even at very low flow rates and easy maintenance.

3.5. Sizing of the Pelton Turbine

To start the initial design, calculations were conducted to size turbine parts. The theory behind these is mainly taken from the 'Micro Hydro Pelton Turbine Manual, by Jeremy,(2000)'. The calculations for design procedure of the Pelton turbine runner involves the following steps.

3.5.1. Calculation of Jet Diameter (d_{Jet})

The pressure at the bottom of the penstock creates a jet of water with velocity, V_{jet}:

$$V_{jet} = K_N \sqrt{2gH_n} \qquad [3.3]$$

where: V_{jet} = Jet velocity (m/s), K_N = nozzle velocity coefficient (are normally around 0.95 to 0.99) *and* H_n=net head at the nozzle.

The flow rate (Q) is then given by this velocity multiplied by the cross-sectional area of the jets:

$$Q=A_{jet}\times V_{jet}\times n_{jet}=\pi \frac{d_{jet}^2}{4}.V_{jet}.n_{jet} \qquad [3.4]$$

Where, n_{jet}=number of jets, d_{jet}=diameter of jets(m)

Combining Eq.3.3, Eq.3.4 and using an average value of 0.97 for K_N, gives:

$$d_{jet} = \frac{0.54}{H_n^{1/4}}.\sqrt{\frac{Q}{n_{jet}}} \qquad [3.5]$$

3.5.2. Calculation of the runner Pitch circle diameter (PCD) and Speed

The PCD is the circle diameter where water strikes the runner, in the middle of a bucket (Fig. 3.7).

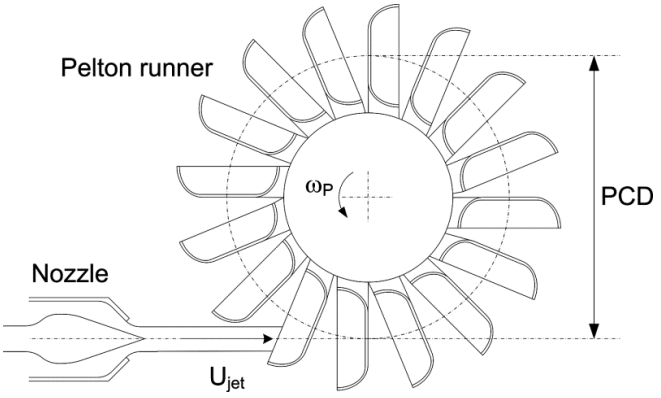

Figure 3.7: Diagram of a Pelton Runner showing PCD (Jeremy 2000).

Beginning with the derived formula to determine the turbine speed which can be expressed as:

$$2\pi \frac{N}{60}.\frac{D}{2} = x.V_{jet} \quad [3.6]$$

Where, PCD (D)= pitch circle diameter (m), x = ratio of runner velocity to jet velocity, (x=0.46 is used to produce the maximum power out of the turbine). N = rotational velocity of runner (rpm). Substituting for $V_{jet,}$ from Equation 3.3, and using x=0.46, Eq.3.6 becomes:

$$D = 37.7 \times \frac{\sqrt{H_n}}{N} \quad [3.7]$$

A spreadsheet was prepared and the results presented in Table 3.2 to determine the turbine speed (N) and PCD.

Table 3.2: Calculation Summary to determine the turbine speed (N) and PCD.

Name	Symbol	unit	Value			
No of jets	n_{jet}	-	1	2	3	4
Jet diameter	d_{jet}	mm	77.0	54.4	44.4	38.5
Runner PCD	PCD	m	699.667	494.740	403.953	349.834
Available PCD	PCD	mm	700	500	425	350
Turbine Speed	N	rpm	371	520	611	742
Gear Ratio	X	-	4.04	2.89	2.45	2.02

More often the speed of the turbine is given by the required RPM of the driven machine, be it a generator or any other end-use equipment. With a given net head, the RPM can be adjusted by changing the diameter of the wheel. Another possibility is not to run the turbine at the optimal speed.

Table 3.2 shows that for a given PCD the speed of the runner may be considerably different from the optimal speed, without having a too large influence on the efficiency of the turbine and thus allowing the manufacturer to have a series of standardized sizes of PCD (Available PCD). All the gear ratios calculated in the table are possible with belt drives.

Runner pitch diameter (D) 350 mm and 425mm with 4-jet and 3-jet respectively have smaller pitch diameter. However, for a turbine of these powers making is very complex and needs considerable expertise, so these are probably not an option. The single jet solution is also possible, but a 700mm PCD runner makes a very big turbine. The best solution is the 500mm, 2-jet turbine as recommended by Jeremy 2000 book, and this were taken for the baseline design analysis.

3.5.3. Calculation of Force due to Jet Water, F

Fig.3.8 shows a water jet emerging at speed C_1 from a nozzle, and striking one of the buckets of the wheel, which itself is moving at speed U. Suppose that the relative velocity, as

the water leaves the bucket,W_2 is kW_1, where, k is a velocity reduction factor with a value somewhat less than unity. The relative velocity is inclined at the bucket exit angle β to the jet's direction. The force F generated on the bucket may be found by considering the momentum change in the direction of motion as Eq. 3.8 as follows:

$F=\rho QC_1-\rho Q[U-kW_1\cos\beta]$ [3.8]

Note, the positive sign before the relative velocity at exit, indicating addition of the relative and bucket velocities. Note also that β is greater than 90°, therefore $\cos\beta$ will be negative. The incoming rate of momentum flow in the direction of motion the bucket is ρQC_1, and the outgoing rate is $\rho Q[U-kW_1\cos\beta]$.

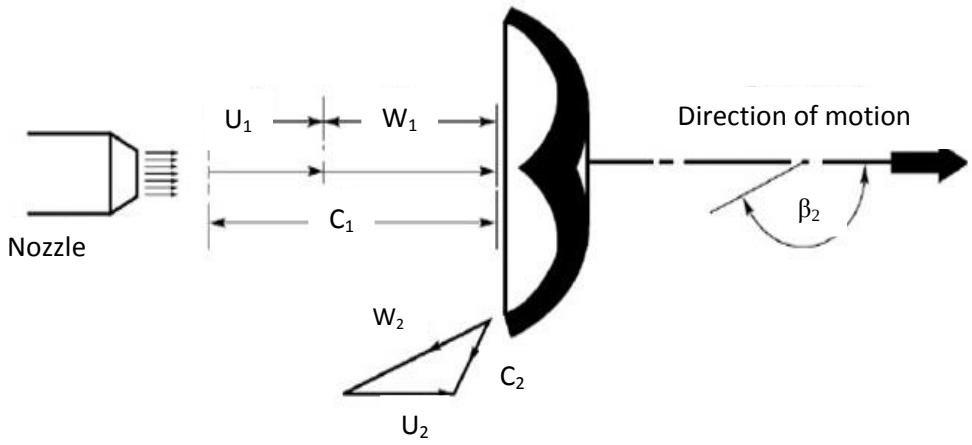

Figure 3.8: Velocity diagram when water jet striking bucket.

For ideal case, blade friction coefficient, k=1, $\beta_2=0$ i.e., water is deflected back by 180^0.

$W_1= C_1-U_1$, and $U_1=U_2=U$,

Therefore, the force (F) can be approximated as:

$$F=\rho Q(C_1-(2U_1-C_1))=2\rho Q\,(C_1-U_1)$$

Where, U - tangential velocity of wheel, C_1- absolute velocity of water at inlet, ρ-density of water, Q- flow rate of water.

Discharge of one Jet, q: It is obtained by dividing the total rate of flow through the turbine by the number of jet which is,

$$q=\frac{0.14}{2}=0.07\,m^3/s$$

If Pelton wheel buckets are held stationary ($U_1=0$, there will be a huge impulse force produced. The force of the water jet on the buckets becomes:

$F=2\rho qC_1$ [3.9]

The force acting on a single bucket by a single jet becomes: $F_{jet}=2\times1000\times0.07\times29.6=4144N$.

This is the structural force exerted by the single bucket on the water. This formula considers that the force is the highest when the runner is beginning to rotate.

3.5.4. Calculation of Torque Exerted on the Wheel

The torque ,T, exerted on the wheel is therefore expressed as:

$$T = \rho Q\, R\, V(1 - \lambda)(1 - k \cos \beta) \qquad [3.10]$$

Where, ρ-density of water, Q- flow rate of water, R-moment arm (Radius of the turbine wheel), k is a velocity reduction factor and λ is the ratio of bucket speed u to jet speed C_1.

From Eqn. 3.10, it is clear that for a particular wheel, supplied with water at some fixed flow rate (so that both mass flow rate and jet velocity are also fixed), torque T varies as $(1 - \lambda)$.

The torque therefore falls linearly from a maximum when λ=0 (when the wheel is stationary) to zero when λ=1 (when the bucket moves at the same speed as the jet). This is referred to as the runaway condition.

3.5.5. Estimation of Efficiency and Power output of the Turbine

To estimate the final system power output and efficiency, [Jeremy 2000] book also provides reasonable efficiency values for the nozzles, turbine, and generator (Table 3.3), which is also used in the usually design of Pelton Turbine.

Table 3.3: Pelton Turbine Parts' Assumed Efficiency *[Jeremy 2000].*

Part	Symbol	Assumed Efficiency
Penstock	η_p	0.95
Manifold	η_m	0.98
Nozzle	η_n	0.94
Runner	η_r	0.8
Drive	η_d	1
Generator	η_g	0.8
Overall Efficiency	η_o	***0.56***

It has proved reasonable in various installations to calculate with such efficiencies [Jeremy 2000].

Estimated electrical power: The power plants will have a power generation capacity of 38.4 Kilowatts. This is enough power to light up over 2856 energy saving bulbs that have been

provided to over 3,600 residents in the area in an environmentally friendly electrical power project. The electricity will also enhance public services by powering one elementary school, one health post in Melkey Herra Keble (selected site for this study).

Power Output of a Turbine: The power generated from hydraulic turbines is a function of the effective head, the flow rate, and the efficiency of the turbine. This is calculated to be 51.2KW.

3.5.6. Specific speed (n_s)

The specific speed of a turbine characterizes the turbine's shape in a way that is not related to its size. According to reference [Nechleba. M, 1957], the specific speed of the Pelton turbine with two nozzle must be between 17 to 50. Hence, the calculated specific speed of the turbine, 28.7 is suitable (see Table 3.4).

3.5.7. Basic design calculation summary of Pelton Turbine

The equations and the resulting values of the baseline design parameters of wheel are collected in Table 3.4 below.

Table 3.4: Basic design calculation summary of Pelton Turbine

Descriptions	**Data/ calculated Values**	**Unit**	**Design Guidelines Jeremy 2000** *[Jeremy 2000]*
$H_{\text{-net turbine}}$	46.5	mm	H-net turbine=$H_{\text{-net}}$× manifold efficiency
K_N	0.97	-	Ranges between (0.95-0.99).
$V_{\text{-jet}}$	29.6	m/s	Velocity of the jet (for n_{jet}=2)
$d_{\_jet}$	54.4	mm	Diameter of the jet (for n_{jet}=2) $d_{\_jet}$ = 0.11×PCD
x(U/V-jet)	0.46	-	For maximum power output (blade speed/V-jet)
Bucket speed	13.6	m/s	U=x.V_{jet}=0.46×29.6
N	1500	Rpm	Standard Generator RPM
η	0.56	-	Total system efficiency
P	38.4	kW	Estimated electrical power=ρg$H_{\text{-Gross}}$ ×Q×η_0
P-turbine	51.2	kW	Turbine Mechanical Power=ρgH-net turbine ×Q×η_r
F	4144	Nm	Force of Water Jet (F=2ρqV_1=2ρqV_{jet})
Ns	28.7	-	Specific speed, $N_s = \frac{N\times\sqrt{P}}{H_n^{1.25}}$

Additionally, a standard generator with 4-pole (running at 1500rpm for 50Hz) was chosen which leads us to design the belt drives as shown in Appendix A.

3.6. Detail Bucket Geometry Design

Fig.3.9 shows the dimensions of the bucket as percentage values of the PCD of the turbine. Like the basic bucket model changing the PCD value within the model allows it to be scaled [Jeremy, 2000].

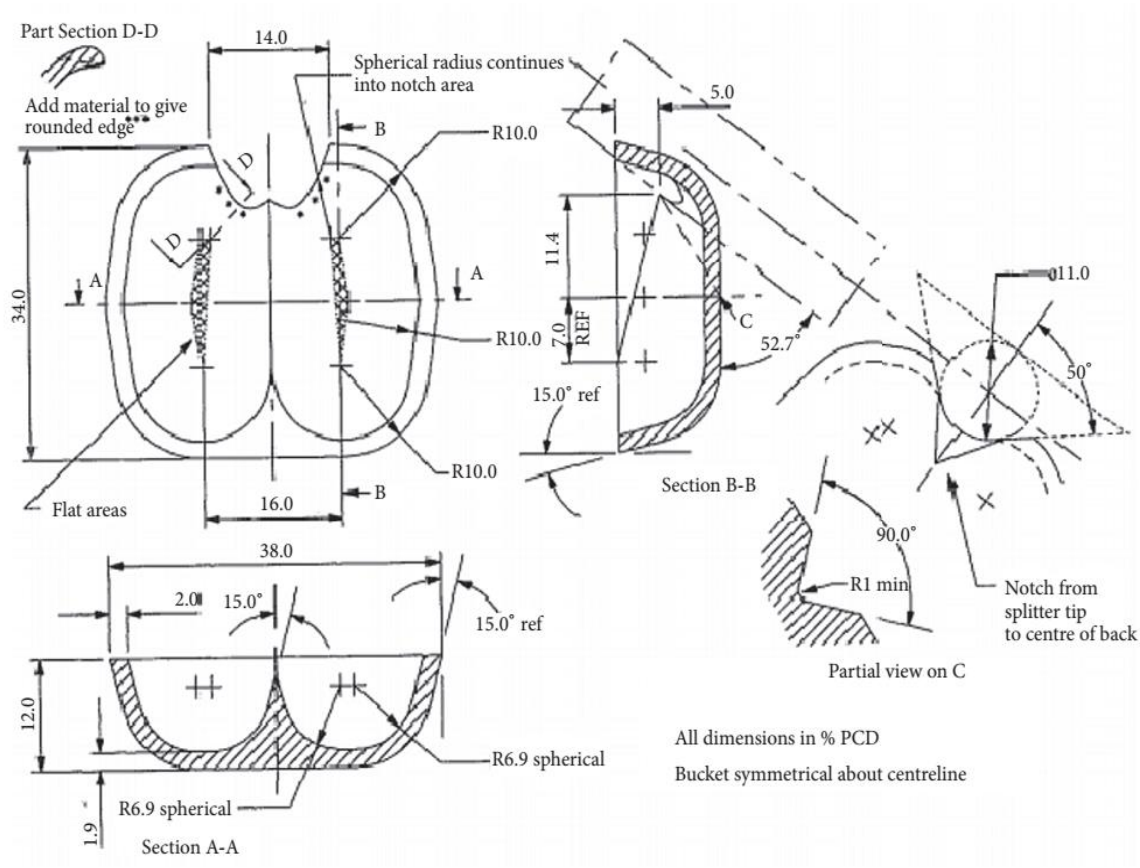

Figure 3.9: A scalable Pelton bucket. All dimensions are in % of PCD [Jeremy 2000].

The bucket stem is not shown in Fig. 3.9, because this can vary; the shape of stem depends on the way the buckets are fixed to the hub. A basic stem for machining, used for bolting or clamping the buckets to the hub, is shown in Fig. 3.10. and is used in this research.

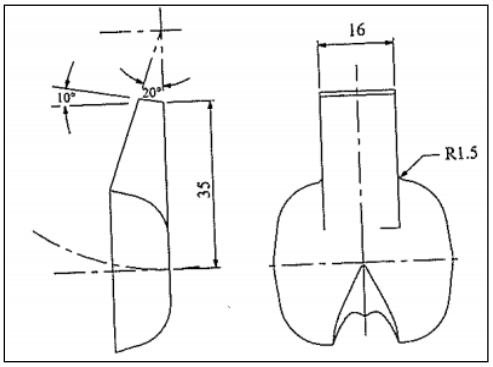

Figure 3.10: A basic bucket stem design for clamped or bolted fixing.
All dimensions are in %PCD [Jeremy 2000].

The dimensions of the bucket are decided based on empirical relations for 500mm PCD (see Table 3.5) which is used in this report as the baseline design case.

Table 3.5: Bucket Baseline dimensions

Parameters, Formula *[Jeremy 2000].*	Calculation	Dimensions
Height of bucket, h=0.34PCD	h=0.34×500	170 mm
Cavity Length: h_1 =5.6%PCD	h_1 = (0.056)×500	28 mm
Length to Impact Point: h_2=0.114PCD	h_2=0.114×500	57 mm
Width of bucket opening, a=0.14PCD	a=0.14×500	56 mm
Bucket-thickness: t_1=0.002 PCD	t_1=0.002×500	1 mm
Minimum number of bucket, z, suggested by Jermey book	-	18
Depth of the bucket, t=0.121 PCD	t=0.121×500	60.5 mm
Width of the bucket, b=0.38 PCD	b=0.38×500	190 mm
Distance between bucket and nozzle, X_{nb}=0.625PCD	0.625×500	312.5 mm

For the baseline bucket design used, the minimum number of bucket is 18, with each bucket 20^0 apart. There are different methods of fixing buckets to the rotor disk. The whole runner can be cast out as one piece. Alternatively, the bucket can be made as a separate item and bolted, clamped or welded to the hub.

As suggested in the [Jeremy 2000] book, single piece casting cannot be an option since it needs good foundry. Bolting buckets to the hub is another method to attach the bucket with the hub. Casting a single bucket is easier than casting the whole rotor. The safety is higher in case a bucket is broken not the whole rotor has to be replaced. For this reason, Bolted buckets are an ideal solution for this project and are chosen as discussed in [Jeremy 2000].

The cast-iron-made buckets are mounted on the runner hub and their design details and geometrical dimensions are given in Table 3.4, and Table 3.5.

The bucket design was specified by defining its outline using the dimensions given in Fig. 3.9 and Table 3.5. The complete 3D geometry of the bucket was created in Solid Works using CATIA V5 software as shown in Fig.3.11.

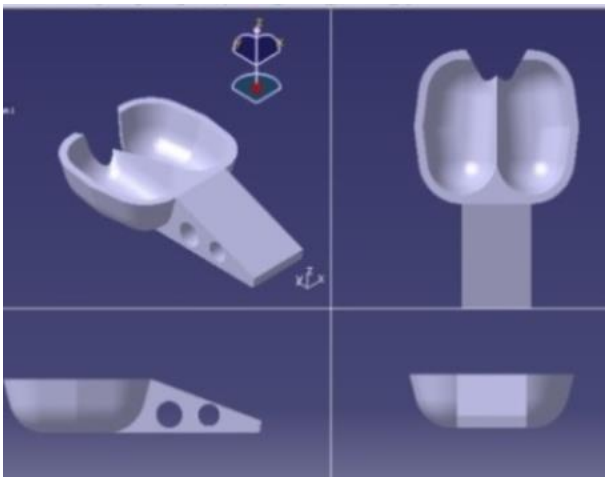

Figure 3.11: Solid model of Pelton Bucket for the selected site data.

For the single piece bucket model shown in Fig. 3.11, the basic runner model is adapted to form an entire bucket by the use of patterning. The runner size is determined by the pitch circle diameter. Two disc plates were used to mount the buckets circularly as shown in Fig.3.12. The discs were to sandwich the buckets into place.

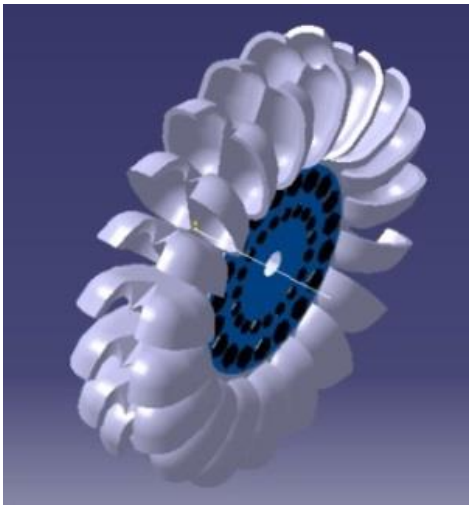

Figure 3.12: Three Dimensional View of the Runner.

3.7. Design of the Remaining Parts of Pelton Turbine

The design of shaft, distributor, nozzle, casing and other components of Pelton Turbine are based on straight forward calculations. This has been done and is found in Appendix A.

(Please refer to Appendix E for the manufacturing/Technical drawing of the optimized design turbine Parts).

CHAPTER 4

PERFORMANCE ANALYSIS OF THE BASELINE DESIGN TURBINE BY CFD

For the selected Melkey Herra's micro hydro power site in Ethiopia, Pelton turbine is the most suitable. Therefore, the main dimensions of the turbine examined here correspond to this ideal plant as designed in chapter 3. CFD simulations are likely considered in this chapter as an available way for investigating the performance of the baseline turbine, in order to reveal the possibility of optimization for the next chapter. This chapter also describes assumptions and methods used for CFD analysis and optimization of scaled model Pelton turbine using ANSYS CFX software.

4.1. Physical Assumptions and Scaling Down

Even a supercomputer does not have enough power to simulate every single aspect of a complex fluid flow problem. Approximations would have to be made. This does not mean that the solution will be inaccurate, sometimes a problem does not have 3D effects or is not time dependent.

The computational domain here was created after removing the features that were assumed to have no or minor effect when comparing the runner designs as follows:

No Casing: modeling the Pelton turbine without casing, similar methods can be found in the literatures *[Židonis, A.,2015, Amod Panthee 2014, Barstad, L. F., 2012]*.

Symmetry: To reduce computational cost, the buckets, nozzle and water-jet are cut in half at the symmetry axis , similar methods can be found in *[Židonis, A.,2015,* Amod Panthee 2014, Barstad, L. F., 2012*]*.

Single Jet: Modeling of only the single jet operation was found in most of the publications reviewed in the literature section *[Židonis, A.,2015, Amod Panthee 2014, Barstad, L. F., 2012],* so we adopted the same approach.

No Hub: The flow will not be interacting with any other part of the runner except for the bucket. Hence, there is no need to include the hub into the CFD model, as suggested in the literatures *[Židonis, A.,2015, Amod Panthee 2014and 13, Barstad, L. F., 2012]*.

Periodic Torque: 3 buckets are enough to recreate the complete runner torque and are used also in this research *[Židonis, A.,2015, Amod Panthee 2014, Barstad, L. F., 2012].*

Scaling down: A model test is a good tool when predicting the performance of the actual turbine, and is beneficial due to the lower production cost of the model because of the smaller size.

Scaling down of the prototype in Computational Analysis is also important to reduce the time consumption and to ease the computational processing in normal computers. On the basis of the above considerations, the scaling factor of 0.53 was used to meet the minimum bucket width standard for model testing. This is based on the international standard IEC 60193 of the International Electro technical Commission which applies to laboratory testing of model turbines *[Amod Panthee 2014].* In this standard, the factor greater than 0.28 was found to satisfy IEC 60193 criteria for Pelton turbines.

Eq.4.1, 4.2 and 4.3 represent head coefficient, flow coefficient and power coefficient for model studies *[Amod Panthee 2014].* In order to achieve similarity between model and prototype behavior, all the corresponding terms must be equated between model and prototype.

$$\left(\frac{H}{D^2 N^2}\right)_{prototype} = \left(\frac{H}{D^2 N^2}\right)_{model} \quad [4.1]$$

$$\left(\frac{Q}{ND^3}\right)_{prototype} = \left(\frac{P}{ND^3}\right)_{model} \quad [4.2]$$

$$\left(\frac{P}{D^5 N^3}\right)_{prototype} = \left(\frac{P}{D^5 N^3}\right)_{model} \quad [4.3]$$

Table 4.1 shows the values for prototype and model with the same speed of 520 rpm.

Table 4.1: Turbine geometry and set up values for prototype and model for the case of baseline design (PCD=500mm).

Parameters	Symbol	Unit	Prototypes' Values	Selected Model operating condition
Flow rate	Q	Lts/s	140	20.84
Head	H	m	47.5	13.34
PCD	D	mm	500	265
Bucket width	B	mm	190	100.7>80mm
Turbine Power	P	kW	51.2	2.14
Number of Bucket	Z		**18**	**18**
Number of jets	n_{jet}	-	**2**	**1**

4.2. Computational Domain Creation

This section describes the methods and models used for conducting the research studies presented in this research. Fig. 4.1 depicts the completed CAD drawings of the rotating and stationary domain which is modeled separately and assembled here to show their relative initial positions.

Stationary domain contains half a cylinder for the inlet and a ring to accommodate an interface between the two domains. Imagine that the rotating domain is aligned with the

stationary domain. When the rotating domain leaves this position, another identical domain is introduced at the top (the same geometry). Thus, one achieves a continuous simulation of a runner [Barstad, L. F., 2012].

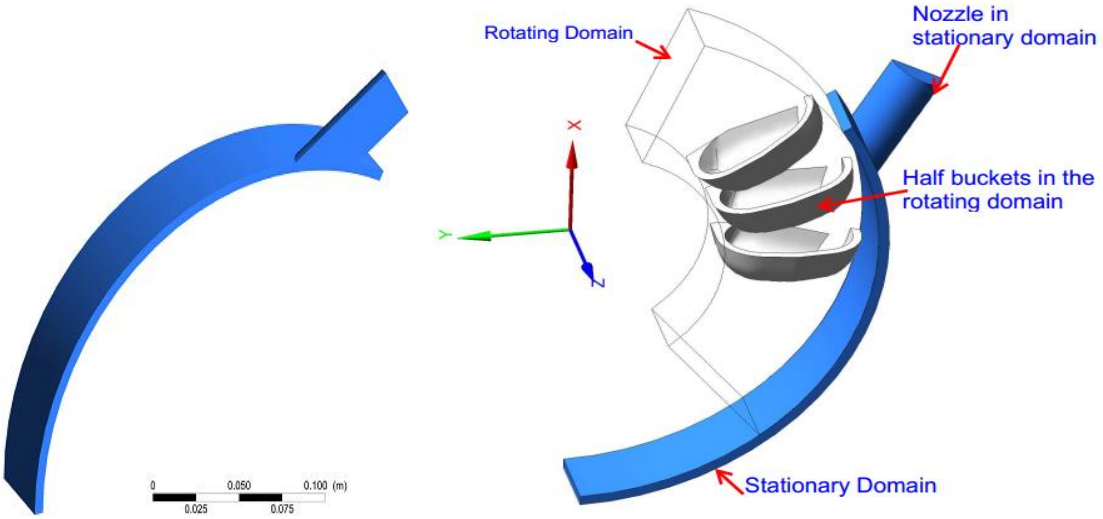

Figure 4.1: Domain geometries: Stationary (left), Assembly of the rotating and stationary domain (right).

4.3. Meshing

As suggested in the literature [Amod Panthee 2014, Barstad, L. F., 2012], unstructured tetrahedral elements were used for the rotating domain meshing because of more complex geometry to be captured by the mesh and also to allow automatic meshing for all the upcoming geometry modifications.

Fig. 4.2 shows both stationary and rotating domains meshed as they are imported into CFX-Pre.

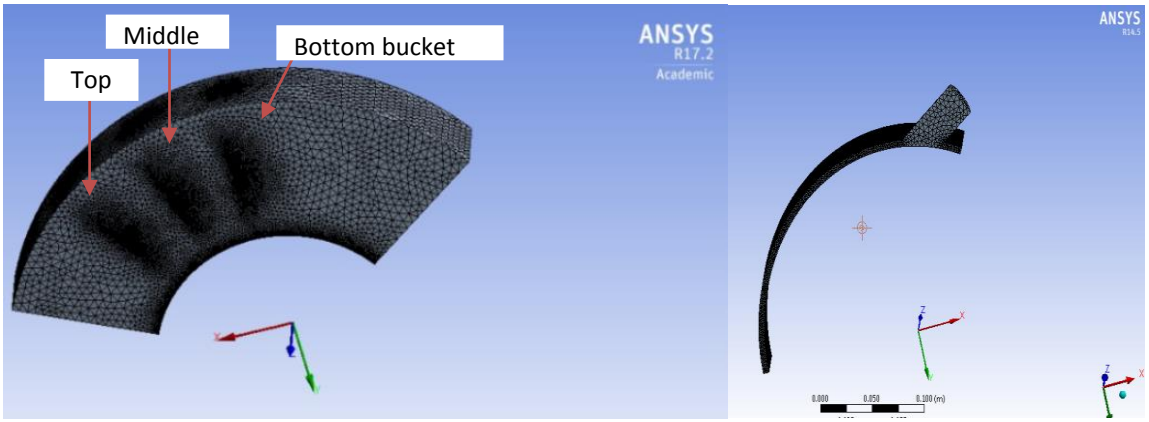

Figure 4.2: Meshed rotating (left) and stationary domain (right):sizing and inflations applied.

4.4. Physical Setup with Ansys Pre-Processing

In this section the essentials of the ANSYS Pre setup are presented.

Analysis Type: In each "Flow Analysis" in ANSYS Pre there is a tab called "Analysis Type".

This is where one defines whether or not the simulation is transient or steady-state, control simulation time and time steps. In this case the transient option was chosen.

Time steps are interval for which CFX solver calculates flow parameters in transient analysis. The time step used for the analysis was 1/20 total time, which corresponds to 0.001714 sec to capture 20 time frames per rotation.

Multiphase Model: The flow through the penstock pipe is having only single phase for the fluid. As the water jet comes out of the nozzle, it is open to the atmosphere and the effect of free water jet may be important. This flow passes through runner buckets, and it will be a free surface flow. This free surface flow glides through internal surface of the buckets and the momentum transfer takes place. The flow leaving the runner bucket will be converted into dispersed water droplets as the fluid leaves contact from the buckets. This way the flow through the Pelton turbine is multi-phase in nature [Amod Panthee 2014, Barstad,L.F.,2012]. Hence, to capture the flow accurately, homogenous multi-phase analysis is performed in this research.

Volume fraction of water: As suggested by the literature [Židonis, A.,2015], the volume fraction of water should change from 0 to 1. In each control cell, the volume fractions of the water and air sum to 1, $\alpha_w+\alpha_g=1$. Then $\alpha_w=0$ denotes cells filled with air while $\alpha_w=1$ denotes cells filled with water and $0<\alpha_i<1$ denotes that the cell contains an interface between the water and air.

In the beginning of the simulation both domains are full of air with 0 m/s velocity. Therefore, the given initial conditions are 0 m/s velocity and 0 Pa for Relative pressure. Initial Water volume fraction is 0 and initial Air volume fraction is 1.

Turbulence model: Shear Stress Turbulence (SST) model is able to capture turbulent scales in flow in high shear stress regions [Amod Panthee 2014, Židonis, A.,2015]. So SST model is chosen for further simulations.

Domain Interface: The interface type between the stationary and rotating domains was Fluid-Fluid *[Amod Panthee 2014].* Interface model for this type was General Connection and the Transient Rotor Stator option was selected for Frame Change/Mixing Model. Pitch ratio was maintained to value 1 between domain interfaces by maintaining equal area in interface region. To apply a rotation to the rotating domain, domain motion in the rotating domain was set to Rotating, and Angular Velocity was defined by the expression "Omega". In this case the angular velocity is negative because the domain was modeled to rotate in the negative rotation direction about the z-axis. This method is also found in the literatures.

Boundary Condition in Rotating Domain: This section contains a list of boundaries and their

conditions. No boundary for outlet is defined in the rotating domain. Rather, opening type boundary condition has been defined. The bucket surface is defined by wall type boundary condition, and an interface type boundary condition at interface between the rotating and stationary domain.

All other remaining boundaries are defined as opening type since it is unpredictable about the actual outlet and flow pattern of fluid through the runner (see Fig. 4.3).

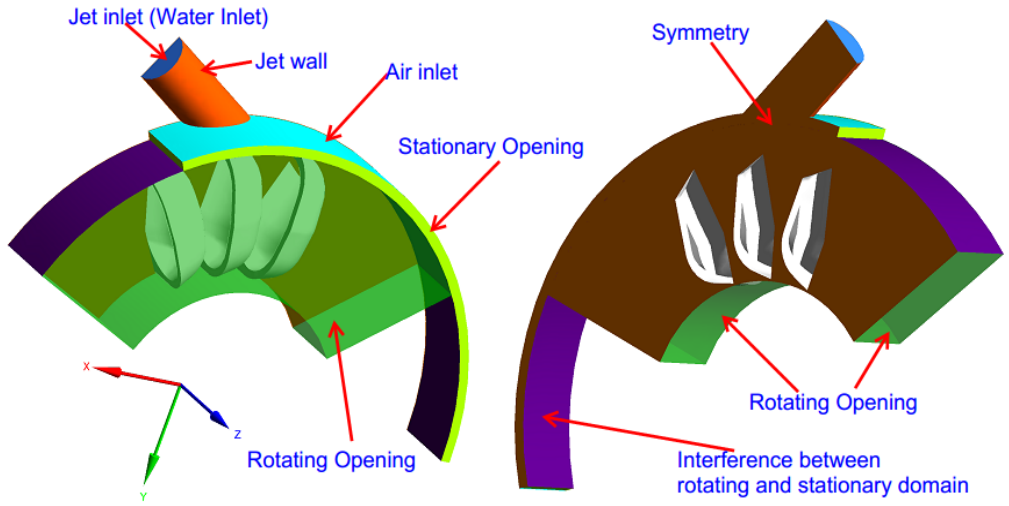

Figure 4.3: Boundaries Applied on the domains.

Solver Control and Output: The chosen advection scheme was High Resolution as according to the CFX Modeling Guide. This gives a good compromise between robustness and accuracy. Second Order Backward Euler option was selected for the Transient Scheme as it is generally recommended for most transient runs in CFX *[Židonis, A.,2015, Barstad, L. F., 2012].*

Monitor Points: The main output of the simulation is the total torque on the middle bucket. A monitor for the expression "**Torque on Middle Bucket Wall**" was added, which logged the torque and made it possible to monitor the torque during the simulation.

The calculated Torque data on the middle bucket was extracted from the simulation using an inbuilt torque function applied to the Named Selections created for the regions for the middle bucket. This function is then plotted as a Monitor Point while the simulation runs, allowing the calculated torque at each time step to be exported.

Expressions: Defining expressions is a good way of streamlining a CFD case. The following expressions in Table 4.2 are used in the setup. This way of defining expressions can be also found in the literatures *[Barstad, L. F., 2012]*.

Table 4.2: Expressions defined in ANSYS Pre for the baseline design.

Name	Expression	Description
Gravity	9.82[ms^-2]	Acceleration due to gravity
Head	13.34[m]	Model Head based on scaling
Turbine radius	132.5[mm]	Model Turbine radius
Inlet Velocity	(2×Gravity×Head)^0.5[m/s]	Water velocity at the nozzle inlet
Omega	Inlet velocity/(2xTurbine radius) [rad/s]	Angular velocity: rotation in the negative direction is selected.
Torque Middle Bucket Wall	Torque_z@Middel Bucket Wall	The entire middle bucket is selected
Total Time	((120xpi)/180)/Omega	Total simulation running time

4.5. Mesh Independency Study

In order to determine the minimum grid size or mesh resolution required to resolve the boundary layer and the mean flow features, a grid independence study was conducted. This allows minimization of errors and uncertainties in the predicted results.

Therefore, grid convergence analysis has been carried out by monitoring torque as a parameter of significant interest. This is done in order to get a solution that does not vary significantly even when we refine our mesh further.

Eight different mesh sizes were tested with an effective head of 47.5m. The mesh size on the rotating domain is controlled by element size. The relevance was increased for finer mesh. Afterwards, for each mesh developed, the orthogonal quality of the mesh have been checked and it was in an acceptable range (0.15-1.00). Each mesh also created with the same physical setup and boundary conditions as stated in section 4.4.

During the simulations, results obtained were directly dependent on the accuracy in quality of mesh. And it was performed while analyzing the torque variation by developing the SST turbulence model.

Table 4.3 indicates the grid information, the calculated torque, the standard torque and the resulting modeled runner efficiency for the baseline design (PCD=500mm). The standard torque was calculated with the power obtained from power coefficient and the angular velocity of runner for comparison.

To calculate the efficiency, power input has to be calculated as well which for a complete turbine is calculated using two variables describing the flow conditions: the net pressure head and the flow rate [Barstad, L. F., 2012, Amod Panthee 2014, Židonis, A.,2015].

$$P_{input}=\rho g Q H_{net} \quad [4.4]$$

$$P_{out}=\frac{2\times\Pi\times N\times T}{60} \quad [4.5]$$

Therefore, runner efficiency in this model was calculated using Eq.4.6 as follows:

$$\eta=\frac{P_{output}}{P_{input}} \quad [4.6]$$

About 3.9 million elements were required to obtain mesh independent result, for PCD=500mm (Table 4.3). One can also observe, a finer mesh gives a solution of a little higher accuracy than required but at the expense of computational power and time.

Table 4.3: Mesh dependent test analyzed for PCD=500mm.

Mesh type	M1	M2	M3	M4	M5	M6	M7	M8
Total no, elements	294952	520687	2011665	2239650	2398044	2861243	3955723	5050204
Calculated total Torque (Nm)	-30.93	-32.20	-34.32	-34.50	-34.69	-34.92	-35.02	-35.25
Standard Torque (Nm)	-35.06	-35.06	-35.06	-35.06	-35.06	-35.06	-35.06	-35.06
Torque Error percent (%)	11.8	8.2	2.1	1.6	1.1	0.4	0.1	0.5

The torque variation curves of the runner obtained using different density meshes are also presented in Fig. 4.4 and. It is seen that, torque increase is gradual and rate of increase is the same for all cases until it reaches a steady values of torque.

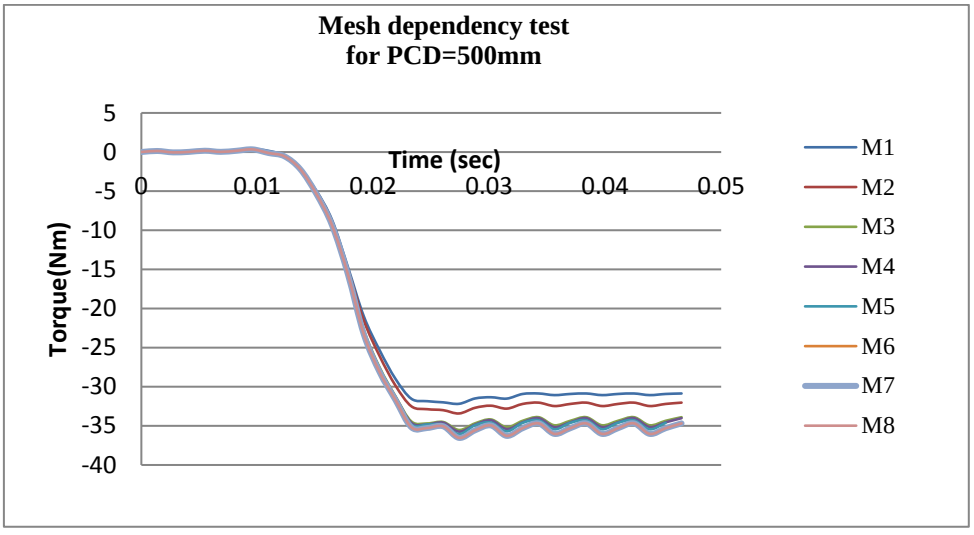

Figure 4.4: Total Torque variations for different mesh sizes for PCD=500mm.

4.6. CFD Result and Discussion

3D-Streamlines of velocity and pressure contours starting from inlet of the nozzle can be seen in all the domains. These were obtained using insert contour and insert streamline commands of menu bar in ANSYS CFX-Post.

4.6.1. 3D-Streamlines of velocity contours in the runner

A visualization of the flow in the baseline design of turbine buckets, starting from the nozzle can be seen in Fig. 4.5 and 4.6 below at different time steps.

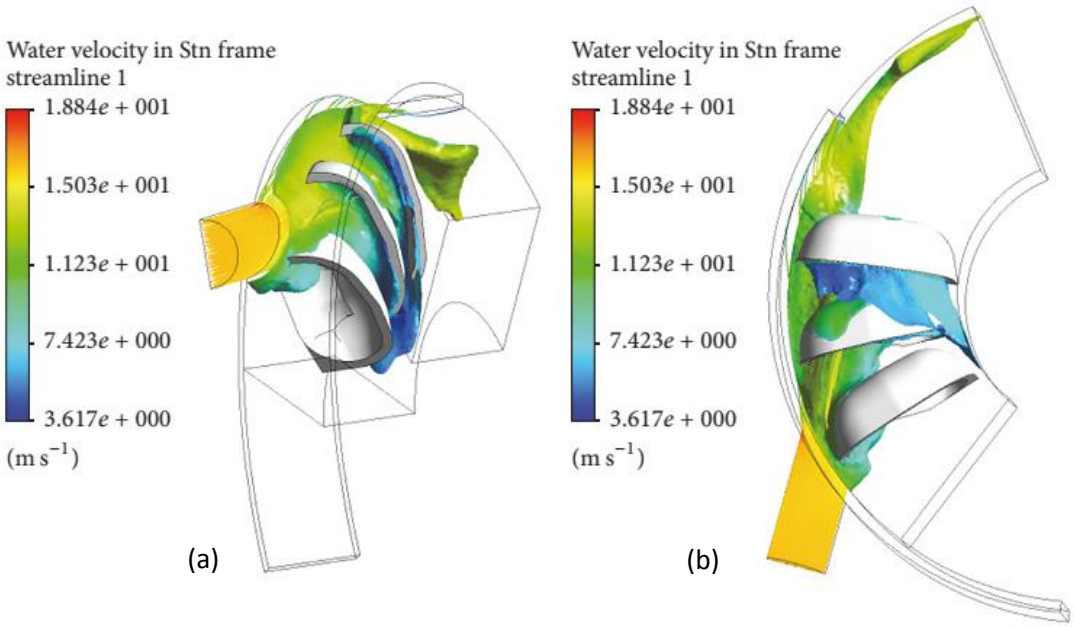

Figure 4.5: Flow visualization of the baseline design, (a). face views,(b). Side views (PCD=500mm).

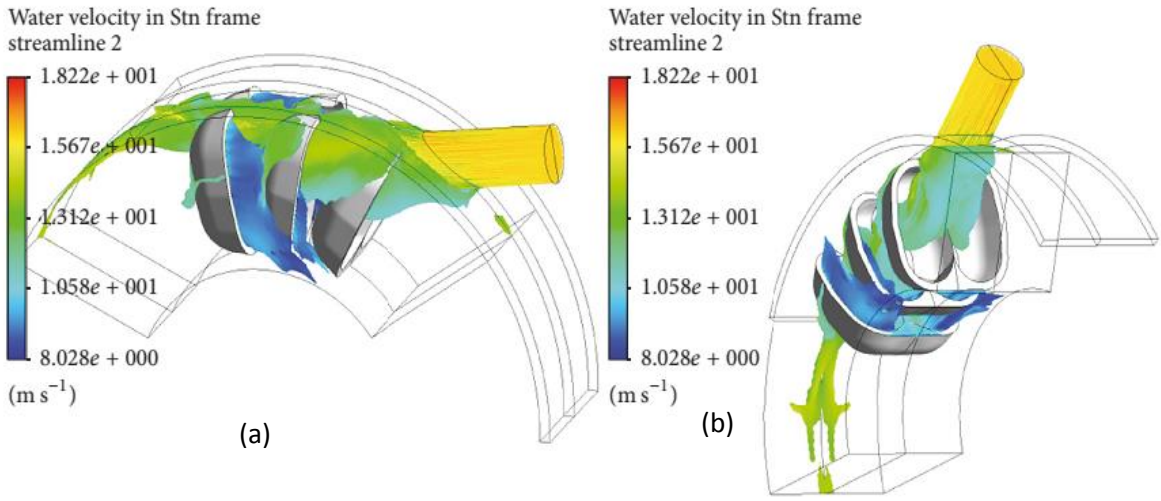

Figure 4.6: Water velocity in stn frame, (a). face views,(b). Side views (PCD=500mm).

Only very small amount of "leaked" water is present next to the bottom bucket with low jet

velocity. These visualizations give good information about the flow pattern. The jet water that came from the nozzle, entered into the runner, hitting the buckets and dividing the jet into three portions. The first portion from the bottom of the jet, touched the outside and inside of the top bucket that is close to the nozzle. The second portion of the jet was the one from the middle, which hit the next middle bucket. Finally, the rest portion of the jet crossed into the latter bucket.

On the face and side view the figures, one can observe also the part of the flow escaping from the cutout of the bucket as well as the lateral sheet flow.

4.6.2. Pressure contours on the surface of the buckets

Next, Pressure contours on the surface of the buckets can be observed as follows.

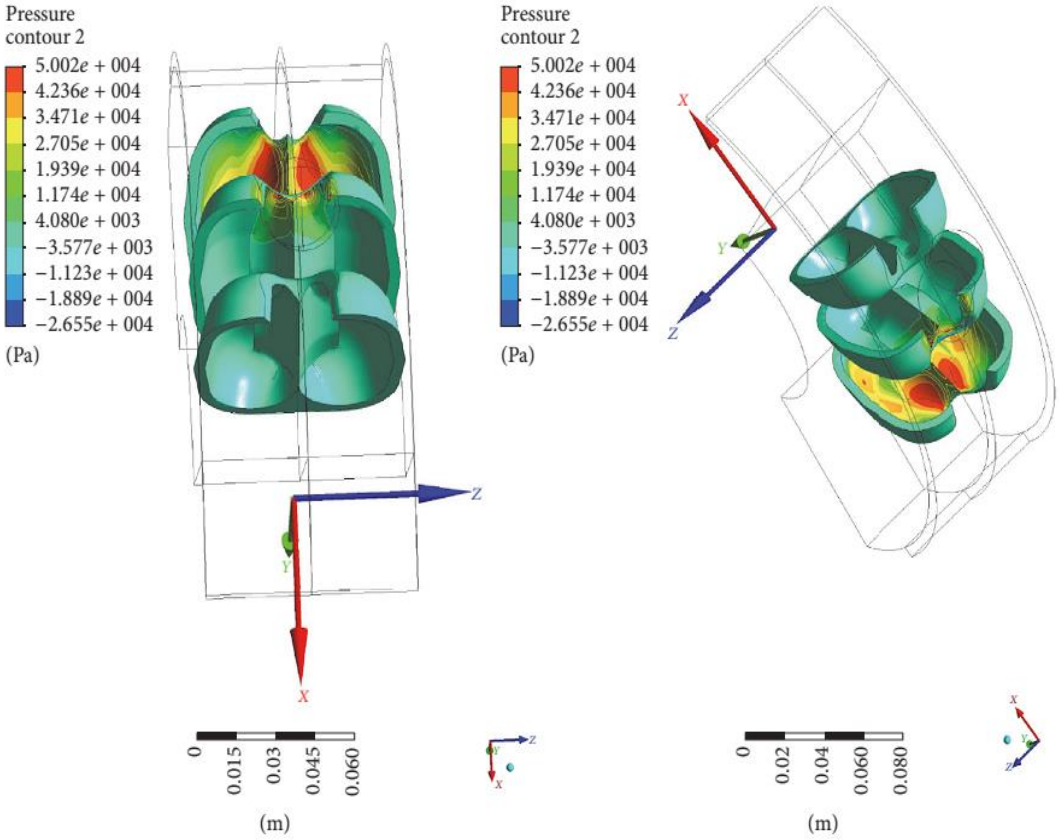

Figure 4.7: Pressure contours on the bucket (PCD=500mm).

It can be observed on Fig. 4.7 that, the maximum pressure point, in red, corresponding to the PCD of the bottom bucket and the tip of the middle bucket which is aligned with the axis of the impinging jet. Similar finding was observed by Amod Panthee (2014).

CHAPTER 5
DESIGN OPTIMIZATION CONSIDERING MANUFACTURABILITY

A baseline (initial Pelton bucket geometrical design), where key design parameters easily can be changed or manipulated, has been done in chapter 3 and numerically tested in chapter 4. This chapter describes the optimization process and the obtained improvement in performance using CFD and finally, the obtained hydraulically optimized geometry of the bucket is further checked for structural safety (strength), to generate solutions to fulfill requirements for manufacturability. In fact, the purpose of CFD is not to make decisions directly, it works in conjunction with experiments and experience in next chapter. Based on the result obtained in chapter 4, this study planned a modification on the baseline design of the bucket which consist of the following new designs being tested:

- Investigate the effect of change in PCD of the runner on the performance of the turbine.
- Changing the length, depth, angular position (Jet bucket interaction) and number of the bucket while keeping all other parameters constant.
- redefining the shape of the lip curve to reduce the leakage.

This way bucket shape proportions with the size of PCD were controlled.

The results, presented at the end of this section, are used to provide insight into the benefit of Pelton design optimization for lowering the manufacturing cost.

5.1. Effect of variation in pitch circle diameter (PCD) of the runner.

The next-generation turbine designs for small-scale hydropower systems seek higher efficiency and low manufacturing costs. The size of Pelton turbine (PCD) is an important parameter to lower the manufacturing cost of a Pelton turbine runner. However, no consistent guidance based on numerical research data is available in the public domain.

This section provides an example of how the size of turbine (PCD) can affect the efficiency of the turbine using CFD simulation. One of the objective was to understand how the turbine performance will change when the flow field is perturbed by reducing the size of turbine from PCD is equal to (500mm) to (400mm) for the same operating condition (i.e. flow rate, head).

This will help to reveal the possibility of optimization by keeping the PCD constant (PCD=400mm).

A detailed explanation of CFD methodology, computational domain creation, assumptions, and setup for Pelton Turbine performance analysis is included in Chapter 4, therefore, it is not repeated here.

5.1.1. Turbine Geometry Modeling For PCD=400mm

The dimensions of the bucket based on empirical relations for PCD=400mm are shown in Table 5.1. Set up values for prototype and model for this case are shown in Table 5.2.

Table 5.1: Physical bucket dimensions:

Parameters, Formula	**Calculation**	**Dimensions**
Height of bucket, h=0.34D	h=0.34×400	136 mm
Cavity Length: h_1= 5.6%D	h_1 = (0.056)×400	22.4 mm
Length to Impact Point: h_2= 0.114D	h_2=0.114×400	45.6 mm
Width of bucket opening, a=0.14D	a=0.14×400	56 mm
Bucket-thickness: t_1=0.002D	t_1=0.002×400	0.8 mm
Approximate number of bucket, z	Z=D/2d+15	18
Depth of the bucket, t=0.121D	t=0.121×400	48.4 mm
Width of the bucket, b=0.38D	b=0.38×400	152 mm

Table 5.2: Turbine geometry and set up values,

Parameters	**Symbol**	**Unit**	**Prototypes' Values**	**Selected Model operating condition for CFD Analysis, Scale Factor=0.53**
Flow rate	Q	Lts/s	140	20.84
Head	H	m	47.5	13.34
PCD	D	mm	400	212
Bucket width	B	mm	152	80.56>80mm
Turbine Power	P	kW	51.2	2.14
Number of Bucket	Z		**18**	**18**
Number of jets	n_{jet}	-	**2**	**1**
Turbine speed	N	rpm	**650**	**650**

5.1.2. Mesh Independency Study

Similar to section 4.5, mesh independency study was carried out for PCD=400mm in order to get a solution that does not vary significantly. The summary of meshing data for eight different mesh has been described in Table 5.3.

Table 5.3: Mesh dependent test analyzed for PCD=400mm.

Mesh type	M1	M2	M3	M4	M5	M6	M7	M8
Total no, Elements	128251	128546	130961	2321026	3019180	4052422	4771226	6855793
Calculated total Torque (Nm)	-18.13	-18.15	-18.29	-21.84	-22.15	-22.27	-22.37	-22.41
Standard Torque (Nm)	-28.05	-28.05	-28.05	-28.05	-28.05	-28.05	-28.05	-28.05
Torque Error percent (%)	35.4	35.3	34.8	22.1	21.0	20.6	20.2	20.1

A total number of 6.8 million mesh elements were required to obtain mesh independent results for the Torque output. A solution was considered grid independent for less than 0.3

difference in the Torque output between three different consecutive mesh sizes. It appears that no significant enhancement is to be expected from a further refinement of the mesh.

Therefore, as seen from the results, a relative error of 20.1%, between the CFD and the analytical data, was found for turbine with PCD=400mm and 0.1% relative error for the baseline turbine (PCD=500mm) at the design-point operating condition (Q =0.14m^3/s and H=47.5m). Hence, high value of relative Torque error indicates that, as there are losses in the reduced size of the turbine, influencing the efficiency characteristics.

The next section will be focused on observing the flow behavior in order to identify the reason for these losses which help to modify the baseline design to get an optimal design geometry.

5.1.3. Water Velocity Contour Plot in the Runner

As seen in Fig. 5.1, when the PCD is reduced to 400mm, a large amount of water does not leave the buckets. However, there is a small amount of the flow that leaves through the cutout with high velocity without being utilized (cutout leakage). This means, the cutout is too wide when the PCD of the turbine is reduced to 400mm. This phenomenon has to be reduced during the optimization stage.

However, it is clearly seen that, as the water starts entering into the top bucket, the inner surface of the middle and bottom bucket will still have some water volume fraction inside it. It means that for a particular instance of time and runner rotation, more than one runner buckets have water volume fraction.

The amount of the water flow touching the runner bucket sides and back surface of the bucket (backwash) is also visible. This water fraction at the back side and side surface of the bucket will impart some force to the buckets and if this fraction is high then the intensity of force on the bucket will be higher and it will reduce the strength of the buckets *[Židonis, A.,2015].* Another effect of this is, the water is acting as a brake on the runner, rather than helping it to turn, and this gives a serious loss of power.

These energy losses occur when jet entering the bucket and providing some amount of counter-torque as the outer side of the bucket hits by the surface of the jet. This means, optimization of design parameters are required on the bucket geometry with PCD=400mm to decrease the energy losses.

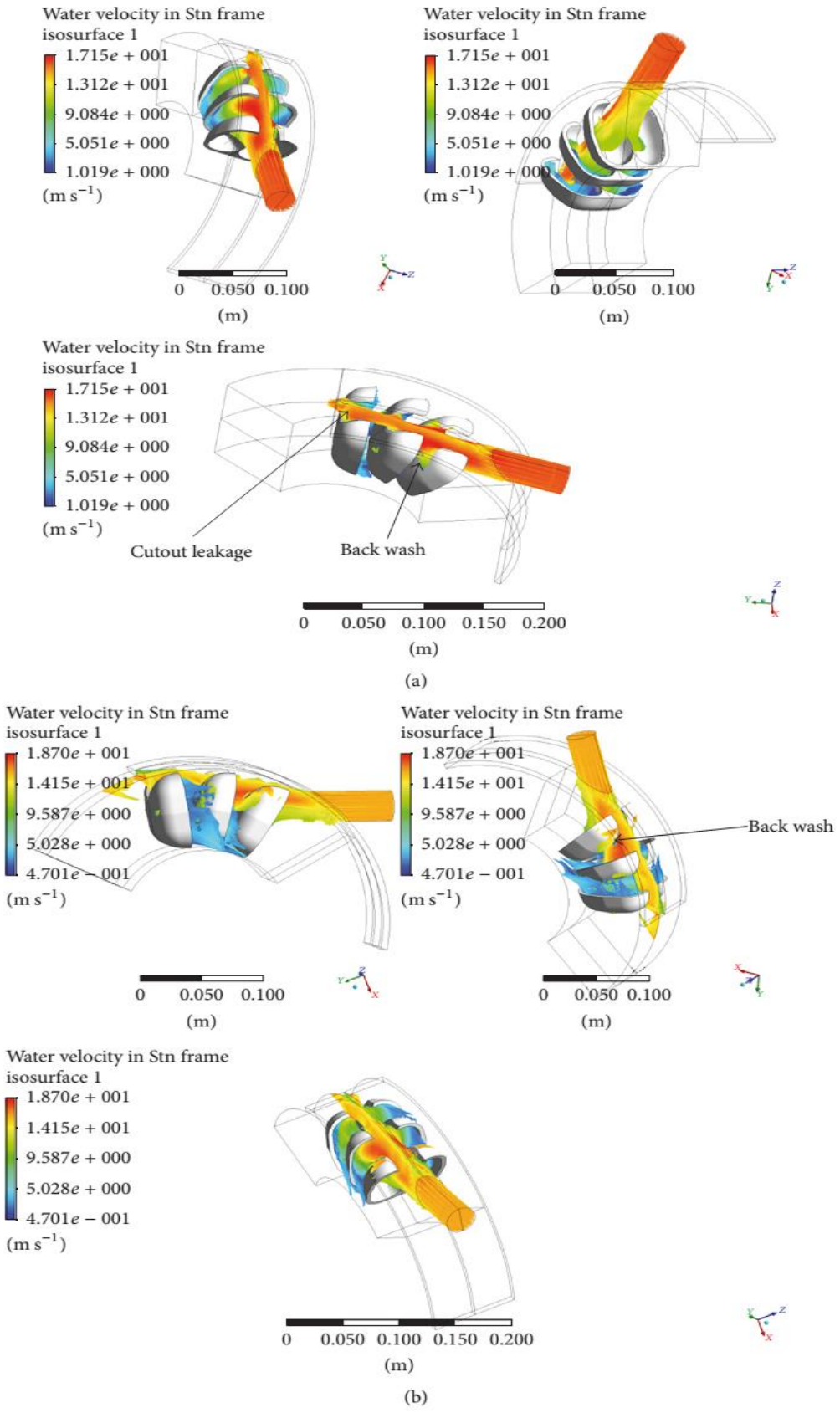

Figure 5.1: Water velocity in stn frame, (a). Side views , (b). face views for (PCD=400mm).

5.1.4. Volume Fraction of Water on the Surfaces of the Buckets

The red and blue regions show respectively water and air in the computational domain. In a more complex situation, the atmosphere also exerts pressure on the surface (water-vapor interface) [Židonis, A.,2015].

The water is also unevenly distributed across the buckets and there are several local accumulations of cells with a high volume fraction of water, most visible in the bottom bucket in Fig. 5.2. This volume of fraction of water will vary with time as the buckets rotate. This occurs when the portion of the jet is going to leave out completely from the bottom bucket and completely enters the next top and consquentive buckets.

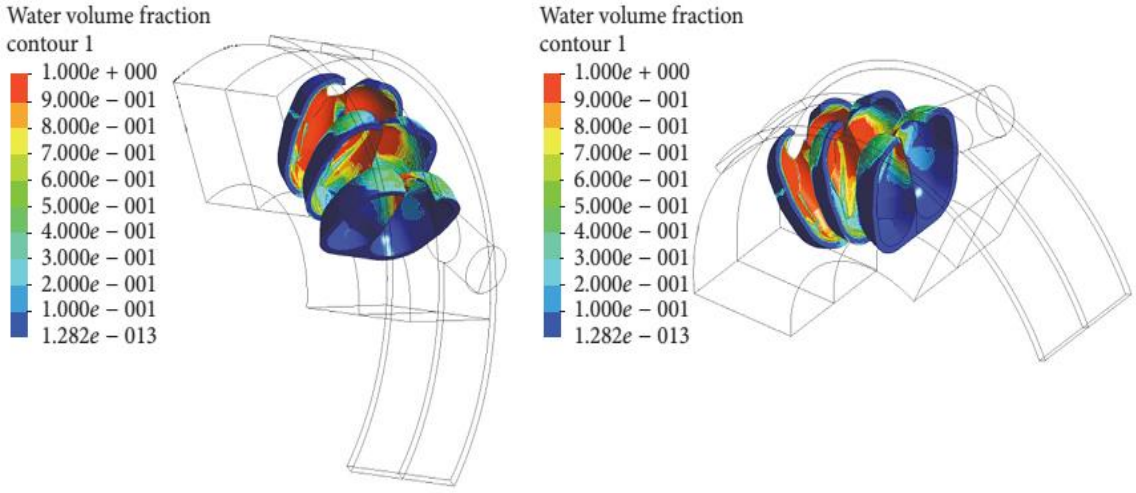

Figure 5.2: Volume fraction of water at a particular time step for (PCD=400mm).

5.1.5. Pressure Contours on the Surface of the Buckets

The pressure distribution in the bucket was due to impact of the jet. This pressure distribution applied on the bucket again varies with the time due to the rotation of the runner. It was found that the pressure peaks are obtained at bucket tip and PCD of the runner. The pressure peak in bucket tip is due to flow disturbance when jet strikes bucket tip.

It is obvious to obtain the pressure peak at the runner PCD since the Pelton runner are designed such that it would convert most of the hydraulic energy to mechanical energy when the jet strikes the runner PCD.

Result showed high pressure with the value of 3.559×10^4 Pa for the first top and the second middle bucket at some degree of rotation of the runner as shown in Fig.5.3. This pressure value is lower than the previous value when PCD=500mm.This might indicate that there is energy loss in the runner.

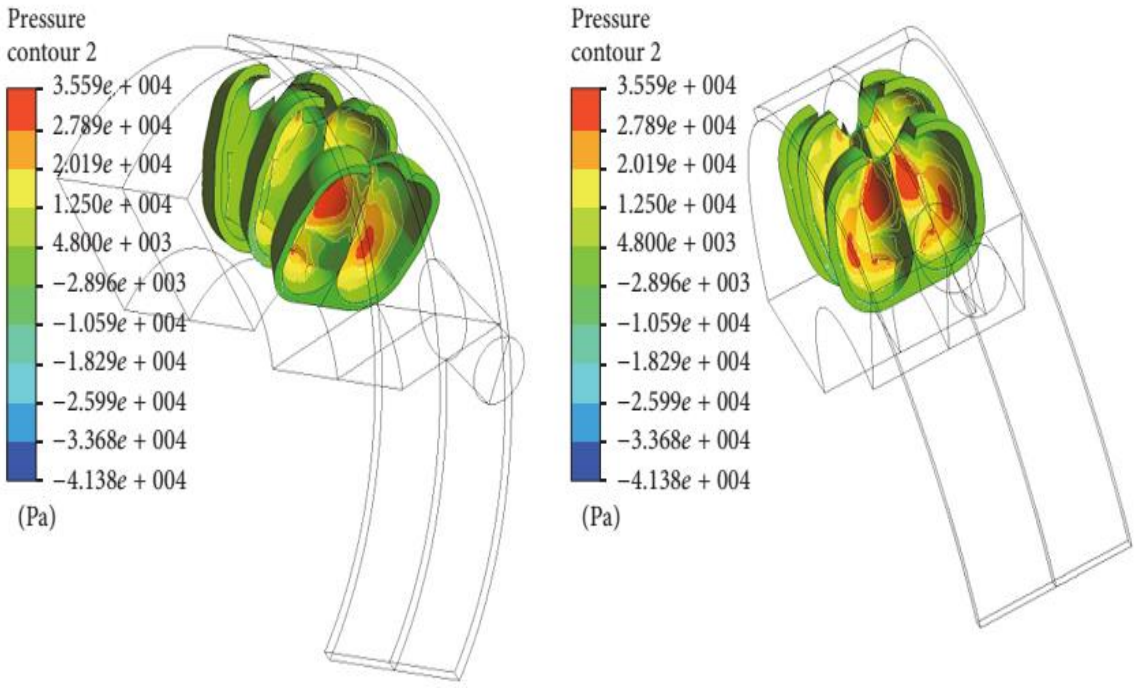

Figure 5.3: Pressure distribution at some degree of rotation of the reference bucket design (PCD=400mm).

The next step will be focused on approximation of the numerical torque.

5.1.6. Prediction of the Torque

Some indicative pictures from the turbine examined here show, how the energy transfer occurred in a single bucket for the two cases of PCD as illustrated in Fig. 5.4. The torque is increasing as more water interacts with the inner surface until the full jet interacts with the bucket to produce the maximum torque.

The shape of the torque curve is also similar to the previous studies by different authors [Barstad, L. F., 2012, Amod Panthee 2014, Židonis, A.,2015], but the irregularity of the curve in this area was attributed due to the Coanda effect and the impact of the back flow which create counter torque on the bucket and makes it slightly differ from the previous studies.

At the start or at the moment of impingement (jet cut in) and at the evacuation of the bucket (jet cut out) a counter torque can also be observed caused by the interaction of the jet with the back surface of the bucket. This value is larger for PCD=400mm, comparing to the baseline design (PCD=500mm).

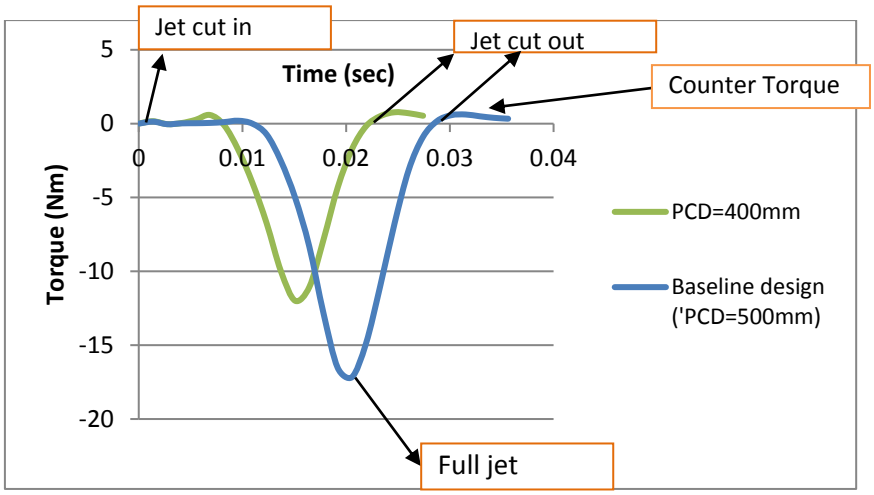

Figure 5.4: Torque generated by middle bucket vs. time.

The maximum torque produced by the baseline design (500mm) is larger than that of a reduced PCD (400mm). The above result shows also smaller turbine are faster than the larger one which is true.

Next, the total curves of the complex unsteady flow in the bucket for all the buckets analyzed can be acquired with the aid of time history views like the ones in Fig.5.5 and Fig.5.6 for both the above cases.

In this research paper**,** the torque generated by the middle bucket is replicated over time to determine total torque generated by Pelton turbine. This is done by assuming that at stable conditions every bucket is producing identical torque periodically. The replication was done till the summation graph gave steady values which occurs after three buckets covered by the water sheets at 0.03 sec of the rotation of the runner.

Since, the plot obtained was due to half nozzle and the maximum torque on the runner at a time is given by peak value multiplied by 4 as there are two nozzles in each unit. This runner torque has been taken for power output calculations by taking the average value from 0.03-0.05 sec of the runner rotation.

Methods of calculating the power output from a single bucket torque readings similar to described above are quite common and can be found in the literature **[Barstad, L. F., 2012, Amod Panthee 2014, Židonis, A.,2015].**

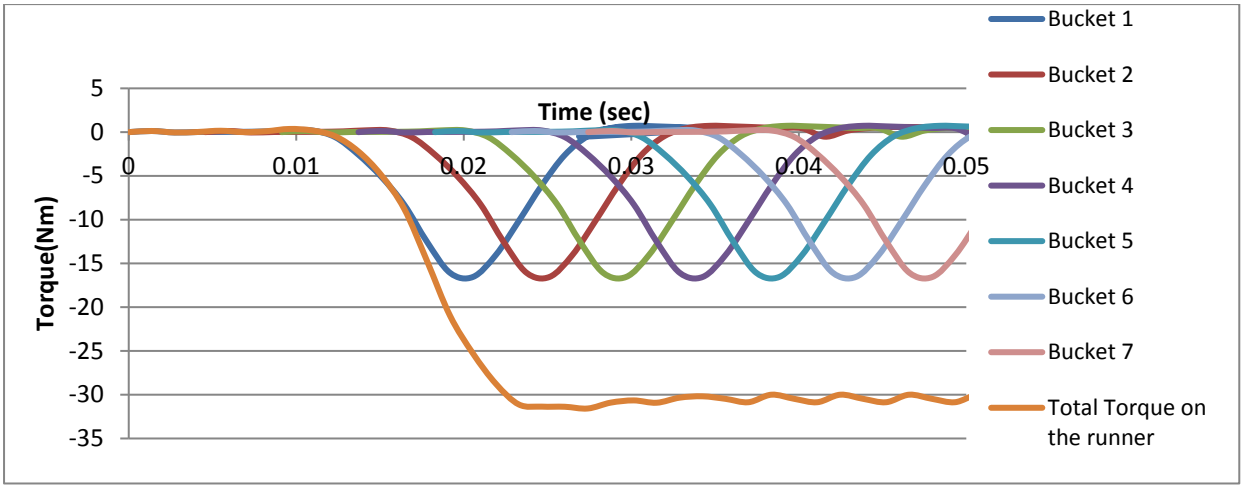

Figure 5.5:Total runner and buckets torque over time for (PCD=500mm) *at constant speed and head.*

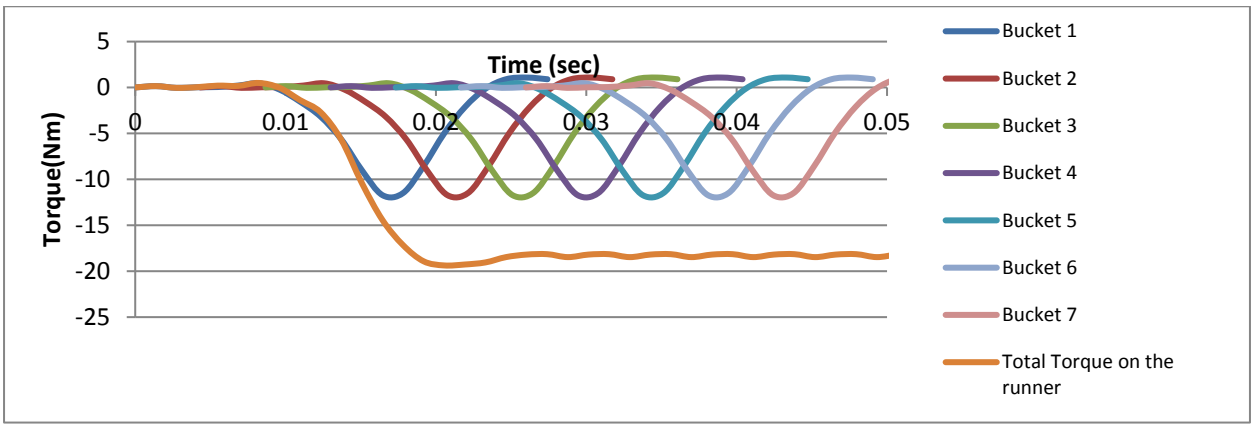

Figure 5.6: Total runner and buckets torque over time for (PCD=400mm) at constant speed and head.

5.1.7. Model Validation

In general rule, a small runner is cheaper to manufacture than the larger one. It takes less material to cast it. Additionally, the housing and associated components also can be smaller. For this reason, in this section consequences of reducing PCD from the baseline design (PCD=500mm) are evaluated and results are compared with that of published results.

The first turbine which is selected for verification of the CFD results has a maximum efficiency of 82.5%, which was studied by Amod Panthee et.al,(2014) for Khimti Hydropower in Nepal. The second turbine has also the same (PCD=400mm) but with a maximum efficiency of 86.7%, which was studied by A.Panagiotopoulos et.al, (2015) using a reference case correspond to a Pelton turbine installed in the LHT, at the National Technical University of Athens.

These were essential for the purpose of computational validation and performance characterization (see Table 5.4).

Table 5.4: Performance Validation of Pelton Runner Model.

Parameters	Unit	Baseline Design (PCD=500mm) Test Cases			Design Test Cases for PCD=400mm			Published Results	
								By Amod Pantee,2014	By Panagiotopoulos et.al 2015
Head	m	47.5	53.9	100	47.5	53.9	100	53.9	100
Flow rate	m^3/s	0.14	0.05	135%BEP	0.14	0.05	135%BEP	0.05	135%BEP
PCD	mm	500	500	500	400	400	400	400	400
Runner speed	Rpm	520	520	520	650	600	1000	600	1000
Number of bucket	-	18	18	18	18	22	22	22	22
Model Efficiency	%	78.8	83.5	84.6	62.6	66.1	71.6	82.5	86.7

The computational analysis results presented in Table 5.4 showed that the performance of the baseline's turbine design were very good and in agreement with the published results. But, it can be observed that from the different cases analyzed on the predicted hydraulic efficiency of the reduced size of the turbine are remarkably lower than that of the baseline design where for reduced size (PCD=400mm) the model runner's efficiencies are only 62.6%, 66.1% ,71.64%.

The flow visualization study of this research provide insights on the reasons for inefficiency for the reduced size of the turbine. The low efficiency in the reduced size of the turbine with PCD=400mm is mainly caused by a large amount of water leaving the bucket through the lip and hence transferring not its energy to the shaft. The problem was therefore, the choice of the runner P CD, that could give the best advantages in terms of efficiency.

For example, the post processing visualization of the baseline design (refere back to Fig.4.6) is able to qualitatively show that the reason for the better performance for the case of baseline design, which may be explained by less cut-out leakage and a more optimal bucket design for its intended use.

Moreover, it is observed that for flow rate and number of bucket equal to $0.05m^3/s$, 22 respectively, more water is caught by the inner surface of the buckets. This could explain why the predicted efficiency increase rapidly for volume flow less than the design flow rate.

The lower efficiency of the model at off-design condition (PCD=400mm) is mainly due to a little backsplash (the breaking effect) on the bucket and the missing jet velocity (leakage flow rate) because of a non-optimized bucket design. As this phenomenon highlighted before, the qualitative view of Fig. 5.1 is reasonable for the lower efficiencies in the off-design cases.

Thus, the goal was left to compare flow visualization at these two conditions, using image post-processing, in order to explain the difference in runner performance. An explanation for the discrepancy is that, due to a decrease in PCD from the baseline design, would lead to high hydraulic losses, despite, it will result less value of manufacturing cost.

It is important to note that, the bucket shape used in the baseline design in this paper is based on [Jeremy 2000] book. It is, ''the design jet diameter is 11% of PCD" which will give a PCD of

approximately 500mm. Therefore, if we optimize/change the shape of this bucket for each cases analyzed above, the optimum results presented in both published results above and the reduced size of the turbine (PCD=400mm) might be different from this study.

In the next section, the design optimization of this turbine bucket will be made by keeping the PCD to be 400mm, to lower the manufacturing cost and improve efficiency of the runner.

Therefore, in the next step, it was decided to change the length, depth, angular position (Jet bucket interaction) and altering the surface close to the lip and redefining the shape of the lip curve to reduce the leakage, intern to reduce the energy loss.

5.2. Modification in the Baseline Design Geometry of Bucket.

Modifications of the bucket have been done in the literature, [Židonis Audrius, 2014, et.al]. To evaluate the effect of these modifications computational fluid dynamics (CFD) was applied. It was also observed that the coarse meshes slightly under predict the efficiency as compared to the fine mesh simulations. Furthermore, it was assumed that this under prediction is going to be constant when comparing small changes in geometry.

In agreement with the above facts, the coarse mesh simulations were chosen for design optimization in this research so as to reduce the computational cost. And these data should be normalized or standardized to bring all of the variables into proportion with one another. For example, if one variable is 100 times larger than another (on average), then the model may be better behaved if it is normalize/standardize.

Therefore, in this research four identifying parameters are used for the design optimization. Finally redefining the shape of the lip curve to reduce the leakage was carried out. These were found out to be an important philosophy behind the design of bucket profile. Each parameters are described below:

Inclination angle: The angular position describes at what angle the bucket is mounted on a runner as measured with respect to a radial line from axis of rotation. This parameter controls the position of the bucket. Therefore, it was decided to investigate the effect of variation of this parameter on the performance of the runner.

Bucket length to width ratio: The width is kept constant as it is related to the jet diameter which is acquired from the operational conditions. Therefore, the ratio is changed by varying the bucket length towards maximizing efficiency.

Bucket depth to width ratio: Again, the width is kept constant. Therefore, the ratio is changed by varying the bucket depth.

Number of Buckets: This parameter controls the positions of the buckets relative to the neighboring buckets, as the spacing angle decreases when the number of buckets is increased.

The basic dimensions were also required to be within the limits suggested in literature, while the exact proportions of the buckets vary considerably, Fig. 5.7 and Table 5.5 are taken as a guide [Adams,1999].

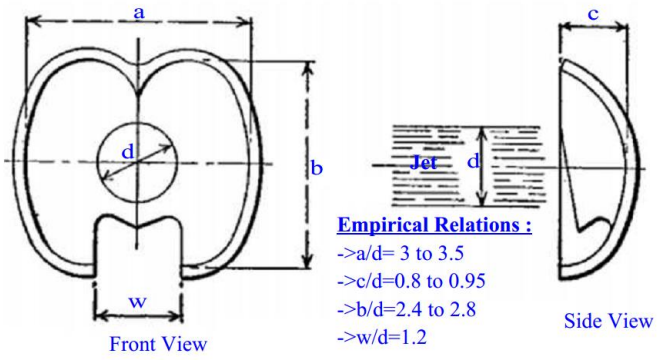

Figure 5.7: Empirical Relations for Bucket Geometry: (Source: Adams, 1999).

Table 5.5: Shape And Position Variation of the Baseline Bucket Design for Same Head and Flow Rate Conditions (PCD=400mm).

Design Parameters	**Unit**	**Symbol**	**Baseline Design values**	**Chosen Interval**	**Recommended Design ranges (Adams Harvey,1993)**
Inclination angle	Degree	θ	5	-20,-15,-10,-5, 0,5,10,15,20	-
bucket length	mm	b	0.34D	0.34D-0.39D	$2.4d_{jet}$-$2.8d_{jet}$
bucket depth	mm	c	0.12D	0.112D-0.133D	$0.8d_{jet}$-$0.95d_{jet}$
Number of bucket		Z	18	13 to 20	-

The simulation process for the optimization follow the following procedure:

- Change one parameter at a time from the baseline design value between intervals suggested in Table 5.5 while keeping the rest of the parameters constant.
- Create the corresponding geometry, mesh, physics setup and Run the simulation.
- Repeat the procedure until we get one final geometry that gives maximum efficiency.

Such a procedure is, more or less, the same as described in the next sections.

5.2.1. Optimization of Inclination Angle

Fig.5.8 provides a diagram showing the main dimensions of bucket positioning. The angular position describes at what angle the bucket is mounted on a runner and the splitter tip circle diameter describes the radial position of the bucket while keeping the pitch circle diameter and the radial distance fixed.

In order to find the best angular position, a minimum of 9 data points (Cases) are taken. Performing such study experimentally would be a costly and difficult process. This is one of

the advantage of CFD based design procedure as explained in the literature section of this paper.

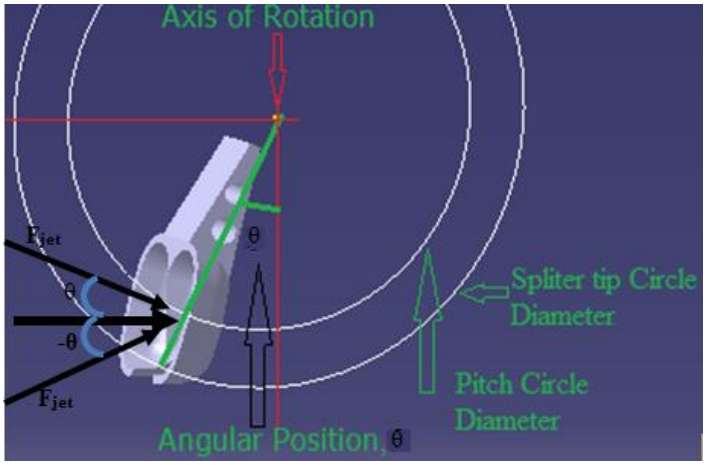

Figure 5.8: Parameters used for bucket positioning.

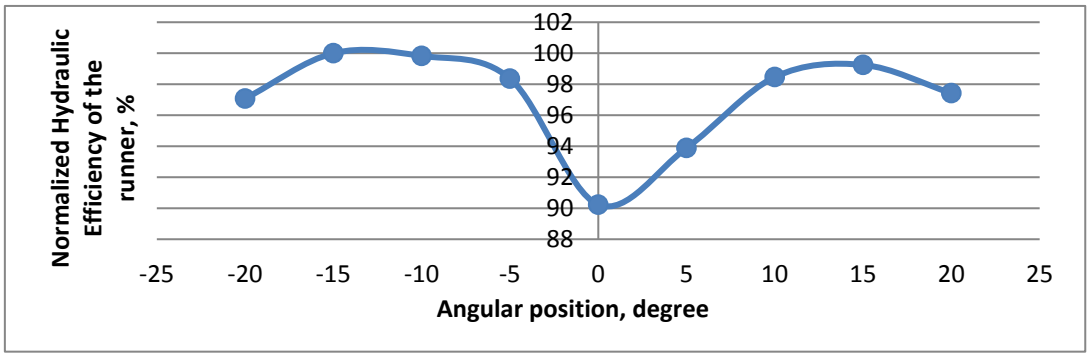

Figure 5.9: Normalized hydraulic efficiency vs. angular position of bucket for PCD=400mm.

The hydraulic efficiency (Fig.5.9) at 0 degree is the lowest compared to the other cases, this is because, there are energy losses associated with jet entering the bucket at 0 degree of angular position and providing some amount of counter-torque as the outer side of the bucket hits the surface of the jet. But, when the bucket is at -15^0 angular position, the maximum average torque can be developed. We take this value computed and then calculate the normalized hydraulic efficiency of the runner based on the maximum hydraulic efficiency achieved which is 66.6%. The procedure is terminated when the analysis cannot improve further the efficiency within a predetermined number of consecutive iterations.

5.2.2. Optimization of Bucket Length

By fixing the width, the angular position and the number of bucket at 152mm,-15^0 and 18 respectively and varying the length of the bucket, different cases analyzed as shown in Fig.5.10. The length of the bucket was changed significantly to understand the effects this would have. The PCD was kept the same (PCD=400mm) so also the number of buckets for the

turbine, the maximum volume of flow inside the bucket would not change. The length chosen to compare to the 136mm long initial geometry were 132mm, 144mm and 152mm. These were chosen to represent extreme values away from the baseline bucket design.

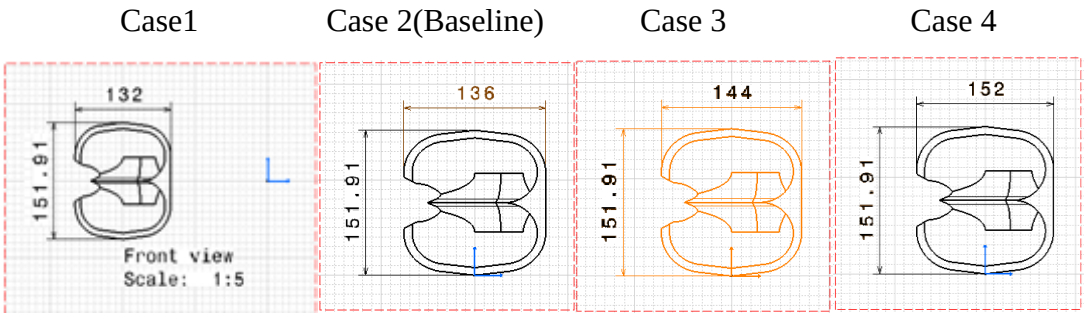

Figure 5.10: Variation of bucket length from the baseline value, dimensions in mm for PCD=400mm.

Taking, the average values of the torques at steady states for each cases separately and normalized with the maximum efficiency of the runner, it is found that, case 3 gives the optimum value as shown in Fig.5.11. The runner efficiency is found to increase by 0.4%.

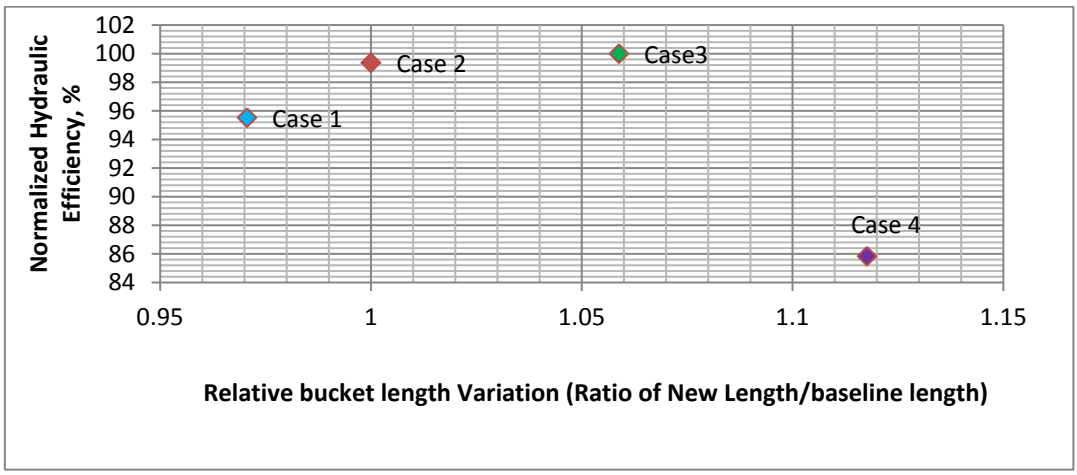

Figure 5.11: Effect of Variation of bucket length on performance of Pelton runner for PCD=400mm.

This study showed that although a greater length means the turbine is able to be in contact with the fluid for longer, potentially being able to extract more of the energy from the flow. However, by being in contact with the buckets for longer, there is a substantial increase in friction losses incurred. Due to this, it is thought that, there is an optimum length where the increased torque produced by the greater length is greater than the reduction in performance due to the friction losses. It is important to find this peak length value, which if increased would result in friction being the domain force, and begin to decrease the performance. Since the size of the bucket was increased perhaps fewer buckets are needed.

5.2.3. Optimization of Bucket Depth

The numerical methodology is also applied here to optimize further the bucket depth in order to obtain the maximum attainable hydraulic efficiency with respect to the depth. This is done by keeping the bucket length at 144 mm, the number of bucket at 18 as in case 3 in section 5.2.2 and varying the depth of the bucket, different cases were analyzed.

The hydraulic efficiency is calculated for each case and normalized by the maximum hydraulic efficiency of the runner, in this case which occurs at case 2 and the result is depicted as shown in Fig.5.12. From this result, it is found out that, there is an incremental in hydraulic efficiency by 0.68%.

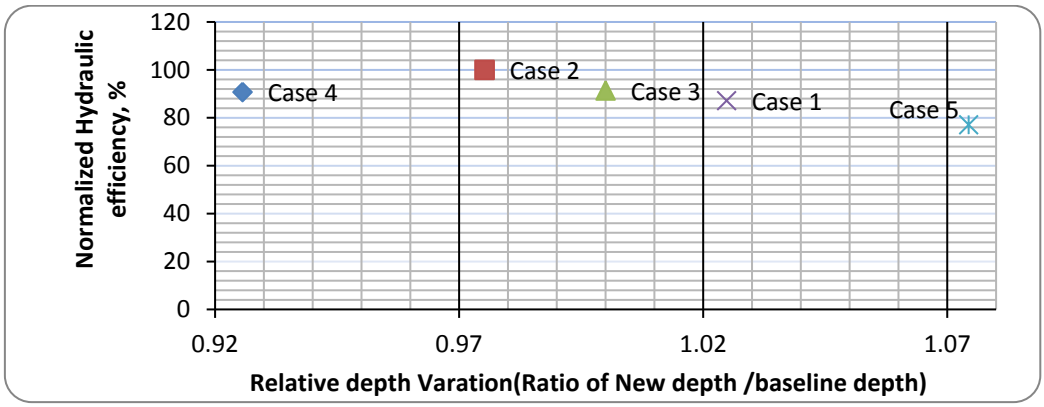

Figure 5.12: Effect of Variation of bucket depth on the hydraulic efficiency of the runner (PCD=400mm).

5.2.4. Optimization of Number of buckets

The number of buckets installed was modified to compare against the 18 buckets baseline design case. As the size, shape of the bucket and its angular positioning is changed the spacing between the buckets might be no longer at its optimum.

Fig.5.13 presents the normalized total torque curves of the runner for different number of bucket at steady states while the PCD kept the same (PCD=400mm). The horizontal axis represents the time, which corresponds to the position of each bucket. The vertical axis shows the relative average torque T/Tmax, where Tmax is the maximum bucket torque.

For each bucket, the predicted unsteady torques of all cases (number of buckets) used the mean value over the number of bucket torques and processed to eliminate variations.

These torque curves show that each case has similar trends. It shows an increase in the magnitude of torque values as the number of bucket is reduced. The reason behind this is, as the number of buckets is reduced the angle between the buckets is increased. This means that the first jet is entering the bucket for slightly longer time before it gets cut off by the following bucket. Consequently, the water from the first jet stays longer in the bucket for lower number

of buckets than higher number of bucket. This means that, the water exerts larger torque in lower number of buckets as presented in Fig.5.13.

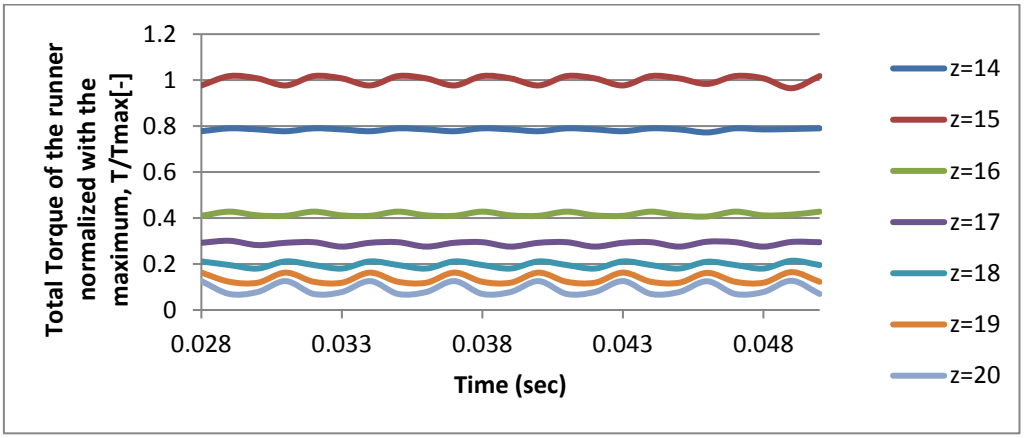

Figure 5.13: Normalized torque values vs time step for different number of buckets (PCD=400mm).

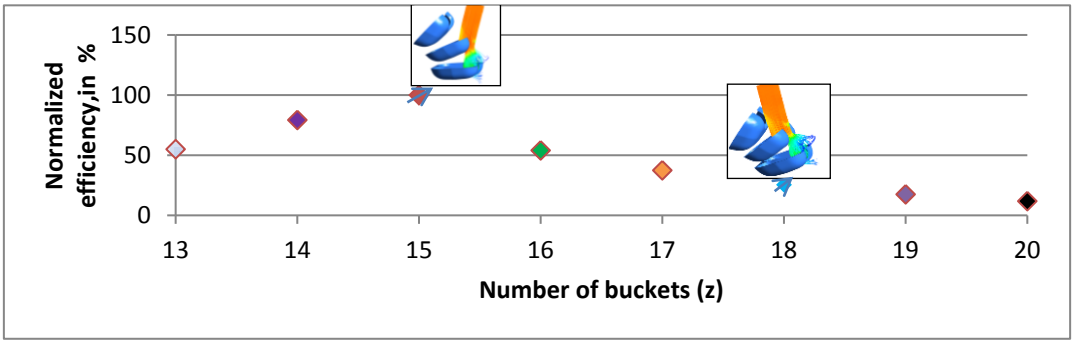

Figure 5.14: Variation of the hydraulic efficiency with respect to number of bucket.

Fig. 5.14 plotted using the normalized hydraulic efficiency for each number of buckets, by taking the maximum efficiencies of each buckets. The peak efficiency is achieved using 15 buckets instead of the initial number of 18 when aiming at the most efficient turbine design at all costs. This improvement in hydraulic efficiency is found out to be 9.6% of the reduced size of the turbine (PCD=400mm).

Also important to note that, the introduction and reduction of extra buckets from the optimum number of buckets reduces the torque values created. Every time the jet enters a bucket some unwanted disturbance is caused to the jet, suggesting that fewer buckets would reduce these disturbances.

This CFD results is in agreement with another similar case study by Veselý and Varner and Židonis Audrius, (2014) and Beucher et al. (2010). According to Beucher et al(2010), CFD modeling shows that with lowering the number and the size of the buckets, friction loss can be decreased by 30%.

5.2.5. Redefining the Shape of the Lip Curve

In modern Pelton bucket has the cutout in the front to ensure smooth flow transition as the runner is rotating. Furthermore, in this research, the undercut on the bucket was modified to avoid the interference of the water jet with the upcoming bucket and to ensure loss free entry of the jet into the bucket.

Redefining the shape of the lip curve was not suitable for parametric optimization and therefore it was optimized by observing the flow behavior and trying to solve the identified problems. As seen in Fig.5.15(A), the cutout was too wide before modification, as a result some part of the flow leave the bucket in high velocity (red) without transferring its energy to the runner, meaning that the losses are the highest at that location. But this problem can be solved by modifying the cutout shape. As presented in Fig.5.15(C) after modification, no water particles were lost at high velocity (red) by failing to hit the buckets during the transition. Further, decreasing of the cutout shape from this was very difficult due to the complex geometry of the bucket. Hence, redefining the shape of the lip curve in each case in order to decrease the leakage gives an incremental in hydraulic efficiency by 8.34%.

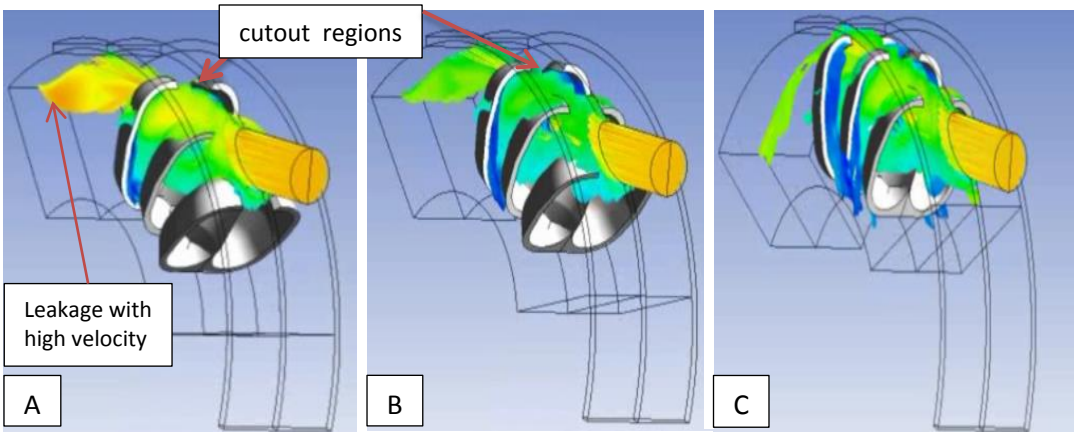

Figure 5.15: Effect of redefining the shape of the lip curve with 15 number of buckets.

5.3. Result Comparison

As explained in section 5.1 and 5.2, various combinations of the design variables are tested using Ansys CFX, in order to assess the relative importance of each one, as well as to determine their variation ranges. It was found that the hydraulic efficiency depends more on the variation in the number of buckets, rather than on main bucket dimensions (length and depth). However, the increase in hydraulic efficiency achieved due to the variation in the angular position of the bucket, depth and length of the bucket cannot also be neglected hence the optimization has to be carried out for all the design variables simultaneously. This

increased the overall efficiency of the turbine, but at the same time ensures that the resulting optimum design is acceptable.

Based on the results and the design trends found, one final optimal geometry was created. A comparison between the baseline design and optimal design for the main bucket dimensions are given in Table 5.6, along with the pitch circle diameter values. A weight reduction of 4.88 kg is achieved through this optimization analysis. The predicted efficiency improvement using CFD was 2.82% of the initial efficiency at the design flow rate. The new shape dimensions are not very different from the baseline design ones. However, we greatly reduced the turbine weight and rotational inertia by reducing the PCD of the runner, allowing quicker initial acceleration to our operational speed.

Table 5.6: Comparison of Runners Geometric Parameters

Parameter	Baseline design			Optimum design		
	%PCD=500mm	Value	Unit	%PCD=400mm	Value	Unit
Jet diameter, d_{jet}	0.11PCD	55	mm	0.1375PCD	55	mm
Bucket length	0.34PCD	170	mm	0.36PCD	144	mm
Bucket width	0.38PCD	190	mm	0.38PCD	152	mm
Bucket depth	0.121PCD	60.5	mm	0.118PCD	47.2	mm
Angular positioning	-	5	^{0}	-	-15	^{0}
Number of buckets	-	18	-	-	15	-
Weight	-	64.523	Kg	-	59.64	Kg
Hydraulic efficiency of the model runner at the design flow rate and head	78.8	%		-	81.62	%

The design and optimization of the runner has the following features and advantages:-

Cost Performance: Reduction of cost of ownership due to less stock (optimization of spare parts stock) and due to possibility to replace few buckets instead of an entire runner.

Technological Performance: Improved behavior of the runner under operation and it has controlled and shorter delivery time. The Pelton wheel runner of this technology has a modified bucket structure as a function of PCD and it is also fitted in the peripheral ring. Compared to the one-piece casting structure, this structure can reduce the manufacturing cost, as well as other costs, by partial replacement of the bucket.

5.3.1. Comparison of Performance at Part Load Operation

So far the above optimization was done for the full load operation, it would be interesting to check the performance of the new design in part load conditions as well. As a consequence, the hydraulic turbine to be installed had to consider both the head variation during the seasonal operation, and the plant's flow parameters. The obtained numerical results for various part load conditions are drawn in Fig.5.16, and compared with the corresponding ones for the baseline design of the bucket with PCD=400mm. It can be seen that the optimum bucket is more efficient at all load conditions (Q/Q_{max}), although its superiority becomes smaller at lower loads. Simulation result shows that torque increases with increases in discharge (load) and hydraulic efficiency initially increases with discharge, attains a maxima and then it starts to decline. Hydraulic efficiency is found to be maximum at 75 % nozzle opening, which is 82.79%. This value is very close to the peak efficiency obtained by Amod Pantee, (2014) 82.5% for a Pelton turbine. But for large scale hydropower, turbine efficiency is generally above 90% [Zhengji Zhang 2016].

Fig.5.16 gives the variation of efficiency with variation of load condition for constant head, (PCD=400mm) and at the design speed of turbine. It was achieved probably due to the lightness of the modified bucket compared to the baseline bucket and the collision produced by the jet water loading on the surface of the bucket, which increased the speed.

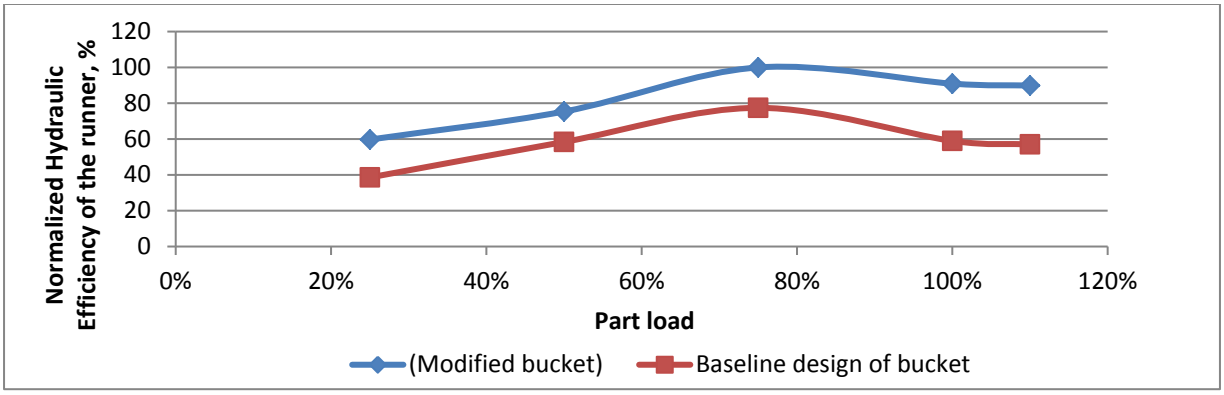

Figure 5.16: Predicted Part load Hydraulic efficiency of the runner with PCD=400mm.

5.3.2 Performance Comparison at Different Pitch Circle Diameter (PCD) of the runner.

As previously stated, the pitch circle diameter was kept constant (400mm) throughout the testing for the modified bucket design. Following the same testing method as the previous, the optimized geometry was run 5 times with the different PCD and Rpm. For these tests, the same geometry was used for each test, with only the rpm modified. Then, the results were directly compared with the baseline (Reference design) geometry values as seen in (Fig. 5.17).

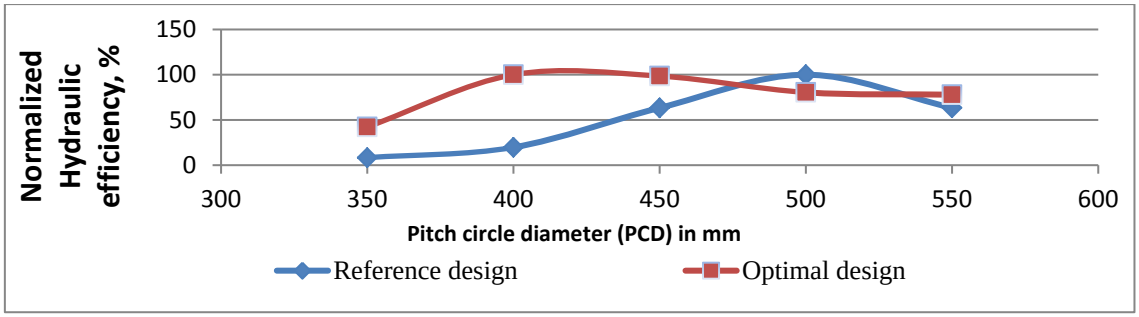

Figure 5.17: Effect of change in PCD on the performance of the runner.

Empirical data suggests that turbine efficiency begins to drop when jet diameter exceeds approximately 11% of PCD for the design of the bucket used in, [Jeremy 2000]. Above this limit, flow interactions inside the turbine cups become more significant and reduce turbine efficiency. However, for a cost effective runner design, smaller turbine is preferable hence further analysis is shown in Fig. 5.17.

The resulting curves verify that the optimization of this parameter gives a cost effective runner diameter, since the efficiency decreases quickly below the optimal value. Also, it is shown that the diameter of the baseline design runner (500mm) is not well selected, although there is a possibility to obtain a slightly higher efficiency with about 500mm diameter. The efficiency drops drastically when much greater or much smaller runner diameters are used (Fig. 5.17), but now this is not the result of volumetric losses, since all the flow still impinge on the inner bucket surface. However, since the runner keeps rotating at the same speed, its peripheral velocity becomes quite different and hence the relative velocity of the particles diverges from the optimum and their angular momentum at the exit of the bucket increases.

It is clear to see from the output data that the PCD is a very important parameter in terms of performance. The results show that the smaller PCD values provide far worse performance characteristics than the larger version. As the PCD decreases, the maximum volume of water within the turbine decreases, therefore there is less force acting on the blades to aid the production of torque. This is especially important when operating horizontally as without the hydrostatic force created by the incline, the primary factor creating the torque is the force within the velocity of the fluid flow. However, the optimization process will not be as simple as decreasing the PCD as small as possible. Fortunately, the optimization processes on the runner together with the bucket surface gives a cost effective result from manufacturing point of view. Finally, it must be noted that in the above examined cases the optimal bucket with PCD=400mm gives higher efficiency than the baseline design model for smaller PCD=400mm and larger rotational speed of the runner.

5.4. Stress Analysis of Bucket

To ensure that the optimized bucket model would be capable of handling the proposed conditions in the prototype, finite element analysis (FEA) using Ansys software was conducted to verify its strength. This simulation of the bucket is done by considering the initial jet impact along the splitter of the bucket.

The assumptions made in this analysis are:-the bucket is stationary, effects of external forces are negligible, and the bucket fixed at its arm acts similar to a cantilever beam.

In this research, depending on the site data, we used cast iron material for the manufacturing of the bucket. A reasonable strength to use for micro-hydro would be 220N/mm^2, or 260N/mm^2, corresponding to grey cast iron to BS 1452 Grade 220 (7150kg/m^3) or 260(7200kg/m^3) [Jeremy 2000].

Fig.5.18 shows that, the first impact force on the splitter is given by F=4144N applied based on the analysis result from chapter 3.

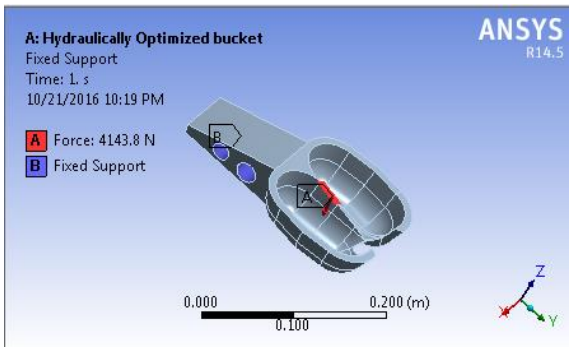

Figure 5.18: Applying the Load

Results of the analysis were analyzed by visualizing the total deformation and the stress levels of nodal solution using the fine mesh.

From Fig. 5.19, it was observed that, it is the tip of the bucket which experience maximum deformation. This value of the optimized bucket is 0.0000359mm.

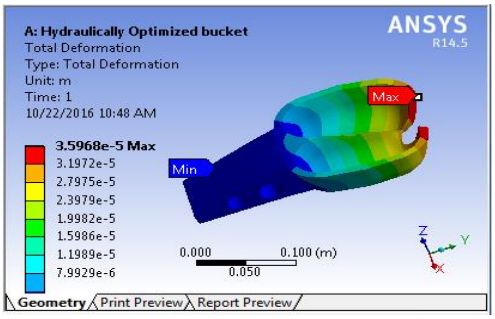

Figure 5.19: Total Deformation.

In designing parts to resist failure, it is assured that the internal stresses do not exceed the allowable limit of stresses of the material. The stress is also analyzed and this value of stress is compared according to the von Mises (Equivalent) stress criteria, which is considered to be most reliable criteria. At the point where jet impinges, maximum stress can be measured.

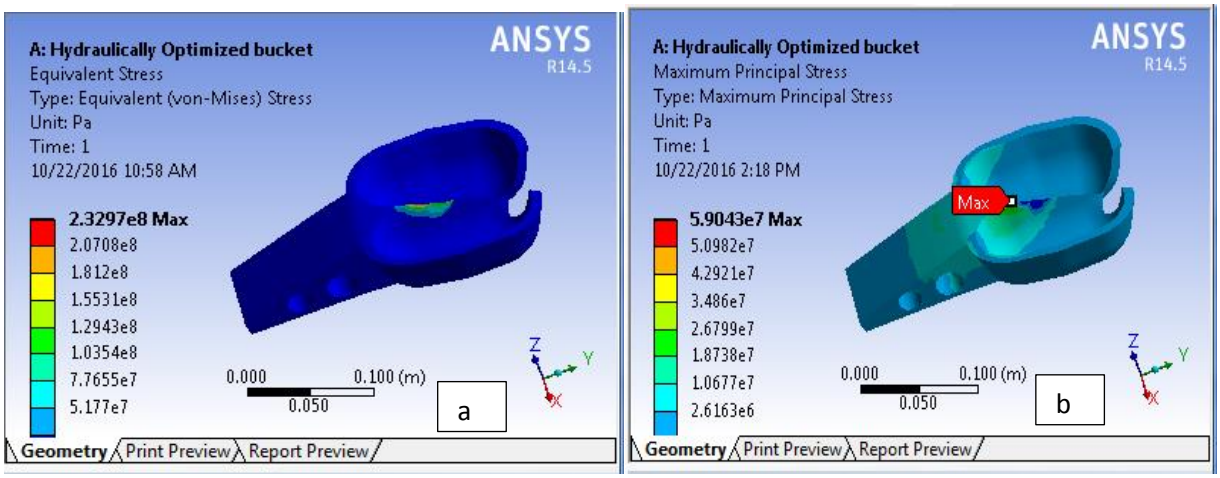

Figure 5.20: Stress analysis (for cast iron Equivalent (von-Mises) stress) and Maximum principal stress.

Based on the maximum principal stress results, the buckets will experience a stress of 59MPa as shown in Fig.5.20b which is below the yielding strength of the material which is 140MPa.

Factor of safety can be calculated by dividing yield stress to maximum Von-Mises stress. Therefore, the safety factor criteria is kept as 2.37. This indicate that, the bucket is safe for given loading. Further, deflection of the bucket is also indicate 0.0000359mm deflection only which is negligible. Hence the bucket passes the structural analysis.

The approach outlined above results in a single solution for the given fine mesh that we have used. Although we are happy that this gives a very good result, but we need to make sure that the solution is also independent of the mesh resolution. After further refinement is made to the mesh and re-analyzing the model until the results converge satisfactorily. The result was found to be almost the same. Hence, the bucket passes the structural analysis. This modeling result showed that the bucket can be operated to produce up to 38.4kW within a good safety factor without fear of failure in cyclic loading.

CHAPTER 6
MANUFACTURING OF THE OPTIMAL MODEL PELTON TURBINE

This chapter describes the manufacturing procedure for the basic components of the optimized Pelton turbine model. CAD graphics of each components and turbine casing can be viewed in Appendix E–Drawing. All the manufacturing activities were carried out at local workshop except standard parts such as bearings, bolts and nuts etc. which were purchased from the market.

6.1. Turbine Bucket Manufacturing Process

3D CAD model the optimized bucket geometry was printed with 3D Printer machine found in Ministry of Science and Technology and used as the master pattern for the mass production of the 15 buckets. The mechanical properties of the material used for the master model have a tensile strength of 36MPa, flexural strength of 52MPa. Fig.6.1 shows photograph of 3D printed model of the optimized geometry of the bucket.

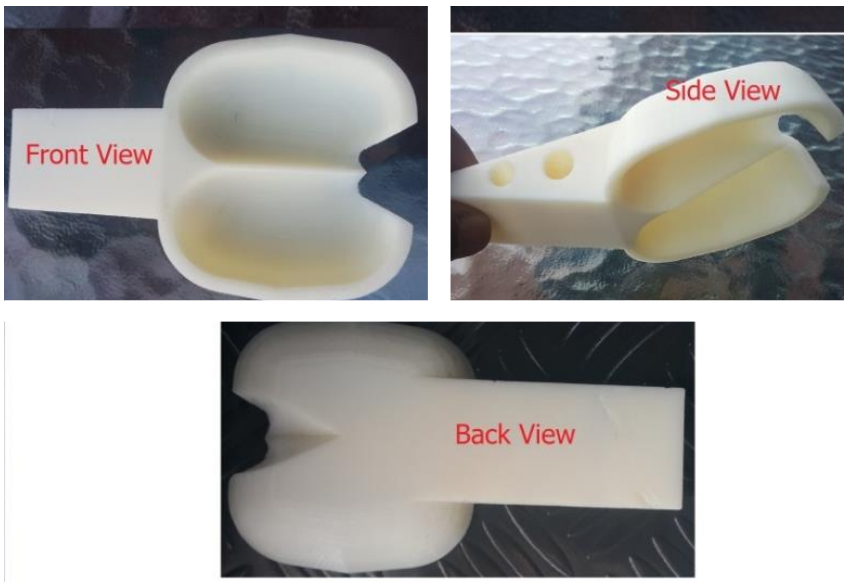

Figure 6.1: Different views of 3D printed model of master pattern for casting.

This, 3D printing technology was used to get an exact and best quality pattern for casting of buckets as far as it withstands the hitting load during sand mould preparation. The 3D Printed bucket was then copied with Aluminum casting. Aluminium alloy with mechanical properties of 518MPa (tensile strength) and 41MPa (flexural strength) have been used for manufacturing of 15 model buckets, due to its resistance to corrosion, cheap cost and suitable structural properties. The external surface, internal surface and handle of the buckets were machined with grinding machine and then rotor grinding was used to surface the internal part of the bucket. Finally, file and sandpaper were used to make smooth and fine surfaces. A cutter

machine was used in addition to the grinding, rotor and file machines and tools to make the part of the bucket. Fig. 6.2 shows photograph of casted buckets.

Figure 6.2: Casted Buckets before machining.

6.2. Turbine Parts manufacturing: Plates, Spacers, Shaft, Nozzle assembly and Casing.

Material: Turbine Parts like shaft, spacers, casing, and Nozzle assembly were fabricated from commercial steel which is very available in the local market.

Runner Plates: The turbine runner plates are the second sensitive part of the turbine components next to runner buckets as the two plates have to fix perfectly which influences the alignment of the buckets that result in loss of efficiency. Thus, the plates were created using plasma cutting machine with thickness 6mm. The discs were then cleaned and made as round as possible using a grinder. The central hole for turbine shaft is bored using boring machine and other holes for the hubs are made using punching machine after marking the exact positions of the holes.

Spacers: The turbine external and internal spacers are manufactured by using lathe machine's turning, facing and boring operations. The spacers were designed to add rigidity and stiffness to the mid-section of the turbines runner plates.

Shaft: The shaft of the turbine is sized in accordance with the design procedure in the Micro Hydro Design Manual, Harvey (1993). A 80mm diameter and 1000mm long solid steel rod has been used to produce a turbine shaft and using lathe-turning operation a stepped shaft was

created. Chamfering is made on the shaft on the same machine but key ways were created using milling machine. To fit the shaft in the base frame and connect it to the dynamometer , bearing housing of internal diameter 60 mm hole on the base was used. The bearing housing is held tightly with the main frame by using nuts and bolts of 10 mm diameter. To connect the dynamometer and the shaft, coupling is used. For coupling, one part of the shaft is threaded to join the dynamometer. A key slot on the shaft and coupling part has been made with lathe and shaper machine so that, the rotatory motion of the shaft is being transferred to the rotor shaft of the dynamometer.

The second step of assembling of Turbine is Fixing of runner plates, holder, internal and external spacer in between the runner plates. Holder part of the shaft is used to hold all the spacers and runner plates and prevent the side ways motion of all these parts of the turbine. It is fabricated by turning on the lathe machine which makes a stepped shaft. A slot is made on the holder which is used to fix the M6 bolts to hold parts of the turbine like external spacer, internal spacer, and runner plates as shown in Fig. 6.3.

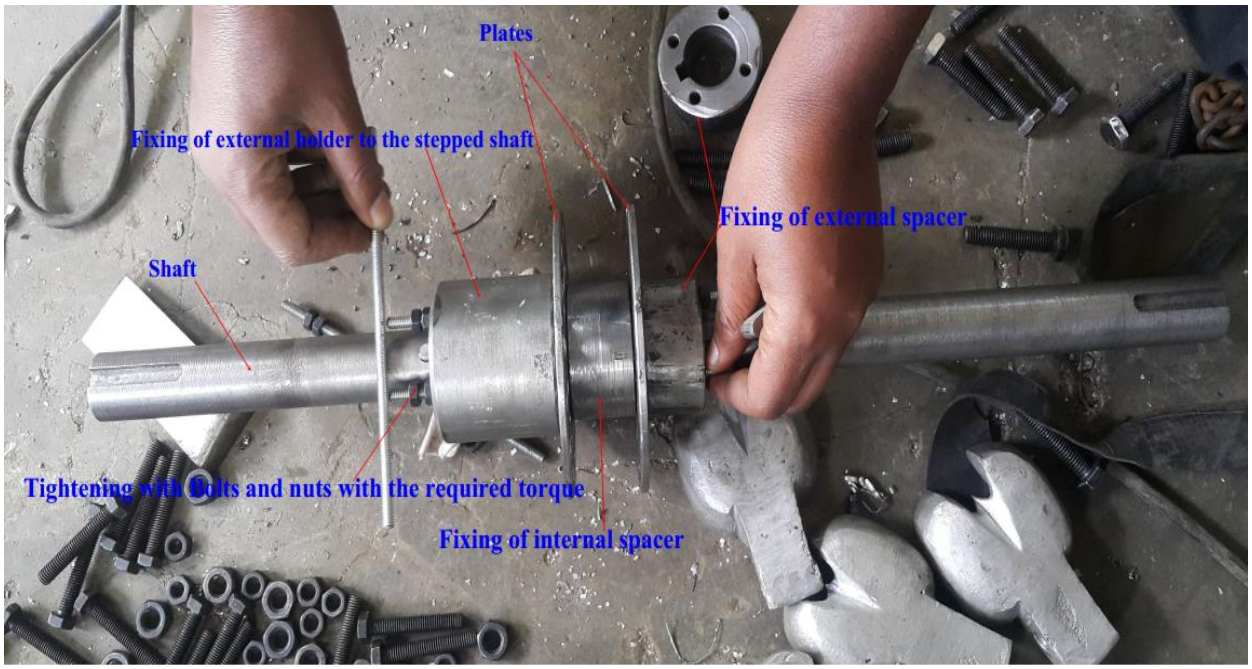

Figure 6.3: Assembly of runner plates, and spacers on the shaft.

Fig. 6.4 shows photographs of Turbine runner assembly of the model with the bearing at the end. All turbine parts were fixed in the holder with four M6 bolts in its slots. This holder is used to prevent the longitudinal movement of the turbine parts and so that, it is used to transfer the rotational motion of the buckets to the shaft effectively.

Figure 6.4. Assembly of the buckets on the plates of the runner.

Bearing Housing: A bearing on each side of the turbine is used to mount the turbine on the casing walls. To select the bearing type, the forces acting on the turbine need to be calculated. This calculation has been done and selected in accordance with Jeremy 2000 book as shown in Appendix A.

Nozzle Assembly manufacturing: a solid shaft of 105mm diameter and a length of 215mm was cut with a power hacksaw and its external surface was faced using a lathe machine until its diameter reached 100mm for the outer facing. Following this, the tip of the nozzle was faced with a lathe machine to make a conical surface to make the included angle 90^o. The remaining steps are organized as follows:

Boring: the first step in boring of the nozzle was to drill with a 30mm diameter drill bit and boring operation of lathe machine has been used to make an internal diameter of the nozzle 92mm and a length of 154mm.

Inner cone facing: the remaining 56mm length of the nozzle was bored at an angle to make a nearly conical surface and an included angle of 53^o was made.

Spear Valve: a 45mm diameter solid shaft was used to make the spear valve. The first operation was to face the shaft a length of 180mm till the diameter becomes 24mm. The second operation was to make the head and tip of the spear valve by facing at different angles to make its head and 26.5^o angle was used to make its tip.

Bushing for axial movement of spear valve: a length of 30mm and diameter 35mm was used to make the bushing to support the axial motion of spear valve to keep its center. The shaft was

drilled at 25mm diameter drill bit in two parallel surfaces and screw was made in the drilled holes. Using these screwed holes, the bushing is suspended to the nozzle body using bolts. The bolts ware lastly welded to the nozzle body.

Bolt and nut for adjustment: a long bolt was welded to the end of the spear valve and this was inserted in a screw made bushing that was welded to a drilled elbow.

Handle: for ease operation of the spear valve, handle was prepared using plate and double nuts. The double nuts were first tightened in the long bolt which was welded to the spear vale and the plate drilled at its center and screwed to the long bolt. Finally two nuts were tightened after the plate.

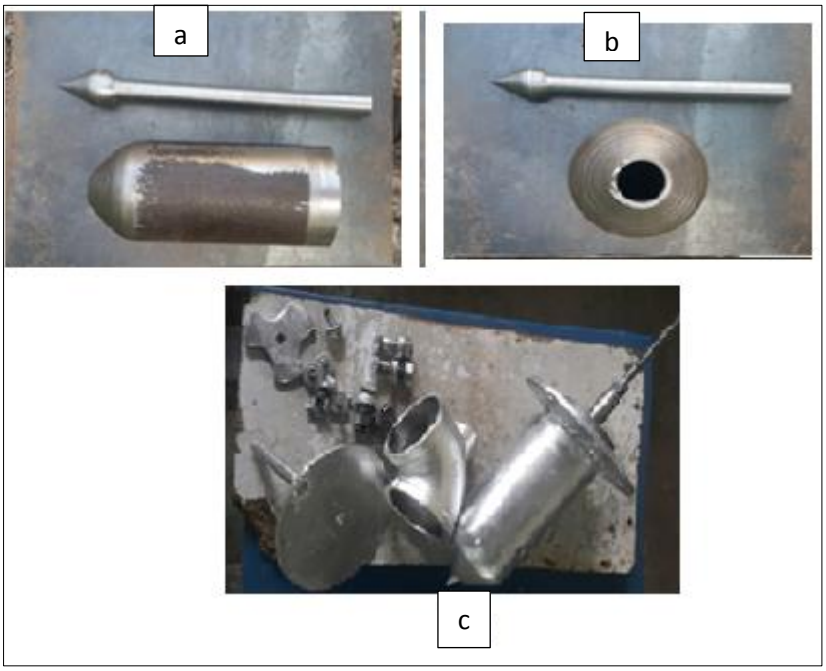

Figure 6.5: a) Side view of nozzle and spear b) Front view of the nozzle and c) Different parts of the nozzle assembly.

Casing: A casing was designed in order to house the turbine during operation. This served several purposes, including: supporting the turbine and alternator; protecting people from moving parts and high-pressure jets; and restricting spray from the turbine. The casing in this model was composed of two components a top casing and a bottom casing. The turbine upper and lower casing are manufactured by cutting the sheet metal to its shape and size as per the design in Appendix A with plasma cutting machine, drilling operation is made with drilling machine. This research (38.4kW micro hydroelectric design research project) uses rigid (6 mm) steel for both the side plates and end plates to ensure reduction of both vibration and noise. Technical drawings for further details information are included at Appendix F. Lastly, the welding of the sheet metal is made by arc welding machines. The main body of the casing

had to be designed in two parts, due to the configuration of the bearing housings and turbine shaft such that the turbine could be more easily assembled in the site. Steel angle is welded around the perimeter of the two casing halves to allow them to be bolted together and also bolted to the base plate. For the prototype, two holes must be cut in the casing for installation of the spear valves and nozzle jets. These are located on the casing top and casing front, nozzle and valve assemblies is attached to the turbine casing using through bolts. The casing is fully sealed at joints using rubber gaskets. Lastly the entire casing is painted with epoxy paint. Appendix E gives detailed as built drawings of all the components making up the turbine casing.

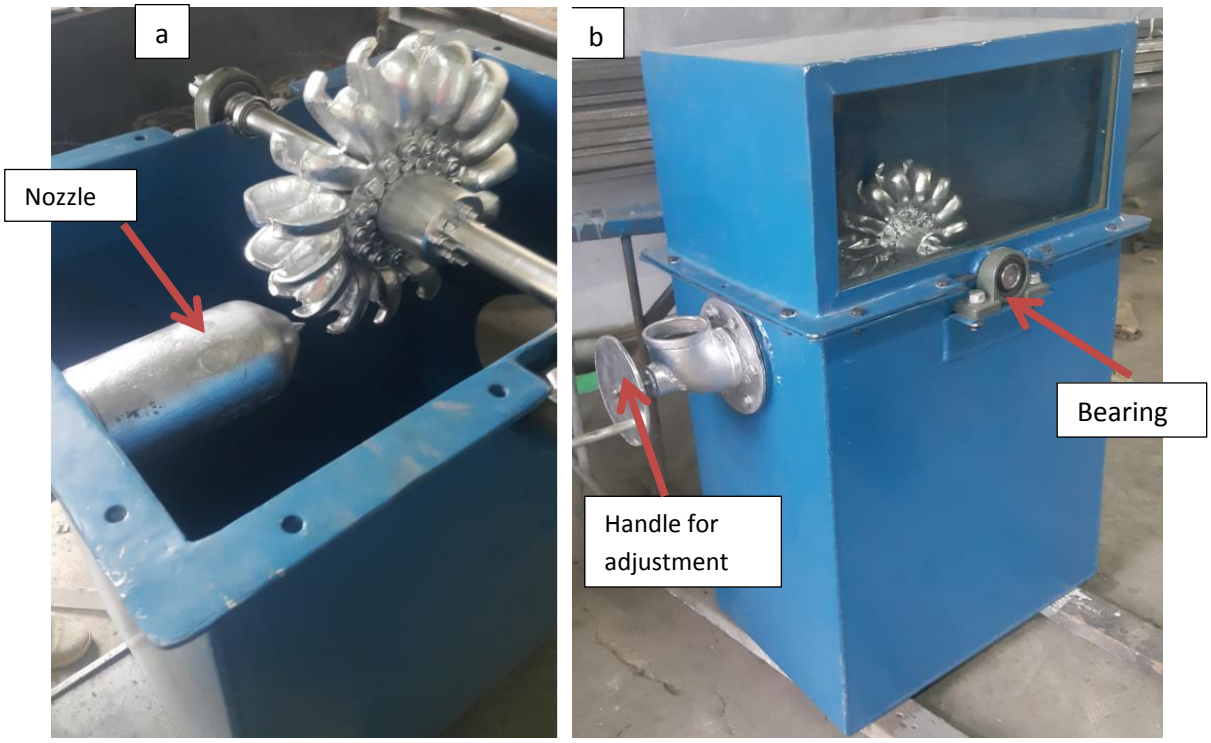

Figure 6.6: a. Fixing of nozzle assembly, runner with shaft and bearing on the lower casing, b. Final phase of assembly of the model Pelton turbine.

Fig. 6.6 shows the assembly of casing, runner and nozzle. Two bearings (NSK 6205 DU) were used for runner mounted on casing.

Next chapter deals with brief description about how the experiment of the model Pelton turbine was conducted in the laboratory to validate/compare with the CFD simulations.

CHAPTER 7
VALIDATION OF THE CFD MODEL

The objective of this chapter is to describe the performance of the constructed model Pelton turbine experimentally and verify that all parts and systems installed in the Pelton turbine are working fine or performing their functions correctly. Moreover, the experiment is done to evaluate the accuracy of the simulation which is important for CFD-based design optimization procedure. In fact, the verification of the simulations in chapter 4 with two published papers is also one part of the validation.

7.1. Description of the Test Set Up

The case study model's performance measurement was conducted on a test rig available at Hydraulic laboratory, AAIT. The set up can accommodate Pelton turbines up to a pitch-circle-diameter (PCD) of 212 mm.

The line sketch of the test set up or scheme of tests loop, Lab layout and various parts of test stand are shown in Fig.7.1. A head tank located in the upper floor of the AAIT building maintains constant water head on the turbine. The tank was used to supply water in the turbine, it was elevated to a height of 13.34 meter and supported by a metal frame. Centrifugal pump used to supply water in the tank from the underground water.

For this investigation, the pump is first switched on to fill the tank and water is released from the tank to drive the turbine when the tank is full, by opening the gate valve in the tank discharge pipe. The water is then discharged (by gravity) back to the wells after driving the turbine. A small mechanical pressure gauge at the inlet of the turbine measures the inlet water pressure (see Fig.7.1 and Fig.7.2) and is used also for reading the available water head. The water exiting the turbine is collected in a releasing basin equipped with a triangular weir (V-notch) at the downstream end to allow measurement of the flow discharge. The laboratory is also equipped with orifice for calibration of volume flow using (V-notch) along with two manometers.

The experimental unit consists of the Pelton wheel, a needle nozzle used as distributor, a Prony Brake drum for loading the turbine, measuring equipment, a housing with a transparent front panel and base for mounting of turbine. The transparent cover enables observation of the interaction of the water flow, the Pelton wheel and the nozzle during operation. The nozzle cross-section and thus the flow rate are modified by adjusting the nozzle needle spear position by means of a hand wheel fitted. When the spear is pushed forward into the nozzle, the amount of water striking the runner is reduced, where as if the spear is pushed back the amount of water is increased. This spear helps to adjust the flow rate to balance the change

caused by site conditions. The parameters that can be measured include; speed, inlet flow, torque and inlet head. These parameters can be used to evaluate hydraulic power and efficiency values for different loading conditions of the turbine.

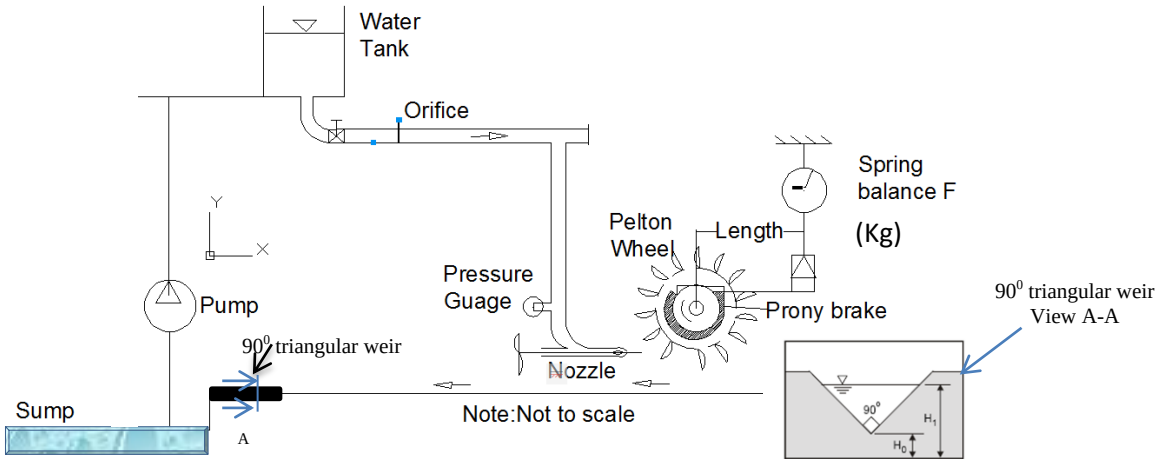

Figure 7.1:Schematic of the Test set up.

The turbine torque is determined by force measurement on a Prony Brake drum coupled with turbine shaft which is also tensioned by a weight hanger with the fixed end being secured via a spring balance to the support frame and read on spring balances. The Prony Brake drum, which in this case physically resembles an automotive disc brake has a reflector and clear cover to work with an optional tachometer to measure the speed of the turbine.

The next step will be to conduct model testing with this design set up, to see how closely the values from CFD and real testing match. Note that prior to the experiments all measuring instruments have been calibrated according to their manuals.

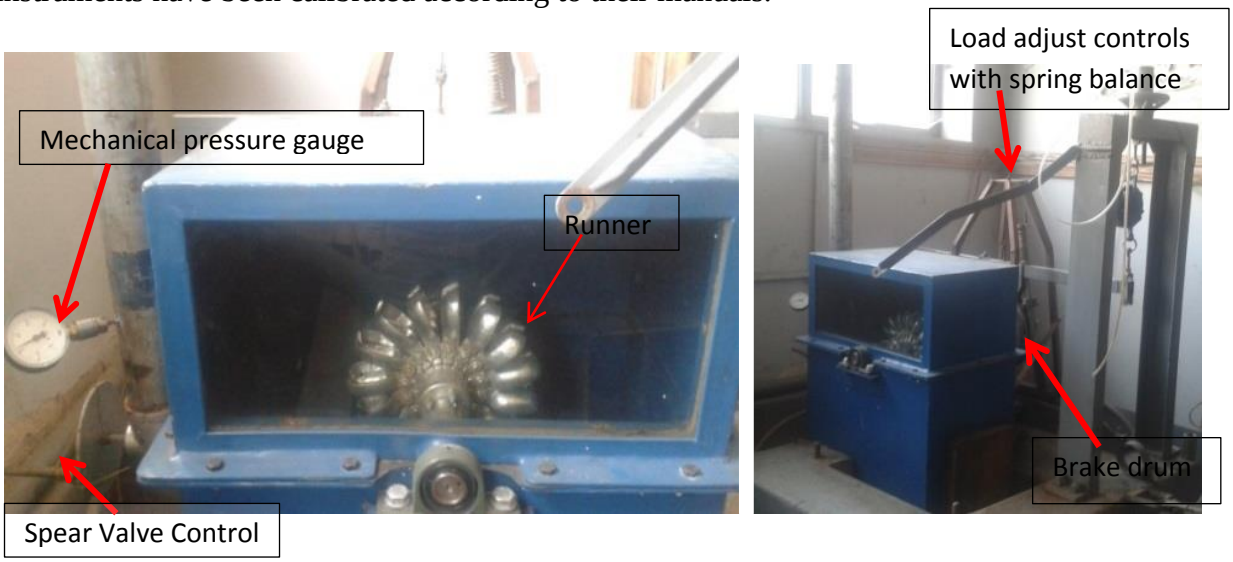

Figure 7.2: Photograph of Test facility/Pelton wheel model in the Laboratory.

7.2. Test Data Measurement Procedures

To ensure consistent results and safe operation, a set of procedures for set-up, startup, and data sampling procedures were created. A water pump was used to generate the pressure head. The volume flow rate and head were controlled by using the valve. The measurement procedure is summarized below:

I. Create blank results table and Performance Calculating sheet, similar to Table 7.1 and Appendix F respectively.

II. Note the number of divisions indicated on the spear wheel, in terms of nozzle opening.

III. Undo the knob that adjusts the dynamometer load so that the disk turns freely and adjust the spring balances to give no load and make sure that they show 0 (zero).

IV. Start the Pump and open the valve just upstream of the pressure gage while opening the spear valve (turn it anticlockwise) until the system flow is at maximum and the spear valve is fully open. Prior to turning the pump on, it must be primed first.

V. Note the inlet pressure and determine the discharge through the system using the weir calibration methods at four spear valve position (approximately 25%, 50%, 75% open and Fully (100%) open) as shown in Appendix F.

VI. Use the contact type or non-contact type tachometer to measure the maximum (runaway conditions) speed of the turbine. To do this, loosen the torque brake so that there is no friction applied on the turbine shaft and put the tachometer against the clear window at the back of the turbine and use it to detect the reflective sticker on the drum.

VII. Slowly increase the load (friction on the shaft of the turbine) in steps to give at least eleven sets of results. The load is adjusted by turning the adjusting knob on the dynamometer. At each step, the upstream head, discharge, speed and torque produced by the turbine are noted down. Stop when the speed becomes unstable or the turbine stops rotating. From the test data the hydraulic power and mechanical power are calculated and the efficiency of the turbine could be derived.

VIII. Repeat the procedure for different opening of the nozzle, keeping each time supply head constant. Repeat the test with the spear valve position approximately (25%, 50%, 75%) open and Fully (100%) open. The exact amount of spear valve opening is not important, as long as they are different from each other to compare the effect. At each condition hydraulic head, discharge, speed of the turbine, torque were measured.

IX. Compare the experimental and Numerical results and discuss some possible reasons for any differences between them.

7.3. Performance Characteristic Equations

This section provides equations used to define the characteristics of a turbine.

During conversion of energy (hydraulic energy to mechanical energy) there occur some losses. They can be in many form and main causes of them are friction, separation and leakage. Considering all losses such as Mechanical and Hydraulic losses as one form, the power generated by the turbine is equal to the sum of the power absorbed by the dynamometer (Useful shaft power output) and the Power loss [Eq. 7.1].

Power Input (generated) = Useful Shaft Power Output + Power Loss [7.1]

Estimation of the mechanical loss of the test rig is necessary for the accurate evaluation of the turbine performance [Zh. Zhang, 2016]. This is treated in Appendix A (Eq. A-11-A-13). Then, the overall efficiency is calculated by using the following formula:

$$\eta = \frac{Power\ output}{Hydraulic\ power\ input\ to\ turbine} \quad [7.2]$$

Hydraulic power input to the turbine is calculated by:

$$P_{in}=\rho g H_{net} Q \quad [7.3]$$

Where, ρ is actual density of water (at actual temperature and pressure) in kg/m^3; g is actual acceleration due to gravity (function of latitude and altitude above mean sea level) in m/s^2; H_{net} is net head of water in m; and Q is discharge rate of water through the turbine in m^3/s. The power input P_{in}, can be re-written in the form of kinetic energy in the jet, as:

$$P_{in}= (½)\rho Q V^2 \quad [7.4]$$

The inlet pressure (read by the pressure gauge) and water flow (measured by the orifice) gives a good approximation of the inlet power from:

$$P_{in}= Q \times P \quad [7.5]$$

Where Q is in m^3.s^{-1} and the pressure (P) is in Pascals.

Turbine Power output: This is the power absorbed by the turbine wheel, taken from water,

$$P_{out} = \frac{2\pi NT}{60} \text{ or } P_w = \omega T \quad [7.6]$$

Torque (T): This is the torque measured by the spring balances. The balances measure the turning force on the drum at the back of the turbine (see Fig.7.2). The torque is the radius of the drum multiplied by the force:

$$T = R_d \times F_d \quad [7.7]$$

Furthermore, in the studies of comparison of the performances of turbines, it is suggested to determine the performance of turbine under unit head (reduce values), such that the efficiency of the turbine remains unaffected. These reduced values make it easier to compare the results

for different operations [IEC 60193-99]. The characteristics equations for these are given below.

Unit speed (Nu): The speed of the turbine, working under unit head (say 1m) is known as unit speed of the turbine. Mathematically expressed as:

$$N_U = \frac{N}{\sqrt{H}} \quad [7.8]$$

Unit power (Pu): The power developed by a turbine, working under a unit head (say 1m) is known as unit power of the turbine. Mathematically expressed as:

$$P_U = \frac{P}{H^{3/2}} \quad [7.9]$$

*Unit discharge (Qu):*The discharge of the turbine working under a unit head (say 1m) is known as unit discharge. Mathematically expressed as:

$$Q_U = \frac{N}{\sqrt{H}} \quad [7.10]$$

Where, H is the head of water, under which the turbine is working; N is the speed of turbine under a head, P is the power developed by the turbine and Q is the discharge.

7.4. Estimation of the Uncertainty in the Instruments

The following procedure was used to estimate the errors in the instruments and compute the uncertainty estimates for the measured efficiency.

The uncertainties in the measurements during the experiments include factors such as inaccuracy within the instruments. To estimate the accuracy, the model acceptance testing standard [IEC 60193-99] provides formula (Eq. 7.11);

$$\frac{d\eta}{\eta} = \pm\sqrt{\left[\left(\frac{dT}{T}\right)^2 + \left(\frac{d\omega}{\omega}\right)^2 + \left(\frac{dP}{P}\right)^2 + \left(\frac{dQ}{Q}\right)^2\right]} \quad [7.11]$$

Where, dT=Accuracy of torque, dω=Accuracy of speed,

dQ=Accuracy of flow and dP= Accuracy of pressure.

To do the calculation, the relative uncertainties for each instruments that has been used in the experimental testing for the measurements of the rotational speed, inlet pressure, flow rate and torque are descried as follows:

Accuracy of digital photo Tachometer: An image of the digital photo Tachometer, (model: Extech 461893) used during the testing is provided in Fig.7.3. This device provides non-contact measurements over a wide range (5 to 100,000Rpm). The relative accuracy for this instrument was within ± 0.05 % and taken for uncertainty analysis.

Figure 7.3: Photograph of Digital Photo Tachometer used for the test.

Accuracy of pressure (dP): The gauge used in this experiment measures pressure up to 1.5bar (see Fig. 7.4A) and is accurate to ± 1.5% over the entire range of gauge.

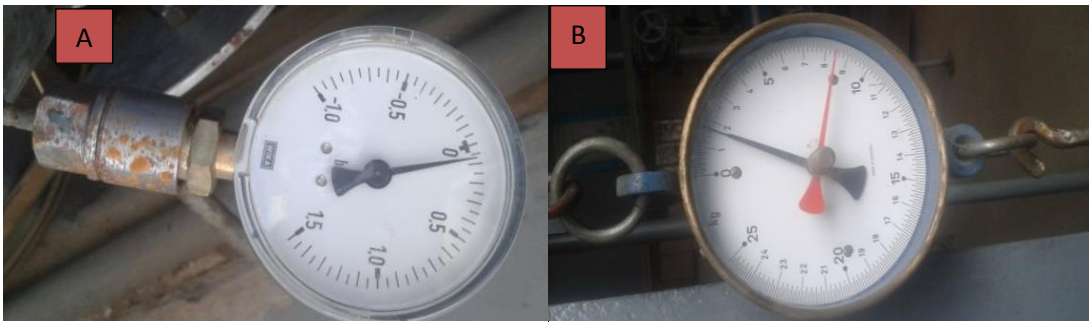

Figure 7.4. Photos of the instruments used in the laboratory: A. Burdon Tube Pressure Gauge used for measuring inlet pressure. B. Spring Weight Balance.

Accuracy of torque (dT): The turbine torque is determined by force measurement on a band brake and is read on spring balances. The spring balance used for this experiment has an accuracy of ± 1 %. It measures weight ranging from 0 to 25Kg, by opposing the force of gravity with the force of an extended spring (see Fig. 7.4B).

Accuracy of flow(dQ): The measurement of the flow rate using an orifice plate has a number of uncertainties. First, there are both bias and precision uncertainties in the measurement of the manometer height that used to measure pressure difference between the two faces of the orifice plate. Secondly, there is uncertainty in the calibration curve that is supplied in the laboratory. We now need to combine the manometer height and calibration uncertainties to obtain the overall uncertainty in the flow rate to be ± 5%.

7.5. Experimental Data Observation and Results

Turbines are often required to work under varying conditions of head, speed, output and nozzle opening. As such, in order to predict their behavior, it is essential to study the performance of the turbine under varying conditions. All these tests are divided in two categories: No Load Tests and Load Tests.

7.5.1. No Load Tests

These tests confirm the operation of turbine and auxiliaries equipment under no load conditions. Accordingly, initially the turbine was allowed to run in its runaway speed for few minutes and the experimental runaway data's were collected as shown in Table 7.1.

The testing was done in different spear valve opening of 25%, 50%, 75% and 100%. The flow rate through the spear valve depends on the opening position of the valve and the fluid pressure. The corresponding performance curves correlate the flow rate variation with the spear opening at the respective constant pressure.

Table 7.1: Experimental data obtained from Pelton turbine at No –load.

S. N	Percentage of Nozzle Spear Valve Opening Position	Measured Inlet Pressure (bar)	Measured Speed in (rpm)	Measured flow rate, Q (liter/sec)
1	25%	1.45	957	3.4
2	50%	1.40	1038.8	5.5
3	75%	1.35	1066.4	7.8
4	Fully Open (100%)	1.30	1076.4	10.41

According to Jermey, (2000), under ideal conditions, the maximum runaway speed is about 1.8 to 1.9 times the nominal speed. Based on this, the runaway speed is calculated to be 1235 rpm. This is the runaway speed, which the turbine can theoretically attain in case of load rejection. However, from the turbine examined here, the experimental data from Table 7.1 show the maximum rotational speed of Pelton turbine at zero torque applied on the shaft is 1076.4 rpm. This means that the maximum runaway speed is found to be 1.66 times of the design speed which is equal to 650rpm. This means, the actual runaway speed is smaller than the frictionless runaway speed. This might be due to the different losses that occurred in the manufactured turbine. Therefore, this test also gives the information regarding no-load losses such as friction loss, bearing loss and windage loss as a sum of the mechanical losses, a quantity that is not directly measurable. Additionally, during the runaway process, a series of instability phenomena occur that causes a slight vibrations of the runner and the unit. Even though, this speedup begins just after the load rejection, the model turbine run without any mechanical problem and the runaway process of the model Pelton turbine was successfully tested.

Additionally, it was seen that the position of nozzle, the distance between spear valve tip to bucket, the alignment of spear valve are as per the design and the dynamic balance of the

turbine was acceptable. Thus, everything seems under control, verifying the normal operation of the test rig in the entire flow range.

Moreover, the pattern shown in Fig. 7.5 is typical for spear valves opening which is similar to the characteristic curve normally obtained from the turbine model tests conducted by the manufacturer. Therefore, the turbine is ready to undertake the next load test.

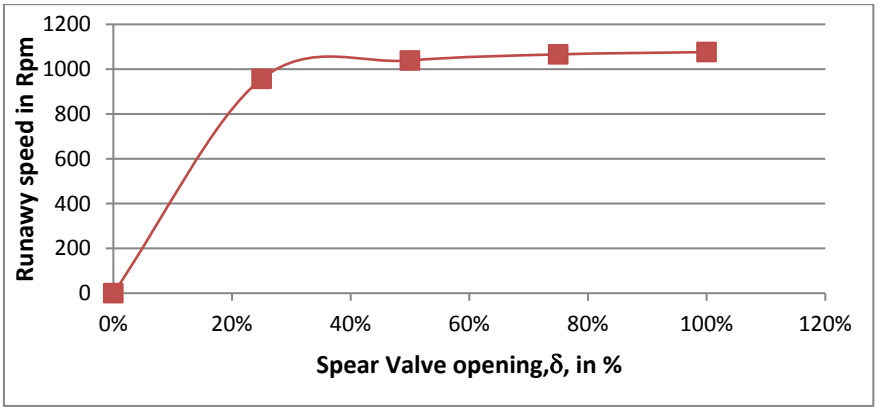

Figure 7.5: Runaway speed at different flow rates.

7.5.2. Load Test

These tests confirm the operation of the turbine under load condition. Following these, the results presented using the form of appropriate plots/curves. According to IEC 60193 test standard, these are curves which help in studying the performance of the turbine under various conditions.

7.5.2.1. Characteristic Curves at Constant Design Flow Rate

Firstly, for a given opening of the spear valve (keeping the head and discharge constant), the speed may vary by adjusting the load on the turbine. These conditions are possible only in the laboratories. The curves so obtained for such conditions are known as *main characteristics* curves [IEC 60193-99].

The pressure head was maintained at 13.34m throughout this test and was monitored by the pressure gauge. Then, the speed of the turbine wheel is varied by adjusting the tension on the Prony brake spring, thereby varying the torque, T_{shaft}, applied to the output shaft. When the loads are increased, the wheel will be harder to rotate due to the increase in torque applied to the wheel and hence the speed reduces.

Table 7.2 shows work for a sample reading of data and analysis of each step to investigate the power produced by the model Pelton turbine at fully open position of the spear valve.

Table 7.2: Part Load operation of Pelton Turbine at fully open needle valve position.

Parameters	Brake Setting										
	1	2	3	4	5	6	7	8	9	10	11
Net spring balance, reading (W-s) in kg	0	1.2	1.4	4.1	6.5	7.1	8.0	8.5	8.7	9	9.1
Measured Inlet pressure, P in kpa	130	130	130	130	130	130	130	130	130	130	130
Inlet Head, H (in meters)=P/ρg	13.3	13.3	13.3	13.3	13.3	13.3	13.3	13.3	13.3	13.3	13.3
Volume Flow Rate, Q litres/sec (measured using Calibration of v-notch)	10.4	10.4	10.4	10.4	10.4	10.4	10.4	10.4	10.4	10.4	10.4
Measured Speed, N in rev/min	1076	1000	940	850	690	650	560	450	370	330	0
Brake Torque τ = (W-s) × g×Rd in Nm R_d=0.15m	0	1.77	2.06	6.03	9.56	10.4	11.8	12.5	12.8	13.2	13.4
Mechanical Power Output, P_{out} in Watts	0	185	203	537	691	711	690	589	496	457	0
Hydraulic Power Input P_{in} = ρgHQ in Watts	1364	1364	1364	1364	1364	1364	1364	1364	1364	1364	1364
Overall Efficiency $\eta=P_{out}/P_{in}$	0	13.6	14.8	39.4	50.6	52.1	50.6	43.2	36.4	33.5	0

Thus, by applying different loads and measuring the speeds at each load, graphs of Torque, power output and efficiency vs. Turbine Rotational Speed were plotted. To draw these curves on the same chart, the unit power Pu, the unit speed Nu, the unit discharge Qu and the overall efficiency are determined for each test based on Eq. 7.8, 7.9 and 7.10 as described section 7.3.

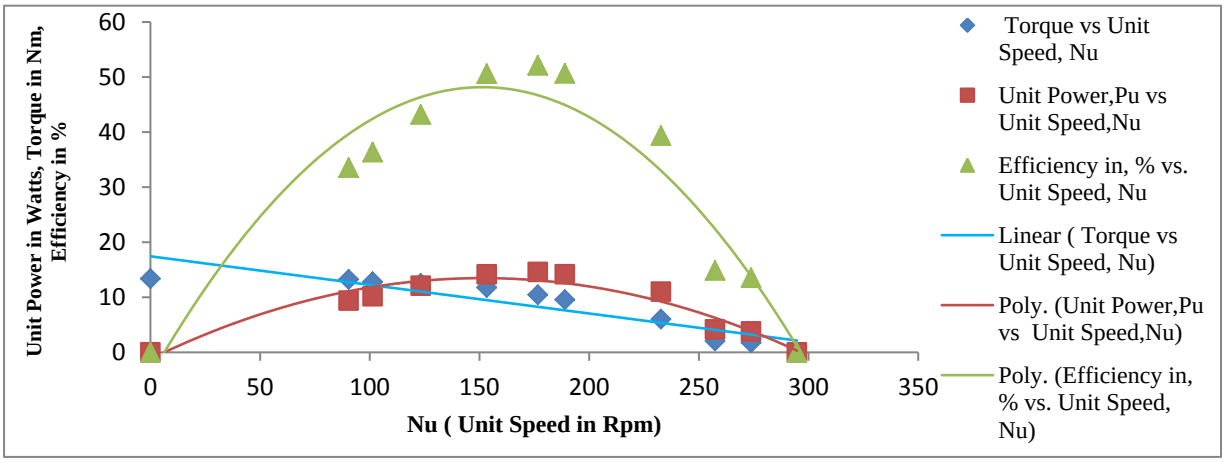

Figure 7.6. Torque, Unit Power and Efficiency Vs. Unit Speed at Fully open spear valve position, δ=100% .

Based on the research, it is found out that the expected graph of torque against wheel rotational speed should show a linear decline of torque value with the rise of wheel rotational speed (see Fig.7.6). Again, if one looks precisely in the efficiency and the power curves, one

can see that measured curve diverts with its shape from the typical efficiency curve which shows a quadratic curve with the rise of rotational speed. Hence, these results suggest that there are certain external factors, which influence the turbine's performance. For this reason curve fitting is used to produce an equation that can be used to find points anywhere along the curve (see Fig. 7.6).

These variation of results from the line of best fit are due to experimental errors. The first error is the fluctuation of measuring instrument's readings whereby when taking the readings of loads, the readings fluctuate and the exact value of the loads' readings were hard to obtain. This leads to less accurate net weight of load, torque and mechanical power readings. The greatest being that, it became really difficult to acquire readings from the spring balance since the setup was vibrating as a result of the operation of the turbine at high rotational speed. This generated vibrations can be of mechanical origin (like unbalance) and of hydraulic origin. This includes the perturbations of the torque developed at the shaft. Naturally, these vibrations could cause uncertainties in collected data.

To reduce these vibrations and their effects on the system, dampers were applied at certain points of the setup. After all, it is found out that, the overall efficiency is to be 52.1% which is lower than the theoretical assumptions in Table 3.3 (56%) at the design point.

The first reason for the difference between these overall efficiency is due to the fluid friction which reduces the kinetic energy of the flow. Secondly, there might be also losses due to the gap necessary between the turbine and the enclosure wall. The efficiency will therefore be very much smaller, because of losses in bearings and by air friction.

7.5.2.2. Characteristic Curves at different Flow Rate

Again, the process is repeated for different flow rates (at 25%, 50% and 75% of nozzle opening), and each time measuring the hydraulic, and mechanical properties as well, and then calculating the efficiencies or losses. Next, performance curves (see Fig. 7.7 and 7.8) are plotted from the results of the tests performed on turbines under the above nozzle opening conditions. These curves also give a good idea about how the performance of the turbine alters with the volume flow rates.

It should also be pointed out that in the "real world" systems, as the electrical load demand of the consumer network increases and decreases, minute by minute, someone or something is compensating for that change by using a spear valve to change the volume flow rate through the turbine, allowing the above tests to be repeated at different flow rates to maintain the 50Hz power frequency standard. As the load on the turbine changes, the flow of water is regulated via the spear valve to maintain the turbine at the required operating speed.

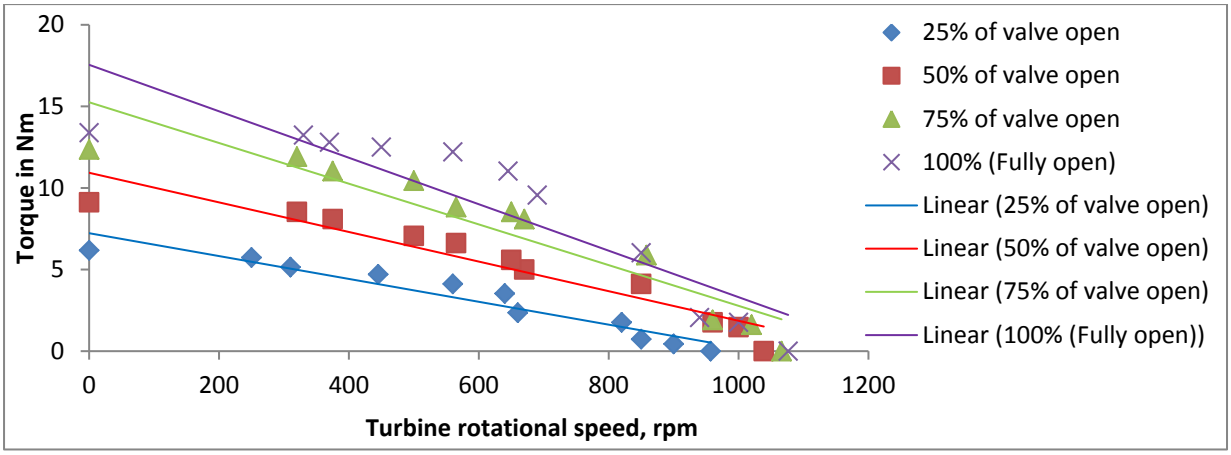

Figure 7.7: Brake Torque vs Turbine rotational speed at different flow rates.

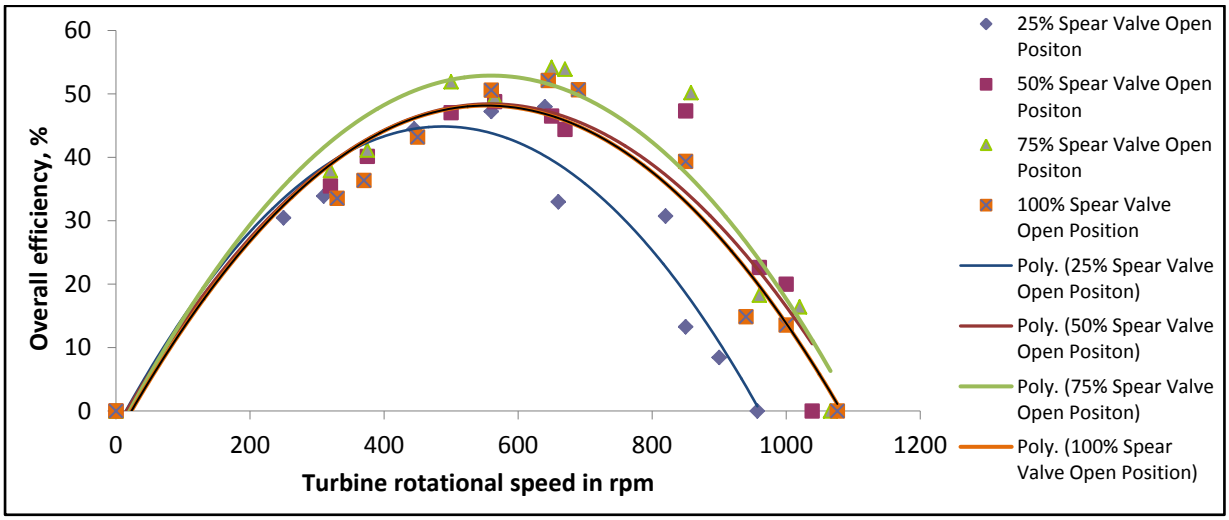

Figure 7.8: Overall Efficiency vs. Speed at different flow rates.

As seen in Fig.7.7 and 7.8, the spear valve position affects maximum speed, torque, power and efficiency. A curve fit second-order polynomial trend lines are added to the data and used to calculate the average maximum efficiency. Relatively, at fully open and 75% of fully open position of the spear valve have more force to move the wheel thus have the highest speed compared to 25% open spear valve position. Moreover, the above figures show that the maximum limits of rotational speed of the turbine and the maximum limits of torque and efficiency increase when the volumetric flow rate increase for every nozzle opening. As it is also observed in Fig.7.8, it was amazing that the efficiency of the runner with the optimized bucket design at 75% of open spear valve position produce maximum overall efficiency of 54.2% which is higher than at fully (100%) open spear valve position which is 52.1%. This result was unexpected. The only reasonable explanation for this is that, the reduction of buckets accommodation effectiveness might have occurred at fully open spear valve position. This creates a loss because some part of the water jet will not contribute to the energy

conversion. Some part of water jet may re-enter the runner section after impacting on the casing walls, and may also interfere with the nozzle jets and cause surface perturbations. This implies that a somewhat higher efficiency could be achieved if the nozzle opening is correctly placed at 75 % fully open with the help of spear valve. This tests was also checked with CFD simulation using various flow and head conditions, resulted in approximately the same preferred operating point (see Fig 7.9 in the next section or refer back to section 5.3.1).

7.6. Comparison of the CFD and the Experimental Results

Although the Pelton turbine model is installed at the laboratory test rig and the total efficiency of the turbine has been measured experimentally, a direct comparison between numerical and experimental results was not easy.

The measured efficiency represents the total efficiency of the turbine including all losses according to the IEC standards, while only the hydraulic efficiency of the runner can be calculated numerically. The simulations were not also carried out on the buckets geometries destined to the real case, but on a scaled down model, to have a direct comparison with the experimental data obtained in the laboratory rig.

Therefore, to compare CFD results with experimental data, measuring/estimation of the mechanical loss of the test rig is necessary for the accurate evaluation of the turbine performance [see AppendixA-6] .

Based on analysis of available reports from, recent scientific publications [Barstad, L.F., 2012, Židonis, A.,2015, Zh. Zhang 2016], textbooks and manufacturer's materials, the amount of mechanical losses were estimated using IEC 60193-99 testing standard manual and some research experience as explained in Appendix A-6.

The operating conditions, numerical and experimental efficiencies and uncertainty values are tabulated in Table 7.3 and are also graphically represented on Fig.7.9. Experimental uncertainties for all calculated values of efficiency based on Eq.7.1 and Eq.7.8 were estimated to meet International Electro technical Commission (IEC) standards for ensuring the validity of the results. On the process of analysis, four operating conditions were selected in the CFD simulation to compare with the experimental test results' efficiency. The efficiency in the numerical analysis was calculated from torque averaged over time with only the last three periods. A detailed explanation of analysis based on CFD is included in Chapter 4, therefore it is not repeated here.

In Fig.7.9 performance curve was plotted at different volume flow rate and from the simulation data, the plot was overlaid with experimental data to make a comparison.

Table 7.3: Part-load Performance Characteristics of the turbine at n=650rpm.

Percentage of nozzle opening (%)	Inlet pressure (bar)	Flow rate (lit/sec)	CFD efficiency (%)	Experimental Hydraulic efficiency (%)	Experimental Uncertainty (%)	Relative error (%)
25%	1.45	3.4	71.47	70.86	3.38	0.86
50%	1.40	5.5	72.35	71.94	3.03	0.57
75%	1.35	7.8	82.79	81.64	2.55	1.34
Fully open (100%)	1.30	10.41	81.62	80.44	4.80	1.44

The best efficiency was obtained at 75% of nozzle opening from both experiment (81.64%) and simulation (82.79%) which find good agreement with each other. This predicted efficiency value by CFD simulation show an improvement of this runner is 3.9 % of the baseline design runner efficiency. This prediction was checked experimentally and it was found out that the efficiency improvement of the optimized runner design is 2.8 % of the baseline design efficiency.

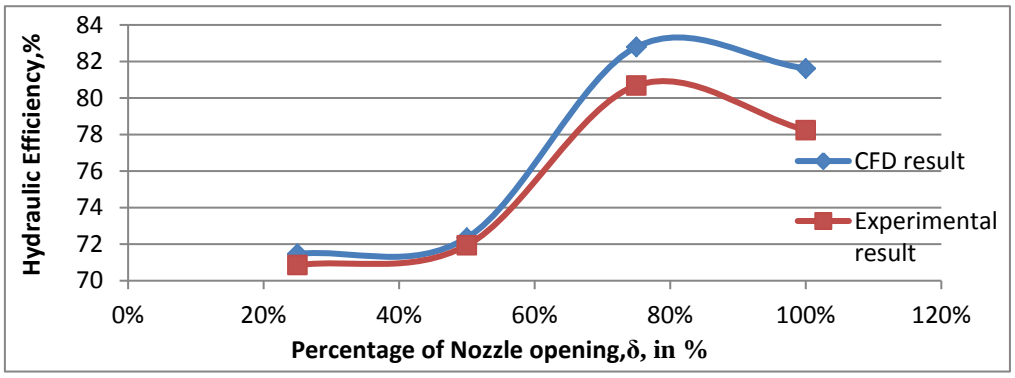

Figure 7.9: Comparison of the Part-load efficiency predicted by CFD with that obtained by Test.

The general pattern of all these results is quite similar with many reference research results, verifying the proper and qualitative design and construction process of the model turbine followed in the laboratory. The variation in the deviation between the CFD and experimental hydraulic efficiency measurements in this research, is smaller than the uncertainty of the experiments. These deviations are confirmed by other published numerical results [Barstad, L. F., 2012, Židonis, A.,2015,]. As can be observed in Fig.7.9, this discrepancy in value is much less at partial load than at full load. This might be due to the losses that have not been

incorporated in CFD analysis. If we consider the losses from the experiment on the simulation, the curve follows the trend of the experimental characteristic curve.

Evidently, for the purpose of validation and performance characterization, two Pelton turbines reported in the literatures were considered as mentioned in Chapter 5. Nevertheless, the design of the buckets suggested by these turbines are different, they were identical in terms of PCD with this study. The first turbine has PCD=400mm, a maximum efficiency of 82.5%, which was studied by Amod, (2014) for Khimti Hydropower in Nepal. The second turbine has also the same PCD (=400mm) but with a maximum efficiency of 86.7%, which was studied by A. Panagiotopoulos et.al, (2015) using a reference case correspond to a Pelton turbine installed in the LHT, at the National Technical University of Athens. Even though, the optimum efficiency presented in that research report might be different from this study because of the difference in bucket design used for the study, the result of this study is close enough to be validated for the design power range. Additionally, in agreement with these literatures, one can expect the CFD model results to over-predict that of the experiments. An over-prediction is indeed expected because the model does not account for various losses. These losses are mainly caused by the quality of manufacturing especially casting of buckets and back flow or splashing and water interference effect caused by the presence of a turbine housing in the experimental set up. Since a small amount of water which drops back to the Pelton wheel has been observed in this experiment, these losses were not included in the CFD model. There can be also human and instrumental errors in this experimental testing and also due to the discretization of the domains and solution of the differential equations in the use of computational methods for performance evaluation of our turbine model. This will lead to a bit increase in the hydraulic efficiency. However, based on the literature review and these experimental results, it is evident that power output of the turbine is close enough to be validated. This shows that the optimized design is the best in terms of lowering the manufacturing cost of the Pelton turbine.

7.7. Efficiency Scale-Up

The efficiency conversion from the model turbine to the prototype under consideration of the Reynolds number and other influence factors is called the efficiency scale-up. In this method, the scale-up calculation of the hydraulic efficiency from the model turbine to the prototype was given by using diverse dimensionless numbers and operation parameters of Pelton Turbines. Besides the bucket volumetric load, especially the Reynolds, Froude, and Weber numbers have been considered as the decisive influence parameters [Zh. Zhang, 2016].

In the simplified calculations, only the Froude numbers and the Reynolds have been used, as defined by Zh. Zhang (2016) using Eq. 7.12 and Eq. 7.13 respectively:

$$Fr = \sqrt{\frac{2gH}{gB}} \qquad [7.12]$$

From Eq. 7.12, the Froude number for this research model calculated to be, F_{rm}=18.17,for that of prototype is F_{rp}=25.

$$Re = \frac{\sqrt{2gH}}{\nu}.B \qquad [7.13]$$

Here, H and B are the net pressure head and the bucket width, respectively. Eq.7.13 gives the Reynolds for the model turbine and its prototype respectively as: Re_m=1.294×10^6,and Re_P=4.613×10^6 .

The corresponding proportion parameters between the model turbine and its prototype are denoted using Eq. 7.14 and Eq. 7.15 as follows:

$$C_{Fr} = \frac{F_{rp}}{Frm} \qquad [7.14]$$

$$C_{\mathrm{Re}} = \frac{\mathrm{Re}_p}{\mathrm{Re}_M} \qquad [7.15]$$

The corresponding proportions parameters calculated to be: C_{Fr}=1.376,and C_{Re}=3.565.

The bucket volumetric load can also be represented by the flow rate of a single injector (Q_{jet}). According to [Zh. Zhang,2016], it is thus defined by:

$$\prod_B = \left(\frac{d_o}{B}\right)^2 \qquad [7.16]$$

This yields 0.128 as design criterion for the bucket width. It is simply expressed by the ratio of the jet thickness to the bucket width.

According to Zh. Zhang (2016), the scale-up calculation of the turbine efficiencies is conducted by considering the difference in the efficiencies between the model and the prototype turbines as:

$$\eta_p = \eta_M + \Delta\eta \qquad [7.17]$$

With,

$$\Delta\eta = \frac{8.5\times10^{-7}}{\prod_B^2}\left(C_{Fr}^{0.3}\,C_{\mathrm{Re}} - 1\right) + 5.7\times\prod_B^2\left(1 - C_{Fr}^{0.3}\right) \qquad [7.18]$$

This yields Δη=-0.0092. Therefore, using Eq. 7.17 and 7.18, the corresponding prototype efficiency at the design flow rate and head of the turbine becomes, η_p=81.6%. The efficiency scale up diagrams are shown in Appendix E, Fig.E2.

CHAPTER 8
CONCLUSIONS AND RECOMMENDATIONS

This chapter includes the summary of the pertinent information of the research and reflects on the goals set and success in meeting them. Recommendations for the future work are also provided.

8.1. Summary

Information about the development of Pelton turbine is generally kept confidential by commercial companies; hence not much have been reported in literature, especially in the recent years. Therefore, the main objective of this thesis was to design, optimize, fabricate, and performance testing of a micro-hydro Pelton Turbine to fill this gap.

The required design data for turbine design like head and volume flow rate of a potential site in Ethiopia were taken from Oromia Energy office. The head of the water is 50m and the volume flow rate is 140 liter per second. The Pelton turbine has been designed to generate 38.4kW output power, assuming its overall efficiency of 56%. The design calculations used to generate the initial geometry of the Pelton runner (baseline design) were all based on those found in: [Jeremy, 2000 and Adams,1999] books.

Performance evaluation of a Pelton runner was accomplished with the help of CFD analysis tools. The simulation was performed on key part of the turbine which is the runner, by taking symmetrically sliced three buckets, half nozzle with 120°domain angle. This was done based on the suggestions of most recent studies using CFD methodologies that were available in the literature.

Different optimization methods for modeling and analysis were used. In each step large numbers of CFD analysis were carried out and the best geometry (Turbine runner) was selected for manufacturing.

Manufacturing of the model Pelton turbine set was done as per design specification of the optimal design by comparing it with the standard catalogue of Pelton turbine and availability of pattern for buckets of turbine. Manufacturing of bucket was done using sand casting using the 3D printed bucket as master pattern. This method was good to obtain the acceptable efficiency of the turbine and hence the method can be scaled up. Furthermore, manufacturing methodologies were developed to fabricate other parts of the turbine which play a significant role in gaining a good efficiency and hence the procedures can be used as a manufacturing manual for micro/small turbines fabrications.

Lastly, the model test was also carried out to verify the accuracy of CFD simulation following the guidelines of the international testing standard IEC 60193–Model acceptance tests. The input variables for the experiment was extracted from the CFD analysis model data in order to match the output of the simulation with the experiment. A water pump was used to generate the pressure head and volume flow rate in the AAiT laboratory. The volume flow rate and head was controlled by using the valve. When the valve was fully opened, the maximum volumetric flow rate and maximum head were obtained. In addition, the main uncertainties in each measuring instruments are also discussed in detail. As a result, the model test is proved trustworthy for simulating at different operating conditions. While in the case of 75 % of open spear valve position, the model test for the optimum design gives the best performance than the others, where the percentage in overall efficiency is found out to be 54.2% (82.79% hydraulic efficiency).

Overall, the final runner design differed from that of the baseline design in that the PCD was less by 100mm and the number of buckets was decreased from 18 to 15. Through the analysis, a weight reduction of around 7.6% is achieved. Moreover, since the main objective of this research was to improve the efficiency of an existing baseline design, the optimized design was compared to the baseline design under the same conditions. From the graph plotted, volume flow rate vs. efficiency, it was observed that efficiency developed at the optimum point was matching with the efficiency developed by the experiment. It was predicted by CFD simulation results that the efficiency improvement of this runner is 3.9 % of the baseline design runner efficiency. This prediction was checked experimentally and it was found out that the efficiency improvement of the optimized runner design is 2.8 % of the baseline design efficiency. This means, the results of CFD solved using commercial software ANSYS CFX over predicting the improvement in efficiency. The first reason for this deviation might be the quality of manufacturing (especially casting of bucket) and inconvenience test rig at AAiT. The second reason of the discrepancy appears to be due to the mechanical losses that were not possible to evaluate experimentally. The other reason is due to the assumption that the runner is not bounded by the casing and also due to the discretization of the domains in the use of CFD which were not taken into account in the CFD simulation.

The turbine examined here is a scaled down model of 1:0.53 of the full scaled design (Prototype). Hence, the efficiency result of the model runner was scaled up using scaling laws to that of the prototype to be 81.6%.

The model test is valid for efficiency test and Runaway test and in line with the literature references, verifying the turbine model design effectiveness, which gives reasonable

confidence in the accuracy of the CFD simulation model. Therefore, the presented results of the research, although a model, ensure availability of documented procedures for designing, constructing and performance testing of Pelton turbine. It would then no longer be necessary, to start the design from scratch.

8.2. Recommendations

Despite the fact that each hydropower site is unique, there is a potential for using this design for different high head flow condition, since it is standardized with PCD of the turbine runner. As a result, having a turbine of reduced size is a positive point, as it would reduce construction costs of the turbine itself and the costs associated to housing the turbine.

Finally, the presented results, along with the provided detailed geometric dimensions of the Pelton model runner, can be a benchmark for extended research. According to observation made during this research, the following recommendations can be reached that can be conducted for better prediction of the turbine efficiency. This can be done in order to get results with minimum errors.

- Further studies can be done on the all geometry of the Pelton turbine including the casing using CFD simulation. Neglecting the casing in the CFD simulation model might have caused inaccuracy in the result. This is one of the limitations of this research which should be considered for future works.
- Performance of the Pelton runner can be increased by various changes in the design that have an effect on different phenomena. Hence, other design parameters could be selected that are expected to influence the runner efficiency.
- Occurence of cavitation on the bucket surface need to be investigated.
- The manufacturing process of buckets was difficult as there is no experience in the country, hence further manufacturing technology and methods should be studied for casting of Pelton buckets.
- The design process should focuses on local contents in terms material selection and manufacturing facility for achieving maximum Pelton turbine efficiency.
- As hydraulic turbines are usually coupled to AC generators which run at a constant speed, it is essential in the future to design speed control system for Pelton turbine.
- A slight vibration of the model setup was experienced during the testing, causing scattered results. It is suggested to increase the stability in future tests by fixing the casing of the turbine with the ground.

Finally, this study recommends capacity building in Micro hydro power technology, transformation of research findings into real products to solve rural electrification problems.

REFERENCES

1. Adams Harvey,1999, *Micro hydro design manual*, a guide to small scale water power schemes.
2. Aklilu Dalelo(n.d.), *"Rural Electrification in Ethiopia":* opportunities and bottlenecks, Addis Ababa University, College of Education.
3. Anagnostopoulos, J. S. and D. E. Papantonis, 2012. *A fast Lagrangian simulation method for flow analysis and runner design in Pelton turbines.* Journal of Hydrodynamics, Ser. B 24(6), pp.930-941.
4. Anderson, J. D., 1995. *Computational Fluid Dynamics: The Basics with Applications.* New York: McGraw-Hill .
5. ANSYS Inc. ANSYS CFX- Solver Theory Guide, Release 12.1 (2009, November).
6. ANSYS Inc. ANSYS Modeling and Meshing Guide, Release 10.1 (2005, August).
7. ANSYS Inc., 2013a. ANSYS CFX Solver Modeling Guide, Release 15. Canonsburg, USA: ANSYS, Inc.
8. ANSYS Inc., 2013b. ANSYS CFX Solver Theory Guide, Release 15. Canonsburg, USA: ANSYS, Inc.
9. ANSYS Inc., 2013c. ANSYS Fluent Theory Guide, Release 15. Canonsburg, USA: ANSYS, Inc.
10. Atthanayake, I. U., 2009. *Analytical study on flow through a Pelton turbine bucket using boundary layer theory.* International Journal of Engineering and Technology *9*(9), pp. 241-245.
11. Avellan, F., P. Dupont, S. Kvicinsky, L. Chapuis, E. Parkinson and G. Vullioud, 1998. *Flow Calculations in Pelton Turbines*,-Part 2: Free Surface Flows. In: IAHR Proceedings of the19th IAHR Symposium, Singapore, Republic of Singapore, 1998, Vol. 1. No. LMH-CONF-1998-002.
12. Barstad, L.F.,2012. *CFD Analysis of a Pelton Turbine*. Master. Norwegian University of Science and Technology.
13. Batchelor, G. K., 1973. *An introduction to fluid Dynamics.* Cambridge: Cambridge University Press.
14. Benzon, D.,A. Židonis, A. Panagiotopoulos, G. A. Aggidis, J. S. Anagnostopoulos and D.E.Papantonis,2015a. *Impulse turbine injector design improvement using Computational Fluid Dynamics.* Journal of Fluids Engineering 137(4), p. 041106.

15. S. Melessaw, *"Ethiopia's Small Hydro Energy Market-GiZ–target market analysis-hydro-Ethiopia,2009"* http://www.germanenergysolutions.de/enwww.gtz.de/projektentwicklungs program.
16. Y. Beucher, E. Boulawz Ksayer, D. Clodic, 2010,*Characterization Of Friction Loss In Pelton Turbine:* Center of Energy and Processes, Ecole des Mines de Paris, Paris, FRANCE
17. Eisenring, M., 1991. *Micro Pelton turbines.* St. Gallen, Switzerland: Swiss Center for Appropriate Technology.
18. European Commission, 2009. Directive 2009/28/EC of the European Parliament and of the Council of 23 April 2009 on the promotion of the use of energy from renewable sources and amending and subsequently repealing Directives 2001/77/EC and 2003/30.
19. European Small Hydropower Association. *Small hydropower for developing countries, 2005*,http://www.esha.be/fileadmin/esha_files/documents/publications/publications/Brochure SHP for Developing Countries.pdf [accessed 08.02.2011].
20. Favre,J.,H. Garcin and E. Parkinson, 2005.*Computational analysis in Pelton hydraulic turbines.*
21. Ferreño, D., J. Álvarez, E. Ruiz, D. Méndez, L. Rodríguez and D. Hernández, 2011. *Failure analysis of a Pelton turbine manufactured in soft martensitic stainless steel casting.* Engineering Failure Analysis 18(1), pp. 256-270.
22. Fulton, A., 1937. *Present Tendencies in Water Turbine Machinery*. Proceedings of the Institution of Mechanical Engineers 135(1), pp. 387-444.
23. Furnes, K., 2013. *Flow in Pelton turbines.* Master. Norwegian University of Science and Technology.
24. Gupta,V.,V. Prasad and R. Khare, 2014. *Effect of Jet Shape on Flow and Torque Characteristics of Pelton Turbine Runner.* International Journal of Engineering Research and Application 4(1), pp. 318-323.
25. Gupta,V. and V. Prasad, 2012. *Numerical investigations for jet flow characteristics on Pelton turbine bucket.* International Journal of Emerging Technology and Advanced Engineering 2(7), pp. 364-370.
26. Hana, M., 1999. *Numerical analysis of non-stationary free surface flow in a Pelton bucket.* Ph. D. Norwegian University of Science and Technology.
27. Hydraulic Turbines, Storage pumps and pump turbines- Model acceptance tests (IEC 60193), 1999 .

28. Janetzky, B., E. Göde, A. Ruprecht, H. Keck and C. Schärer, 1998. *Numerical simulation of the flow in a Pelton bucket.* In: IAHR, Proceedings of 19th IAHR Symposium on Hydraulic Machinery and Cavitation, pp. 276-283. Singapore, 9-11 September 1998.
29. Joseph E. Shigley, Charles E. Mischke and Thomas H.Brown, jr.mechanical engineering design, 8thed., McGraw Hill, New York 2008
30. Jošt, D., P. Mežnar and A. Lipej, 2010. *Numerical prediction of Pelton turbine efficiency.* In: IAHR, 25th IAHR Symposium on Hydraulic Machinery and Systems, IOP Conf. Series: Earth and Environmental Science, 012080. Timisoara, Romania, 20-24 September 2010.
31. Jošt, D.,A. Lipej and P. Meznar, 2008. *Numerical Prediction of Efficiency, Cavitation and Unsteady Phenomena in Water Turbines.* In: ASME 2008, 9th Biennial Conference on Engineering Systems Design and Analysis, pp. 157-166. Haifa, Israel, 7-9 July 2008.
32. Keck, H. and M. Sick, 2008. *Thirty years of numerical flow simulation in hydraulic turbo machines.* Acta mechanica 201(1-4), pp. 211-229.
33. Klemensten, L.A.,2010. *An experimental and numerical study of the free surface Pelton bucket flow*. Master. Norwegian University of Science and Technology.
34. Koukouvinis, P. K., J. S. Anagnostopoulos and D. E. Papantonis, 2010. *Flow Analysis Inside a Pelton Turbine Bucket Using Smoothed Particle Hydrodynamics*. In: HYDRO 2010 International Conference. Lisbon, Portugal, 2010.
35. Krause, E., 2014. The Millennium-*Problem of Fluid Mechanics–The Solution of the Navier Stokes Equations.* The History of Theoretical, Material and Computational Mechanics Mathematics Meets Mechanics and Engineering, Springer: pp. 317-341.
36. Kvicinsky,S.,J.-L. Kueny, F. o. Avellan and E. Parkinson, 2002. *Experimental and numerical analysis or free surface flows in a rotating bucket.* In: IAHR, The proceeding of the 21st IAHR Symposium on hydraulic machinery and systems, Lausanne, Switzerland, 9-12 September 2002.
37. Liang Q W, Keller M, 2010, *Behaviour of Pump Turbines Operating at Speed no Load* Condition in Turbine Mode.J. Proceedings of Hydro Vision, 27-39.
38. Marongiu, J.C., F.Leboeuf, J. Ë. Caro and E. Parkinson, 2010. Free surface flows simulations in Pelton turbines using an hybrid SPH-ALE method. Journal of Hydraulic Research 48(S1), pp.40-49.

39. Matthias, H. B. and O. Promper, 2004. *Numerical simulation of the free surface flow in Pelton turbines.* In: The 6th International Conference on Hydraulic Machinery and Hydrodynamics. Timișoara, Romania, 21-22 October 2004.
40. Nechleba. M, 1957, *Hydraulic Turbines, Their Design and Equipment.*
41. Panthee, A.,H.P. Neopane and B. Thapa, 2014. *CFD Analysis of Pelton Runner.* International Journal of Scientific and Research Publications 4(8), pp. 1-6.
42. Parkinson, E., G. Vullioud, L. Geppert and H. Keck, 2002. *Analysis of Pelton turbine flow patterns for improved runner-component interaction.* International Journal on Hydropower & Dams 9(5), pp. 100-103.
43. Parkinson, E., H. Garcin, G. Vullioud, F. Muggli, Z. Zhang and E. Casartelli, 2002. *Experimental and numerical investigations of the free jet flow at a model nozzle of a Pelton turbine.*
44. Parkinson, E.,C. Neury, H. Garcin, G. Vullioud and T. Weiss, 2006. *Unsteady analysis of a Pelton runner with flow and mechanical simulations.* International Journal on Hydropower & Dams 13(2), pp. 101-105.
45. Patel, K., B. Patel, M. Yadav and T. Foggia, 2010. *Development of Pelton turbine using numerical simulation.* In: IAHR, 25th IAHR Symposium on Hydraulic Machinery and Systems, IOP Conf. Series: Earth and Environmental Science, 012048. Timisoara, Romania, 20-24 September 2010.
46. Pelton Water Wheel Company, 1898. *The Pelton Water Wheel.* Embracing in Its Variations of Construction and Application the Pelton System of Power. San Francisco, USA: Pelton Water Wheel Company.
47. Rainbow Micro Hydro Instruction Manual, Certified by: OFFICE OF ENERGY (NSW) Certificate of Suitability Number: 6273.
48. Perrig, A., 2007. *Hydrodynamics of the free surface low in Pelton turbine buckets.* Ph. D. Thesis. École polytechnique fédérale de Lausanne.
49. Perrig, A., F. Avellan, J.-L. Kueny, M. Farhat and E. Parkinson, 2006. *Flow in a Pelton turbine bucket: numerical and experimental investigations.* Journal of Fluids Engineering 128(2), pp.350-358.
50. Solemslie, B. and O. Dahlhaug, 2012. *A reference Pelton turbine design*. In: IAHR, 26thIAHR Symposium on Hydraulic Machinery and Systems, IOP Conf. Series: Earth and Environmental Science, 032005. Beijing, China: 19-23 August 2012.
51. Sanam Pudasaini, Hari Prasad Neopane, Amod Panthee, Anuj Pathak and Bhoj Bahadur Chaudhary; *Computational Fluid Dynamics (CFD) analysis of Pelton runner*

of Khimti Hydro-power Project of Nepal, Published in Rentech Symposium Compendium, Volume 4, September 2014.

52. A Santolin; G Cavazzini; G Ardizzon and G Pavesi, *Numerical investigation of the interaction between jet and bucket in a Pelton turbine.* Proceedings of the Institution of Mechanical Engineers, Journal of Power and Energy, 223(6), pp. 721-728.Part A:.
53. Thake, Jeremy, 2000. *The micro-hydro Pelton turbine manual: design, manufacture and installation for small-scale hydro-power*. London: ITDG publishing.
turbo machinery, Vol. 128.
54. Turboinštitut, Rovšnikova, D Jošt, P Mežnar and A Lipej, Ljubljana, 2010, Slovenia, *Numerical prediction of Pelton turbine efficiency*, 25th IAHR Symposium on Hydraulic Machinery and Systems.
55. Tilahun N, Wondwossen B, Feyisa B, and Edessa D, July 2017, *Feasibility study for power generation using off- grid energy system from micro hydro-PV-diesel generator-battery for rural area of Ethiopia:* The case of Melkey Hera village, Western Ethiopia, AIMS Energy vol. 5, no.4, pp.667-690, 2017.
56. *World Small Hydropower Development Report 2013– The Need For Further Resource Assessments,* L. Esser, International Center on Small Hydro Power, Division of Multilateral Development, Hangzhou, CHINA
57. Xiao, Y., T. Cui, Z. Wang and Z. Yan, 2012. *Numerical simulation of unsteady free surface flow and dynamic performance for a Pelton turbine*. In: IOP Publishing, IOP Conference Series: Earth and Environmental Science. 15(5), p. 042033.
58. Xiao, Y., Z. Wang, J. Zhang, C. Zeng and Z. Yan, 2014. *Numerical and experimental analysis of the hydraulic performance of a prototype Pelton turbine.* Proceedings of the Institution of Mechanical Engineers, Part A: Journal of Power and Energy 228(1), pp. 46-55.
59. Zhang, Z. and M. Casey, 2007. *Experimental studies of the jet of a Pelton turbine. Proceedings of the Institution of Mechanical Engineers,* Part A: Journal of Power and Energy 221(8), pp. 1181-1192.
60. Zh. Zhang, *Pelton Turbines,2016,* Springer International Publishing Switzerland, ISBN 978-3-319-31909-4 (eBook).
61. Židonis, A. and G. Aggidis, 2015a. *Pelton Turbine: Identifying the Optimum Number of Buckets Using CFD.* Journal of Hydrodynamics, Ser. B (in-press).
62. Židonis, A. and G. Aggidis, 2015b. *State of the art in numerical modeling of Pelton turbines.*

63. Židonis, A., A. Panagiotopoulos, G. A. Aggidis, J. S. Anagnostopoulos and D. E. Papantonis, *Parametric Optimization of Two Pelton Turbine Runner Designs Using CFD.* Journal of Hydrodynamics, Ser. B 27(3), pp. 403-412.
64. Židonis, A., D. S. Benzon and G. A. Aggidis, 2015. *Development of Hydro Impulse Turbines and New Opportunities*. Renewable and Sustainable Energy Reviews, pp 1624–1635.
65. Zoppé, B., C. Pellone, T. Maître and P. Leroy, 2006. Flow analysis inside a Pelton turbine bucket. Journal of Turbomachinery, vol. 128(3),pp 500-511.

LIST OF APPENDICES

Appendix A: Basic design of shaft, Casing, nozzle, deflector, selection of Bearing and Power loss calculation for Pelton Turbine.

Design Summary:

Site Data:

Rated Discharge=0.14m^3/s, Gross Head=50m, and Net Head at Rated Discharge=47.5m.

Arrangement: horizontal with runner on turbine shaft.

Table A-1:Design Summary of the optimal Pelton Turbine Geometry.

Description	**Unit**	**Value**	**Available Design Guideline**
Generator data	Hz	50	
Generator data	Rpm	1500	4-pole is preferable
Intake Type:		2 – JET	
Runner Pitch Diameter:	mm	400	
Specific Speed at Rated Net Head (turbine) per jet		36.2	
At Maximum Net Head of	meters	47.5	
Maximum Out Put Power of Turbine	KW	48.123	
Runner Efficiency of Turbine Assumed	%	80	[Jeremy, 2000]
Maximum Runaway Speed (at Max. Net Head):	rpm	1235	1.9 times 650
D/B Ratio (Runner Pitch Dia./Bucket Width):	-	2.633	Bucket width>80mm
Approximate Runner and Shaft Weight:	Kg	64.523	
Inlet Diameter of the nozzle	mm	244	
Nozzle Diameter	mm	68	
Jet Orifice Diameter	mm	56	
Needle Stroke	mm	61	
Centerline to Inlet distance	mm	2374	
Jet to Jet Included Angle: 60 to 90	Degrees	62	[Jeremy, 2000]
Housing/Discharge Geometry:			[Jeremy, 2000]
Centerline to Housing Top:	mm	600	1.5×PCD
Housing Width:	mm	800	3×PCD
Discharge Width:	mm	600	1.5×PCD
Overall Shaft Length:	mm	975	
Turbine Shaft Diameter:	mm	60	

A-1. Clamping of Buckets

For a two bolt clamping arrangement, design decisions taken with reference to Figure A-1. The force on each bolt is made up of two components one which is the direct shear from the jet force, S, and the other, T, which comes from the moment generated by the jet force.

R_1= 80mm (20% of PCD), R_2= 116mm (29% of PCD), Bolt 1 is M10 (2.5% of PCD), Bolt 2 is M12 (3.0 % of PCD),

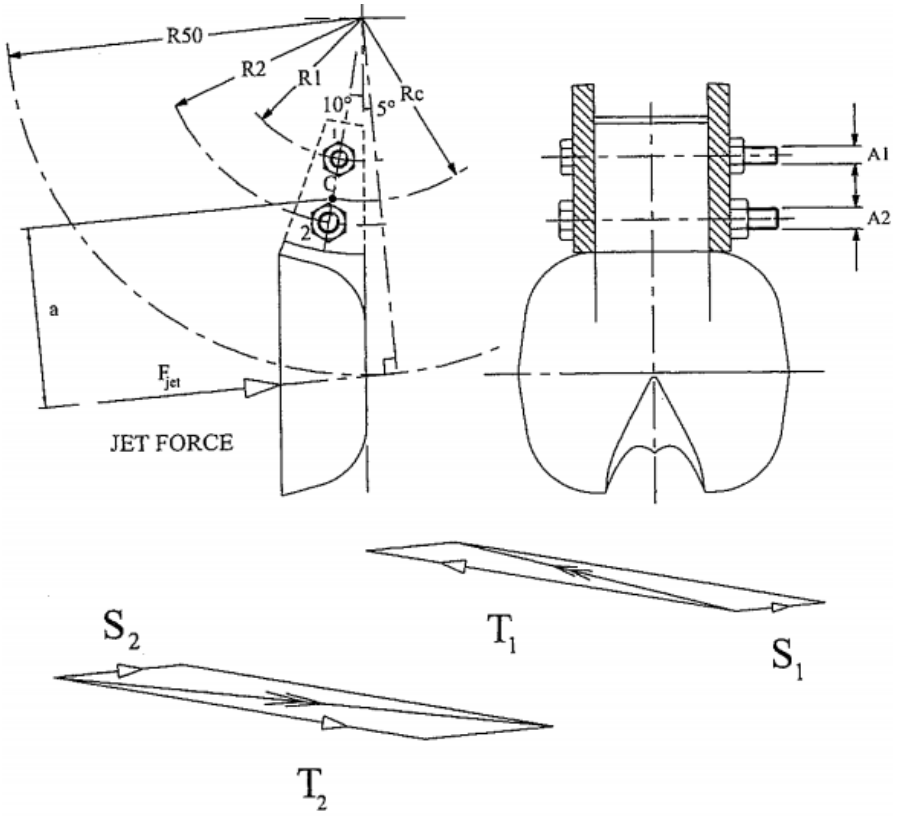

Figure A-1: A Pelton bucket clamped between the two sides of a hub by two bolts [Jeremy 2000].

The shear component in the bolts is given by the following formula:

$$S_1 = F_{jet} \times \frac{A_1}{A_1 + A_2} \qquad [A\text{-}1]$$

$$S_2 = F_{jet} \times \frac{A_2}{A_1 + A_2} \qquad [A\text{-}2]$$

Where, A_1 and A_2 are cross sectional area of bolts 1 and 2 respectively and determined as:

$$A_1 = \pi \times \frac{d_1^{\,2}}{4} = \pi \times \frac{10^2}{4} = 78.5\,\text{mm}^2$$

$$A_2 = = \pi \times \frac{d_2^{\,2}}{4} = \pi \times \frac{12^2}{4} = 113.1\,\text{mm}^2$$

Shear force on the bolts is therefore,

$$S_1 = 4144\text{N} \times \frac{78.5}{113.1 + 78.5} = 1697.8N$$

$$S_2 = F_{jet} \times \frac{A_2}{A_1 + A_2} = 4144 \times \frac{113.1}{113.1 + 78.5} = 2446.2N$$

The moment component is given by:

$$T_1=T_2=F_{jet}\times\frac{a}{R_2-R_1} \quad [A\text{-}3]$$

Where, R_1 and R_2 are radius from runner centerline to centers of bolts 1 and 2 respectively. The dimension 'a' is the moment arm of the jet force about the centroid 'c' which lies between the bolts at a radius calculated by:

$$R_c=\frac{A_1R_1+A_2R_2}{A_1+A_2} \quad [A\text{-}4]$$

The centroid 'c' for the bolts is:

$$R_c=\frac{A_1R_1+A_2R_2}{A_1+A_2}=\frac{78.5\times80+113.1\times116}{78.5+113.1}=101.25mm$$

The force vectors found above drawn on the bucket where the shear component vectors drawn parallel to the jet force and the moment components drawn perpendicular to the radial line through the bolts center at their centroidal point 'c'. So vector addition of S_1 + T_1 and S_2 +T_2 gives the force on each bolt. So the value of a (the moment arm) is 102.2mm. The moment components become:

$$T_1=T_2=F_{jet}\times\frac{a}{R_2-R_1}=4144\times\frac{102.2}{116-80}=11764.35N$$

Using the cosine law, we can find the resultant force R_1:

$R_1^2= S_1^2 + T_1^2 - 2\ S_1T_1\cos\beta$

$= (1697.8^2 + 11764.35^2 -2\times1697.8\times11764.35\cos15^0)^{1/2}$

$R_1 = 10.1KN$

Similarly for resultant force R_2 on bolt 2:

$R_2^2= S_2^2 + T_2^2 - 2\ S_2T_2\cos\beta$, which gives:

$R_2 = (2446.2^2 + 11764.35^2 - 2\times2446.2\times11764.35\cos165)^{1/2}$

$R_2= 14.14KN$

From the Table A-2, bolt and bolted joint properties for Grade 8.8 M10 and M12 high tensile steel we have friction load capacity of 4.8KN for bolt 1(M10) and 7KN for bolt 2(M12). This is less than the bolt load, so the clamping is insufficient by itself.

Table A-2: Bolt and Bolted Joint Properties [Jeremy 2000].

Grade 4.6 Black mild steel				**Grade 8.8 high tensile steel**	
Bolt dia.(mm)	Pitch(mm)	Friction load (KN)	Torque(Nm)	Friction load(KN)	Torque (Nm)
M5	0.8	0.5	2.6	1.2	6.8
M6	1	0.6	4.5	1.7	11.6
M10	1.5	1.9	21.7	4.8	55.9
M12	1.75	2.7	37.9	7	97.5
M16	2	5	94.4	12.9	242.9
M20	2.5	7.9	184.4	20.2	474.4
M24	3	11.3	318.7	29.1	819.7

For Grade 8.8 M16 and M20 bolts the figures increases to 12.9KN and 20.2KN, which are OK. We have also a safety factor of 1.3 for bolt 1 and 1.43 for bolt 2. Friction clamping alone would be acceptable for this case.

A-2. Design of a Pelton Turbine Shaft

The shaft design has been based on the maximum bending moment criterion and returns a conservative result. Following is the procedure followed [Adam Harvey,1999]:

- Calculation of Belt Tension
- Calculation of Bearing Loads
- Calculation of Maximum Bending Moment and shaft diameter using formula:

Generally two types of arrangements are used in Pelton turbines: Horizontal shaft and Vertical shaft arrangement. Vertical units require less floor space and are often used for large capacity multi-nozzle units [Adam Harvey,1999]. The main argument for choosing a horizontal installation in this research project is:

- Its flexibility and horizontal shaft turbines are suitable for small hydro applications that have less water available.
- The horizontal rig also has the benefit of making it easier to observe the model turbine during testing.

A-2-1. Shaft lay out/ Geometric Analysis

The general lay out of a shaft to accommodate shaft elements example bearings, pulley and turbine must be specified in the design process in order to perform a free body force analysis and to obtain a shear moment diagram. Considering the turbine and drive system shown diagrammatically in Fig. A-2. We chose a horizontal shaft, 2-jet pelton with one jet vertical one jet horizontal. Each jet acts on the runner with a force of 4144N as calculated before. The

shaft is supported on two bearings. The weight of the shaft can be ignored. The turbine drives a generator through a flat belt drive system as shown in Fig.A-2.

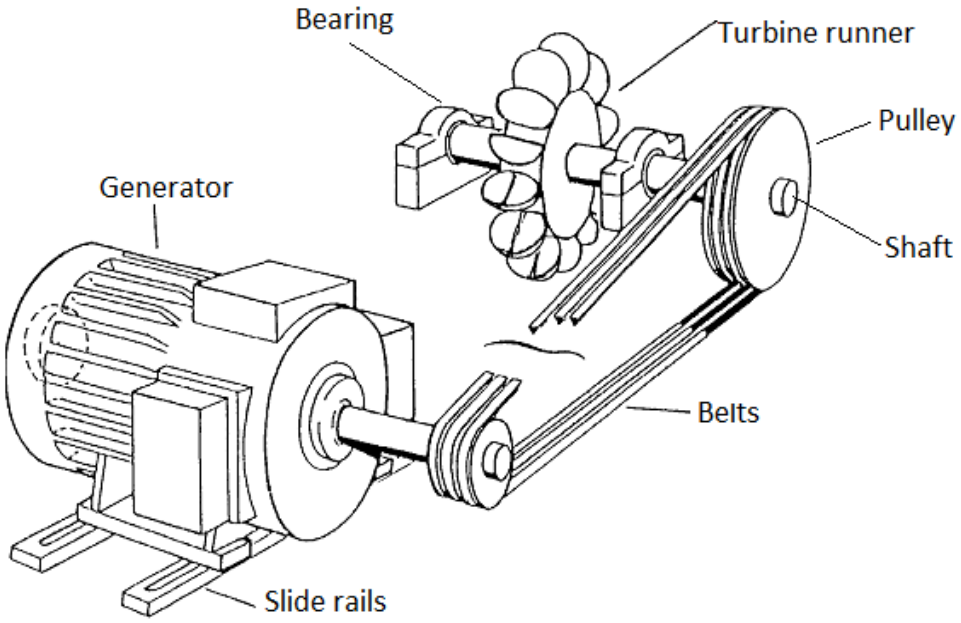

Figure A-2: Pelton Turbine belt drive system [Adams Harvey,1999].

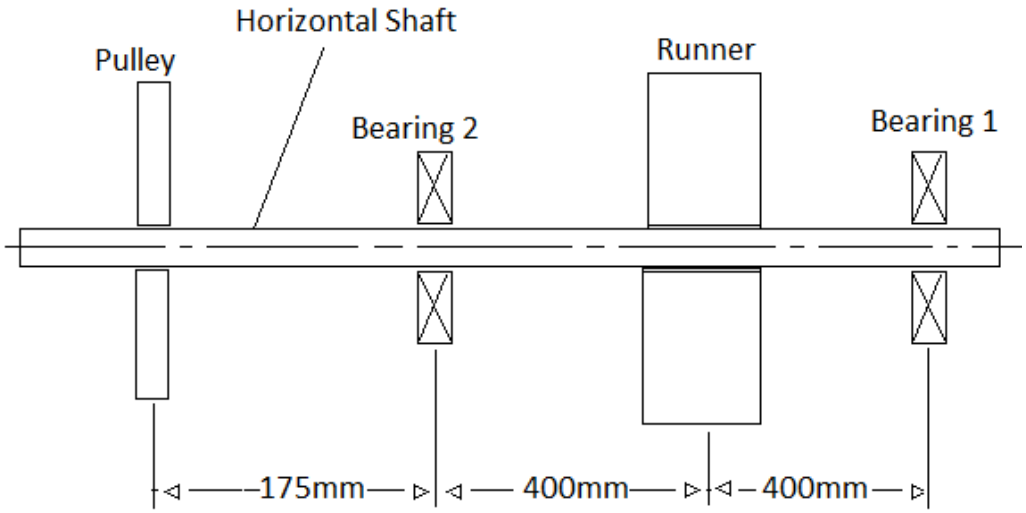

Figure A-3: Shaft Lateral Dimension

For the calculation of the shaft diameter of the turbine rotor, bending moments and torsion moments must be considered. The shaft mostly has a larger diameter in the middle than at the ends. An idealization of the system is given in the sketch in Fig. A-3 and Fig. A-4.

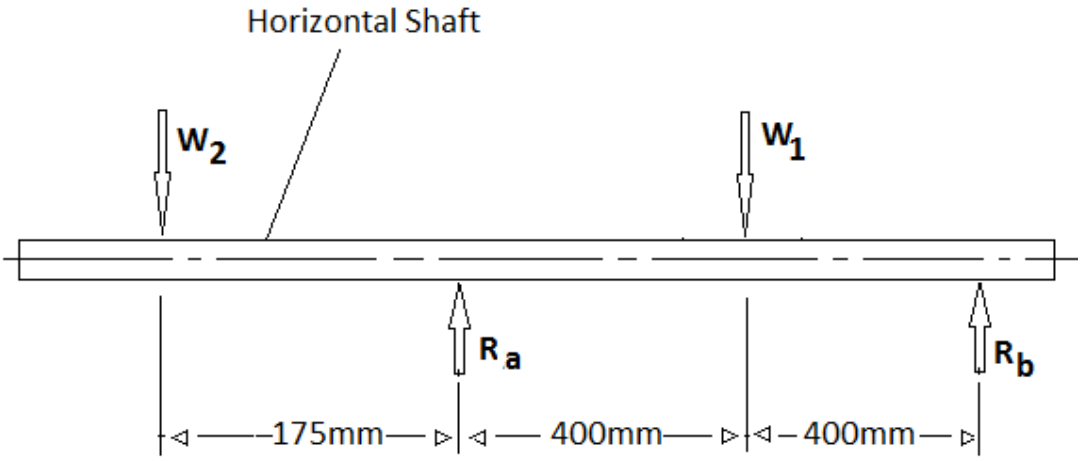

Figure A-4: Idealization of turbine as a simply supported beam system.

The turbine is idealized as a simply supported beam of length 800mm with cantilevered length 175mm. The weight of the turbine itself is modeled as a load W_1, the load due to tension force imparted by the belt is modeled as W_2. A Pelton turbine shaft has torsion and bending forces acting on it. The torsion transmits the power out from the runner. The bending moment arises from the jets forces on the runner, the weight of the runner and shaft, the bearing reactions, and from the belt tension.

Weight of pulley and belt:-The most common types of drive for micro hydro systems are flat belts or v/wedge belts [Jeremy 2000]. Table A-3 gives some recommendations for the schemes, and the approximate speed ratios that can be safely achieved.

Table A-3: Recommended belt types for different scheme sizes [Jeremy 2000].

Power	Up to 8kW	8 to 20kW	20-50kW	Over 50kW
Recommended type	Any	Any flat belt wedge belt	Synthetic flat belt wedge belt	Synthetic flat belt only
Maximum ratio	1:5	1:4	1:3:5	1:3

From the above table, we can select Synthetic flat belt. Based on a real micro hydro plant, the weight of the pulley (W_2) is 1000 N [Jeremy 2000].

Weight of runner (W_1):- Calculated using the volumetric dimensions of the turbine and the densities of the materials used. The mass of a Pelton runner with 400mm PCD and casted from cast iron is near 64.523kg. This is determined using Catia V5 as shown in Fig. A-5. The weight of turbine (W_1) is found out to be 633N.

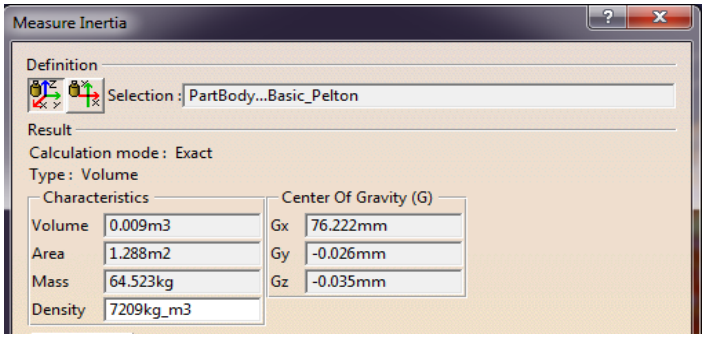

Figure A-5: Determination of Inertia using Catia V5

Force from jet:- On the previous section, we show that the jet force is F_{jet}=4144N. The inclination angle for the jet force was optimized to be -15^0 from the horizontal axis. The outer surface of the bucket inclined from the vertical axis at -5^0. Hence, the force of the jet in the z and y plane can be calculated as:

$(F_{jet})_z$=4144 cos -5^0=4128N, $(F_{jet})_y$=4144 sin -5^0=361N

Force from pulley initial tension:-The turbine drives a generator through a flat belt drive system, which acts on the turbine pulley with a force of 6000N, 15^0 below horizontal [Jeremy 2000]. So $(F_i)_z$=F_i cos β=6000×cos 15^0=5795.6N, $(F_i)_y$=Fi sin β=6000×sin 15^0=1553N.

The torque produced by the jet: $T = F_{jet} \times \frac{PCD}{2} = 4144 \times \frac{400}{2} = 828.8Nm$

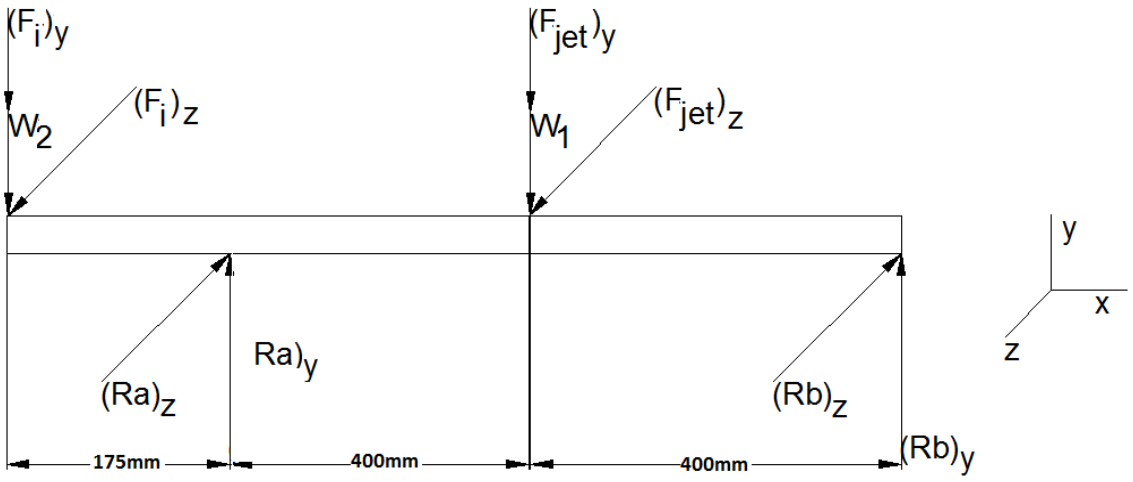

Figure A-6: Forces acting on the shaft and their arrangment.

$(F_i)y + W_2$=1553N+1000N=2553N. This is the tensile force attributed to the belt tensioning of the transmission system and includes weight of the pulley.

$(F_{jet})y + W_1$=361N+633N=994N

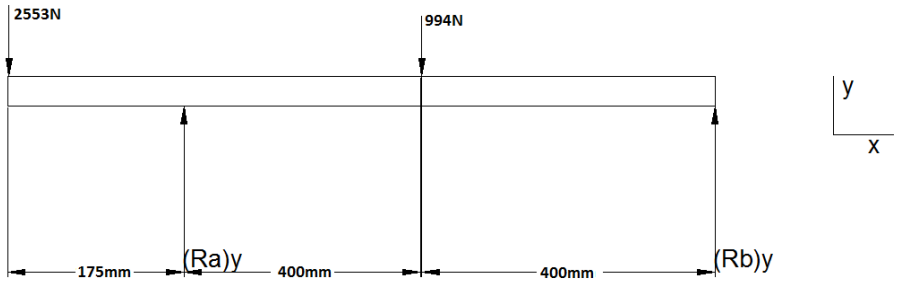

Figure A-7: Force on XY plane

Finding the reactions :

$$\sum M_b = 0 \rightarrow (Ra)_y \times 0.8 = 2553N \times 0.975m \Rightarrow (Ra)_y = 3111.5N$$

$$\sum Fy = 0 \rightarrow (Ra)_y + (Rb)_y = 2553N + 994N \Rightarrow (Rb)_y = 435.5N$$

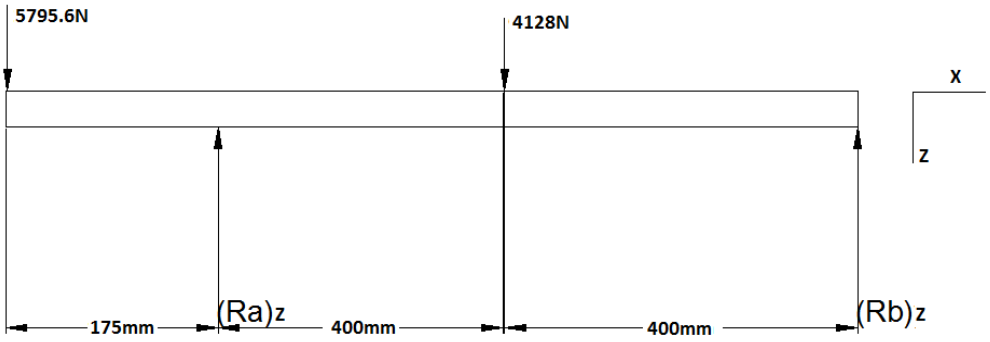

Figure A-8: Force on xz plane

Finding the reactions:

$$\sum M_b = 0 \rightarrow (Ra)_z \times 0.8 = 5795.6N \times 0.975m \Rightarrow (Ra)_z = 7063.4N$$

$$\sum Fy = 0 \rightarrow (Ra)_z + (Rb)_z = 5795.6N + 4128N \Rightarrow (Rb)_z = 2860.2N$$

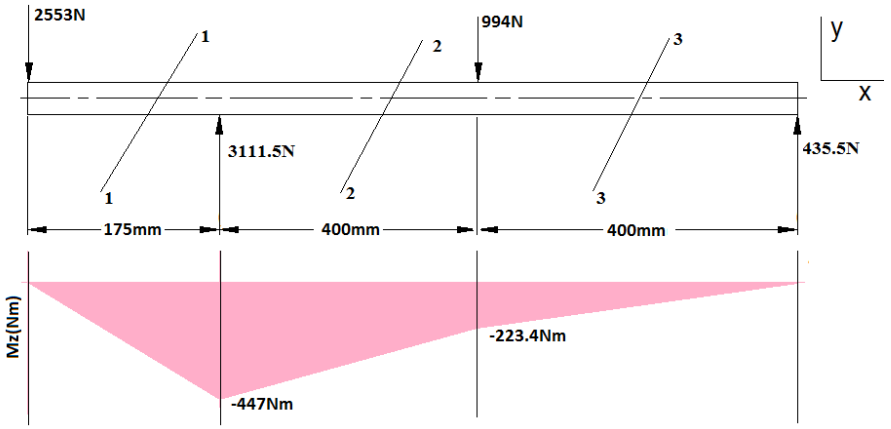

Figure A-9: Moment's diagram on a Pelton shaft xy plane.

Section 1-1 (0mm<x<175mm)

V=2553N, Mz=-2553x Nm

Section 2-2 (175mm<x<575mm)

V=3111.5N-2553N=558.5N, Mz=-2553x+ 3111.5(x-0.175) = (558.5x-544.5) Nm

Section 3-3(575mm<x<975mm)

V=-435.5N, Mz=435.5(0.975-x) = (-435.5x+424.6) Nm

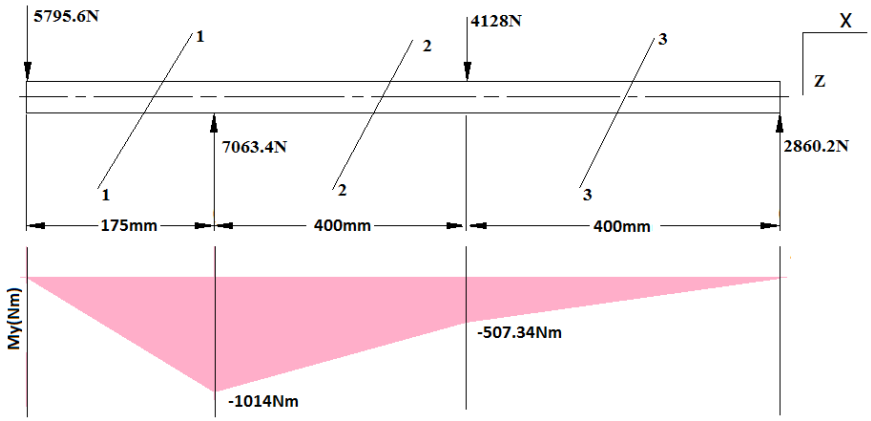

Figure A-10: Moment's diagram on a Pelton shaft xz plane.

On the XZ plane:

Section 1-1 (0mm <x<175mm):

V=5795.6N, My=5795.6x Nm

Section 2-2(175mm<x<575mm):

V=5795.6N-7063.4N=-1267.8N, My=5795.6x-7063.4(x-0.175) = (-1267.8x+1236.1) Nm

Section 3-3(575mm<X<975mm):

V=2860.2N, My=2860.2(0.975-x)

Combine orthogonal moment vectors to get total moments:

$$M = \sqrt{\left(M_y^2 + M_z^2\right)} = \sqrt{\left(1014^2 + 447^2\right)} = 1108.2Nm$$

Start with the point at which the bending moment is high, there is a stress concentration at the shoulder and torque. When the diagrams are drawn, the result is that both the largest bearing force and the greatest bending moment are found to be at bearing 2.

The calculation of nominal shaft diameter is based on the torque transmitted with typical safety factors. On horizontal Pelton turbines, side forces (runner weight and hydraulic thrust loads) are accounted for, in the calculation of the shaft diameter, as necessary, to limit excessive shaft bending. The shaft about to be design should sustain the largest magnitude at bearing 2 with a magnitude of 1108.2Nm. Using the usual design methdology**.** Assume generous fillet radius for the turbine position.

According to *Joseph E. Shigely,2008,* for first iteration estimates for stress concentration factors is:

$Kf = Kt = 1.7, Kfs = Kts = 1.5$

The selected materials where **AISI 1050 CD steel** with properties :

$Sut = 690MPa, Sy = 640MPa$

The endurance limit S_e is: $S_e = Ka * Kb * Kc * Kd * Ke * Kf * Se'$

For S_{ut}<200kpsi (1400MPa), $Se' = 0.5Sut0.5 * 690MPa = 345MPa$

The load factor, Ka , is: $K_a = aSut^b$ where a=4.51, b= -0.265

so $K_a = 4.51 * 690^{-0265} = 0.80$

Guess K_b=0.8(size factor), $Kc = Kd = Ke = Kf = 1$ for first estimate [*Joseph E. Shigely,2008]*, $Se = KaKbKcKdKeKfSe'$=0.8×0.8×345Mpa=221Mpa

For first estimate at the small diameter at the shoulder point, use the DE Goodmann criterion [*Joseph E. Shigely,2008]*. This criteria is good for the initial design, since it is simple and conservative with $Mm = Ta = 0$, design factor of safetey(n)=1.5, the equation reduced to:

$$d = \left\{\frac{16n}{\pi}\left(\frac{2(KfMa)}{Se} + \frac{[3(KfsTm)^2]^{\frac{1}{2}}}{Sut}\right)\right\}^{\frac{1}{3}} \quad \text{[A-5]}$$

$$d = \left\{\frac{16\times1.5}{\pi}\left(\frac{2(1.7\times1108.2)}{221\times10^6} + \frac{\left[3(1.5\times828.8)^2\right]^{\frac{1}{2}}}{690\times10^6}\right)\right\}^{\frac{1}{3}} = 53.6mm$$

This is the minimum diameter; the shaft could not be manufactured smaller than this diameter. The next standard shaft diameter will be d=55mm. Shoulders are made for each shaft element. Each shoulder is made with an increment of 5mm to make them standard shaft sizes [*Joseph E. Shigely,2008]*. Hence, a nominal 60mm cold drawn shaft diameter can be used.

Check for safety (Check if estimates were acceptable): From groove of round bar in bending and tension [*Joseph E. Shigely,2008]*, we have:

D/d=60mm/55mm=1.09

Fillet radius: r= (D-d)/2= (60-55)/2=2.5mm

So r/d=2.5/55=0.045, K_t=2.18, K_{ts}=1.45

From notch sensitivity chart for steel [*Joseph E. Shigely,2008]*, we have $q = 0.7, qs = 0.9$

So fatigue stress concentration factor K_f:

K_f=1+q (K_t-1) =1+0.7(2.18-1) =1.826, K_{fs}=1+q_s (K_{ts}-1) =1+0.9(1.45-1) =1.405

Size factor K_b is given by:

$K_b = 1.51d^{-0.157} = 1.51(0.052)^{-0.157} = 2.4$

Loading factor K_c, Temperature factor K_d, Reliability factor K_e, miscellaneous factor K_f

$Kc = 1, Kd = 1, Ke = 1, Kf = 1$

The modified endurance limit is:

$Se = ka * kb * kc * kd * ke * kf * Se'$= (0.8) (2.4)345Mpa=662.4Mpa

So alternating stress is: $\sigma_a = \frac{32K_f Ma}{\pi d^3} = \frac{32(1.826)(1108.2)}{\pi(0.052)^3} = 146.6Mpa$

Midrange stress is:

$$\sigma_m = \left[3\left(\frac{16K_{fs}T_m}{\pi d^3}\right)^2\right]^{\frac{1}{2}} = \left[3\left(\frac{16\times1.405\times828.8}{\pi(0.052)^3}\right)^2\right]^{\frac{1}{2}} = 73Mpa$$

Using Goodman criterion

$$\frac{1}{n_f} = \frac{\sigma_a}{S_e} + \frac{\sigma_m}{S_{ut}} = \frac{146.6}{662.4} + \frac{73}{690}$$

$n_{f=}3.1$----------Safe!!

So n_f is calculated to be $n_{f=}3.1$, the shaft turns out to be safer since the safety factor we have is greater than the safety factor we need to attain during the design ($n_d = 1.5$).

A-2-2. Design of Shaft key

There may not be much choice as to how the runner is fitted on the shaft. But if the shaft is made especially for the turbine, there are lots of options as described below.

- Parallel fit with keyway
- Taper fit with keyway
- Hub welded to the shaft
- Single piece hub and shaft

A key transmits torque between a shaft and a hub, but is not the main element of the joint. Think about how the runner is to be serviced. If the runner, need to be changed, is it useful to have to change the whole shaft as well? Usually not, so welding the hub to the shaft or making them out of one piece is not a good idea. Size also plays a part too. A good fit between the hub and a parallel shaft can be dismantled easily if the shaft is small. Tapered fits are preferable for larger runners (over 300mm PCD) [Jeremy 2000]. So **parallel fit with key way** is a best choice since no thrust load present and among much kind of key fits, a rectangular key is selected because of its general usefulness especially when a wheel is to be positioned against a shaft shoulder, since the key slot need not be machined into the shoulder stress concentration

region. The use of the rectangular key also yields better concentricity after assembly of the wheel and shaft [Jeremy 2000]. This is especially important at high speeds, especially for turbine wheel and shaft.

For a shaft diameter of 55mm and 52mm, we can select the dimensions and tolerances of standard keyways from the table below.

Table A-4: Selected parallel metric key and keyway dimensions to BS42345: [Jeremy 2000].

Shaft diameter (mm)		Key size (mm)			Keyway	
From	To	Width, W	Height, H	Length, L	Depth, mm	
					Shaft, t_1	Parallel key hub t_2
50	58	$16\ ^{0.00}_{-0.043}$	$10\ ^{0}_{-0.09}$	45-180	$6\ ^{+0.2}_{0}$	$4.3\ ^{+0.2}_{0}$
58	65	$18\ ^{0.00}_{-0.043}$	$11\ ^{0}_{-0.11}$	50-200	$7\ ^{+0.2}_{0}$	$4.4\ ^{+0.2}_{0}$

Material: AISI 1006 HR is chosen because it is one of mostly used key material and have good mechanical strength as well fatigue resistance.

Properties are: $Sut = 300MPa,\ Sy = 170MPa$

Factor of safety: n= 2.5, assuming minor shock loads from the transmitted power of the turbine.

Design: The torque transmitted by the key is given by:

$$T = \frac{P}{\omega} = 60 \times \frac{P}{N \times 2\pi}$$

$$T = \frac{60 \times 48123}{650 \times 2\pi} = 707Nm$$

The force F at the surface of the shaft: $F = 2 \times \frac{T}{D} = 2 \times \frac{707}{0.055} = 25.7KN$

On the basis shear stress on the key: $\tau = F/wL$

Based on the conservative shear stress theory: $\tau = Sy/2n$

Equating we have: Sy/2n=F/WL, $L = \frac{2nF}{S_y W} = \frac{2 \times 2.5 \times 25.7KN}{170MPa \times 16mm} = 47.2mm$

But the maximum length of the key limited by the hub length and better not exceed 1.5 times the shaft diameter so,

Took, L=47.2mm, $\tau = \frac{F}{WL} = \frac{25700}{16mm \times 47.2mm} = 34Mpa$

Based on the maximum shear force theory:

$n = \frac{S_y}{2\tau} = \frac{170}{2 \times 34} = 2.5$ (Which is not safe!!!). This is because, the yield strength is 170Mpa the key is safe for fatigue loading and the safety factor is 2.5 with maximum shear force theory [Jeremy 2000]. But if we took L=55mm, we have:-

$$\tau = \frac{F}{WL} = \frac{25700}{16mm \times 55mm} = 29.2Mpa$$

So based on maximum shear force theory: $n = \frac{S_y}{2\tau} = \frac{170}{2 \times 29.2} = 3 > 2.5$(Safe!!!)

The crushing stress, σ_c is: $\sigma_c = \frac{4T}{LhD} = \frac{4 \times 707Nm}{55mm \times 10mm \times 55mm} = 93.5Mpa$

Since the yield strength is 170Mpa, the key is safe for fatigue loading with maximum shear force theory. Similarly for the second key with shaft diameter is equal to 60mm and taking, L=60mm we have:

$$\tau = \frac{F}{WL} = \frac{25700}{18mm \times 60mm} = 23.8Mpa$$

Based on the maximum shear force theory:

$n = \frac{S_y}{2\tau} = \frac{170}{2 \times 23.8} = 3.6$ (Safe!!! Since a safety factor of 3-4 could be used [Jeremy 2000]).

A-3. Bearing selection

For the purpose of this research project the type of bearing selected is **single row deep groove ball bearing** because the shaft is loaded for small amount of radial load and it is better to safeguard the turbine from any kind of thrust load due to external factors. This bearing will take radial load as well as some thrust load and will also with stand a small amount of shaft misalignment of deflection. The selection of the bearings geometrical diameter is done based on the bearing life method. The bearing rating value C_{10} is calculated first from the desired reliability, bearing loading and desired rotational speed. The value is compared with the bearing life of the catalog bearing rating life. A bearing with a catalog load rating greater than or equal to the calculated rating is to be selected. From the shaft strength analysis we have the reaction loads acting on the bearings [Fig.A-11].

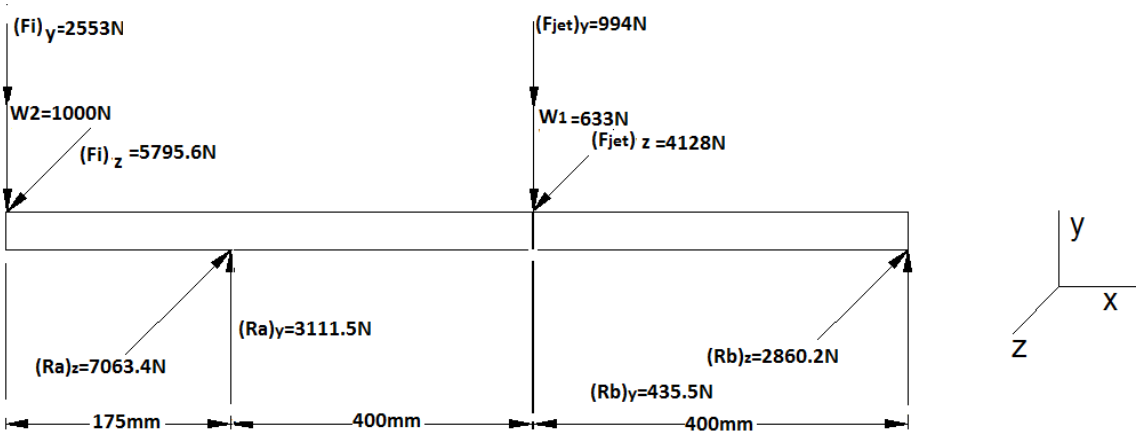

Figure A-11: Forces acting on the Pelton shaft.

Summing up the force vectors orthogonally on bearing 2 and bearing 1 respectively, gives us the maximum load which is:

$$F_2 = \sqrt{\left((Ra)_z^2 + (Ra)_y^2\right)} = \sqrt{\left(7063.4^2 + 3111.5^2\right)} = 7{,}718N$$

$$F_1 = \sqrt{\left((Rb)_z^2 + (Rb)_y^2\right)} = \sqrt{\left(2860.2^2 + 435.5^2\right)} = 2893.2N$$

So the desired radial load to be taken by the ball bearing 2 at point 'a' is F_D=7,718N and by the ball bearing 1 at point 'b' is F_D=2893.2N. The shaft diameter at the bearing location was computed to be (d=55mm).

From SKF Catalogue [*Joseph E. Shigely,2008]*, we have: desired life in hour (L_D), catalogue rating KN, Desired load, F_D=7,718N for bearing 2, Desired speed, n_D=650rpm (Turbine rotational speed),Desired reliability of R_D =0.99 and a bearing service life of one year is assumed. The C_{10} catalog entry to be sought (or exceeded) when searching for a deep-groove bearing in a manufacturer's catalog on the basis of 10^6 revolutions for rating life is calculated as:

$$C_{10} = a_f F_D \left[\frac{X_D}{x_0 + (y)(1 - R_D)^{1/b}}\right]^{1/a} \qquad \text{[A-6]}$$

Where, the application factor a_f for machinery with light impact ranges between 1.2 and 1.5[*Joseph E. Shigely,2008]*. We have chosen the mean value, which is 1.35.

The Weibull parameters are given by x_0=0.02 (guaranteed, or minimum value of the variant, ($y=\theta-x_0$) =4.439, θ is characteristics parameter corresponding to the 63.2121 percentile value of the variant, and b=1.483 (Shape parameter that controls the skewness) [*Joseph E. Shigely,2008]*.

Taking, a=3 for ball bearings. The desired life of the bearing in revolution L_D is calculated as: L_D=N×60×life in hours. In a year there are: 365.25×24=8766 hours.

Therefore, L_D =650×60×8766=341.874×10^6 revolutions

Design life measure dimensionless variate, $x_D=L_D/L_{10}$

$$x_D = \frac{L_D}{L_{10}} = \frac{341.874\times10^6}{10^6} = 341.874$$

Substituting all the above values in Equation A-6 yields:

$$C_{10} = a_f F_D \left[\frac{X_D}{x_0 + (y)(1-R_D)^{1/b}}\right]^{1/a} = 1.35\times7{,}718\times\left[\frac{341.874}{0.02+4.439\times(1-0.99)^{1/1.483}}\right]^{1/3} = 120.6KN$$

Similarly for bearing 1 with F_D =2893.2N we have C_{10} =45.3KN. Both the dynamic rating calculated values are greater than the catalog load rating value [*Joseph E. Shigely,2008]*. As a result the bearing selected is 02-series Deep-Groove ball bearing with a bore diameter of 55mm.

Bearing Housing: For this turbine different housing arrangement could be sought for the selected bearing. The housing to be selected should consider ease of maintenance and since it is a corrosive environment that the turbine is to operate in, the housing and the bearing should be put further away from contacting the flowing water. For this reason a housing which could be mounted on the outside of the turbine is selected [Fig. A-12].

Figure A-12: bearing housing UCP series pillow block UCP211 with 55mm bore inserting bearing manufactured from steel (http://uk.rs-online.com/web/p/ball-bearings/).

A-4. Design of Casing/Housing

The casing is an essential part of the turbine. It has to drain off the water coming out of the buckets without hindering the runner. Casing should have enough strength to meet the mechanical/structural requirements. The housing of a Pelton turbine with a horizontal shaft normally consists of at least two parts. Usually the housing can be split horizontally at the level of the shaft [Jeremy 2000]. The casing was composed of three components a base plate, a top casing and a bottom casing. The main body of the casing had to be designed in two parts, due to the configuration of the bearing housings and turbine shaft such that the turbine could

be more easily assembled. Steel angle was welded around the perimeter of the two casing halves to allow them to be bolted together and also bolted to the base plate [Jeremy 2000].

According to [Jeremy 2000 book], the casing of a Pelton turbine does not perform any hydraulic function. But it is necessary to safeguard the runner against accident and to prevent the splashing of water and lead the water to the tail race. So there is no formula, and every engineer is free for designing the shape he wants.

Basic dimensions for horizontal-axis housings are given in Fig. A-13. These are good minimum dimensions, but they can be varied. The performance of the turbine will not be affected if larger dimensions are used, and it may even improve marginally. Care should be taken when reducing the dimensions [Jeremy 2000].

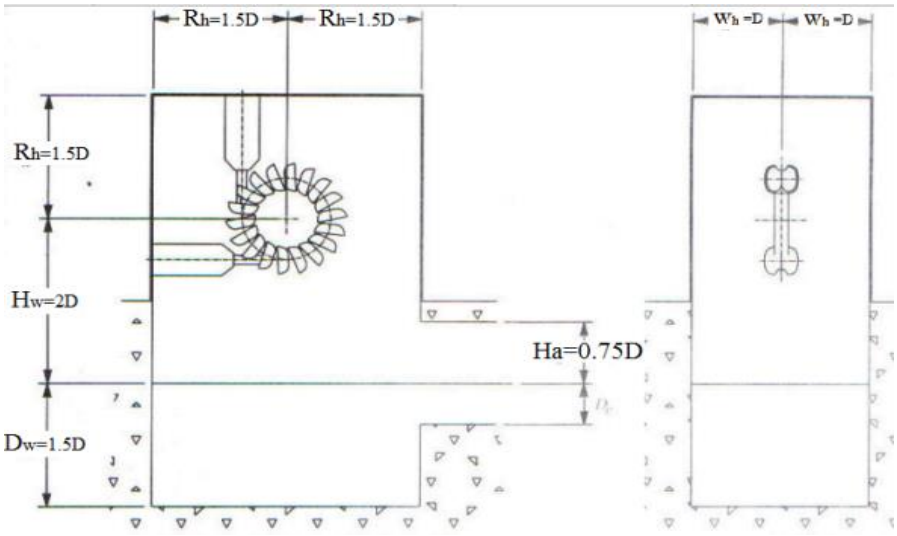

Figure A-13: Representations of Suggested Housing Dimensions [Jeremy 2000].

The Pelton turbine housing is designed to account for the forces applied by the manifold and bearings [Jeremy 2000]. Jeremy suggests that horizontal axis micro hydro turbine systems contain side plates that are thicker than the top plates and end plates to reduce vibration and noise from water hitting them [Jeremy 2000]. For a system of a few kilowatts, a 2-3 mm steel plate are suggested; whereas for a system of 50-100 kW, 6-8 mm side plates and 5mm end plates are suggested [Jeremy 2000]. This research (36.5kW Micro hydroelectric design research project) uses rigid (6mm) steel for both the side plates and end plates to ensure reduction of both vibration and noise.

With the Pitch diameter (D) of 400mm, the minimum suggested dimension values of the Pelton turbine housing can be calculated as follows (Fig. A-14 and Fig. A-15 show 3D views of the housing):-

R_h=1.5(D), H_w=2(D), D_w=1.5(D), H_a=0.75(D) and W_h=D.

For this particular research, we have the following design values of R_h=0.6m, H_w=0.8m, D_w=0.6m, H_a=0.3m and W_h=0.4m.

As shown in Fig. A-14 and Fig. A-15 transparent housing in the upper front casing is used for observing the Pelton wheel and needle nozzle.

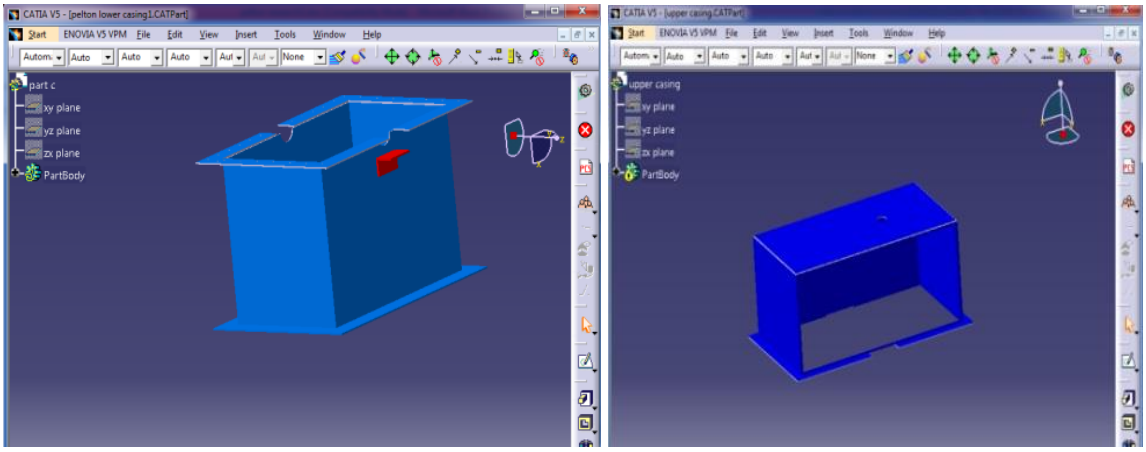

Figure A-14: Lower casing(left side) and Upper Casing(right side).

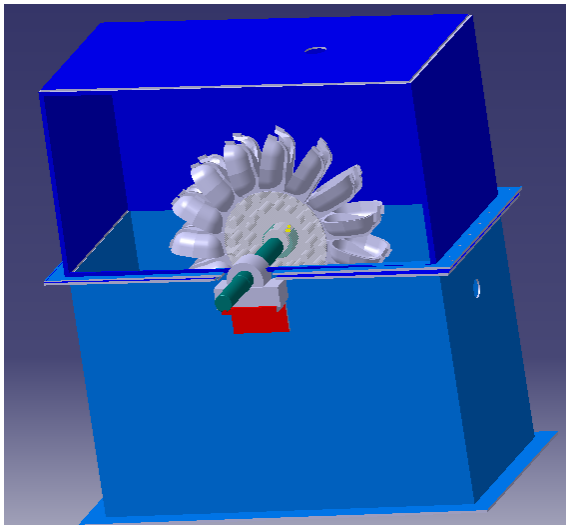

Figure A-15: 3D View of double jet Pelton turbine housing assembly.

A-5. Design of Nozzle and Deflector

I. Design of Nozzle: The dimensions of the nozzle are determined as follows:

The nozzle length can be calculated as:

$$L_n = \frac{(D_{pn} - D_j)}{\tan\beta}(\text{m}) \qquad \text{[A-7]}$$

$$D_{pn} = \frac{D_{pt}}{\sqrt{n_j}} \quad (m) \qquad \text{[A-8]}$$

where, D_{pt}=244mm: Diameter of penstock connected to the turbine (m).

D_{pn} :Diameter of penstock connected to the nozzle (m)

$$D_{pn} = \frac{D_{pt}}{\sqrt{n_j}} = \frac{0.244}{\sqrt{2}} = 0.17 \quad (m)$$

Substituting into Eq. A-7, we have:

$$L_n = \frac{(0.17 - 0.0544)}{\tan 14^0} = 0.46(m)$$

The nozzle exits have to be located as close to the Pelton runner as possible to prevent the jet from diverging the designed diameter. The distance between the nozzle and runner should be 5% of the runner circle diameter, plus an extra (3) mm clearance to account for emergency deflectors as:

$$X_{nr} = 0.05 \times PCD + D_t \quad (m) \qquad \text{[A-9]}$$

$X_{nr} = 0.05 \times PCD + D_t$, take PCD = 400mm, $X_{nr} = 0.05 \times 400 + 3 = 23mm$

The distance between nozzle and bucket taking into account the minimum clearance between the nozzle and buckets was given as:

$$X_{nb} = 0.625 \times PCD \quad (m) \qquad \text{[A-10]}$$

$X_{nb} = 0.625 \times PCD = .62 \times 400 = 250mm$

The dimensions given here are to give an idea of the sizing of the nozzle used in experimentation. The mechanism for the valve adjustment is based largely on a design suggested by the literature Adams Harvey 1999 (Fig. A-16). The dimensions of the nozzle are determined according to the diameter of the jet (d_{jet}).The calculated results in Table A-5 are parameters of nozzle design.

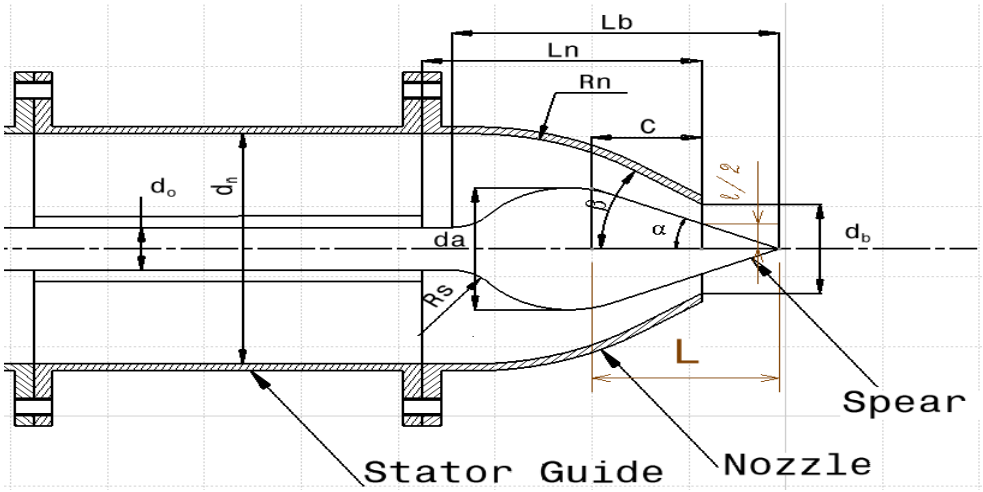

Figure A-16: The nozzle of the Pelton turbine [Adams Harvey,1999].

A converging conical nozzle with a manually adjustable needle valve was designed for the purpose of experimentally validating the models presented in this research.

Table A-5: Results table for nozzle dimensions

Items	Calculated Values, mm	Design Guidelines
Nozzle diameter (Orifice diameter), d_b	68	Nozzle diameter, d_{noz} = 1.15-1.25 times jet diameter, take d_{noz}=1.25djet
Blocking space needle to nozzle tip , C	73.44	Location of needle tip radius, S = 1.35 times jet diameter
Location of nozzle orifice radius, x	27.36	Location of nozzle orifice radius, X = 0.503 times jet diameter
Diameter of spear shaft, d_1	24.48	Diameter of spear shaft, d = 0.45 times jet diameter
Length of needle tip, L_b	172.45	Length of needle tip, L_b= 3.17 times jet diameter
Curve of needle tip radius, r	38.35	Curve of needle tip radius, r = 0.705 times jet diameter
Nozzle orifice diameter (outlet)	56	D_{noz} = 0.14PCD, (Jeremy Thake, 2000)
Height of needle tip, d_a	32.64	Height of needle tip, h = 0.6 times jet diameter.
Distance between Nozzle & Bucket	250	*0.625PCD*
Nozzle Length, Ln	460	$L_n = \frac{(D_{pn} - D_{noz})}{\tan\beta}$
D_{pn} :Diameter of penstock connected to the nozzle	170	$D_{pn} = \frac{Dpt}{\sqrt{n_j}}$
distance between the nozzle and runner	23mm	The distance between the nozzle and runner should be 5% of the runner circle diameter, plus an extra (3) mm clearance to account for emergency deflectors

II. Deflector design

The deflectors serve to bend the jet away from the runner at load rejections to avoid a high speed increase. It also protects the jet against exit water spray from the runner. This emergency deflector system must be installed to protect the generator in case a load circuit failure, and the generator rotates at over speed. Fig. A-17 below shows the attachment of the deflector to the nozzle. 3D model of deflector Jet deflectors have the function of diverting the water flow or part of it between the nozzle and the runner in such a way that it does not hit the buckets (Fig. A-18).

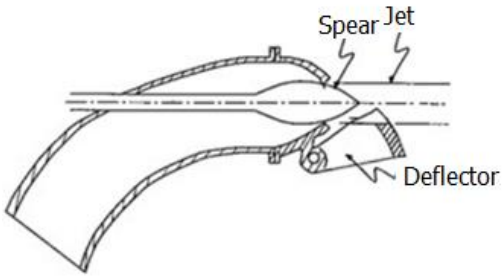

Figure A-17: deflector of the Pelton turbine

The force in each deflector can be calculated as:

$$F_d = \rho_w \times Q_n \times V_j = 1000 * 0.07 \times 19.27 = 1.35KN$$

The required force in each deflector is given as: $F_{dr} = F_d \times s.f$,

Take safety factor 1.5,

$$\text{Therefore, } F_{dr} = 1.5 \times 1.35 = 2.025\text{KN}$$

The bending moment acting on the deflector arm given as:

$$T_d = F_{dr} \times R_d = 2025R_d(N.m)$$

The moment required acting on the deflector arm given as:

$$T_{dr} = T_d \times F_c$$

Where F_C *is* friction factor acted upon by bearings (≅1.2)

$T_{dr} = T_d \times F_c = 2025R_d \times 1.2 = 2430R_d(N.m)$, where R_D is moment arm in m

As the moment arm varies the torque needed to deflect the water jet also increases so the optimum moment arm has to be set regarding the available space and the material cost needed due to the increase in moment arm. This will be decide after the installation of the turbine. Fig. A-18 shows the design dimension based on the literature suggested limit.

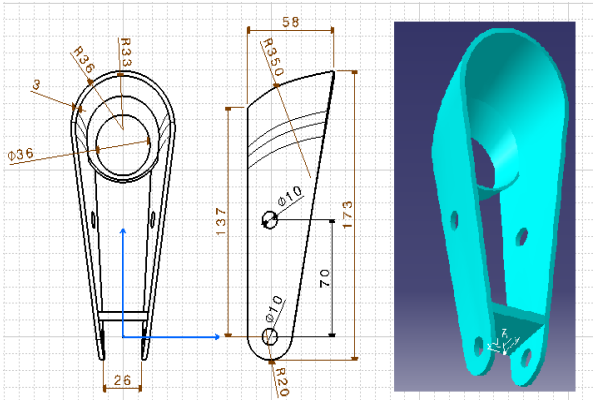

Figure A-18: 3D view of deflector, dimensions in mm.

A-6. Mechanical Power Loss Calculation

The possible mechanical resistances and the resulting efficiency losses in the power transmission are friction and windage losses in the turbine casing and the frictions in the shaft bearings and seals. According to the literature by [Zh. Zhang, Pelton Turbines,2016], for Pelton turbines with horizontal rotation axes, all relevant geometric design parameters are shown in Fig. A-19. The power that is required to compensate for the friction and windage losses is calculated using IEC60041 standard (1991)as follows:

$$P_{wi}=15n^3D^5\left(\frac{B_a}{D}\right)^{1/4}\left(\frac{B_{iu}}{D}\right)^{5/4}\left(\frac{B_{io}}{D}\right)^{3/4}\left(\frac{R_{io}}{D}\right)^{7/4} \quad \text{A-11}$$

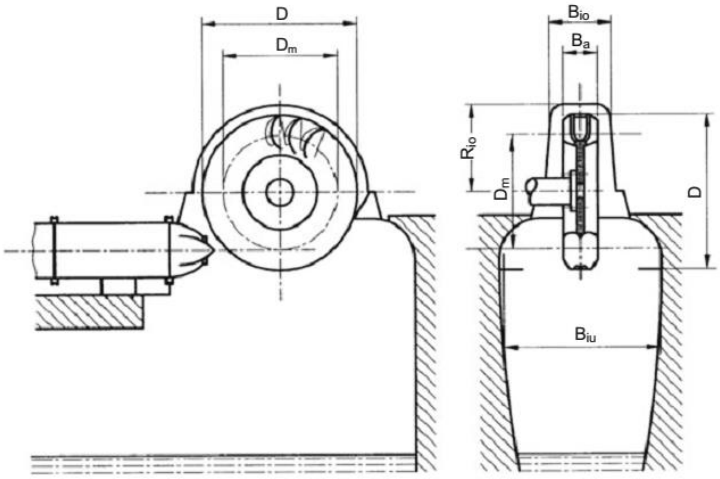

Figure A-19: Parameter definition for calculations of friction and windage losses in a horizontal Pelton turbine according to IEC60041 (1991)[Zh. Zhang, Pelton Turbines,2016].

In Eq.A-11, influences of all casing parameters on the windage power are taken into account and the unit of rotational speed n should be taken as 1/s. For a given Pelton turbine, Eq. (A-12) is rewritten in the following abbreviated form:

$$P_{Wi} = a.n^3D^5\ (W) \quad \text{A-12}$$

Here, a is a constant which combines the air property and design parameters of the turbine casing. Its dimension is kg/m^3, i.e., the same as the dimension of the specific density. Here, windage power only depends on the rotational speed of the Pelton wheel, but not on the flow rate.

Because of the hydrodynamic lubrication behavior, the bearing friction power in the range of fluid friction is expressed as Eq. (A-13),

$$P_{be} = K_{be}n^{1.75} \quad \text{A-13}$$

Here, K_{be} is the bearing friction coefficient. It is a function of the type of bearing, bearing load, dynamic viscosity of the lubricant, and bearing temperature. Equations A-12 and A-13 represent the characteristics of the respective mechanical losses.

Mechanical Efficiency: The mechanical efficiency describes the power transfer from the turbine to the shaft, at the end of which the rotor of the electric generator is positioned. The possible mechanical resistances and the resulting efficiency losses in the power transmission are friction and windage losses in the turbine casing and the frictions in the shaft bearings and seals. According to Zh. Zhang, Pelton Turbines,2016, friction and windage losses in efficiency in the Pelton wheel can be calculated using the formula below:

$$\Delta\eta_{wi} = \frac{a.n^3 D^5}{P_o} \qquad \text{A-14}$$

For the bearing friction loss efficiency can be calculated using the formula:

$$\Delta\eta_{be} = \frac{K_{be}\, n^{1.75}}{P_o} \qquad \text{A-15}$$

Here,P_0 is the hydraulic power of the total number of water jets. With the rotational speed as a variable, the two equations represent the characteristics of the respective mechanical losses. From Eqs. (A-14) and (A-15), the mechanical efficiency of a Pelton turbine is given by:

$$\eta_{mech}=1-\Delta\eta_{wi}-\Delta\eta_{be} \qquad \text{A-16}$$

Therefore, based on the above equations, the mechanical efficiency for our model turbine in this research estimated to be about 84%.

Appendix B: Power Transmission

There are two possible solutions for power transmission from the turbine shaft to the generator shaft, they are: Gears, Belts & Pulleys. Gears are usually avoided in micro-hydro schemes due to their high cost and high maintenance. Belts and pulley mechanism, if properly designed, can well serve the purpose with efficiencies of about 98% [Adams Harvey, Jeremy 2000]. The reason for stepping the rotational speed up to 1500 rpm is such that the four-pole alternator machine employed would be able to generate 50hz AC when spinning around 1500 rpm. As the turbine was designed to spin at only 650 rpm, it was necessary to step the system up using different pulley diameters. The estimated power output of the system was to be 36.5KW as per the turbine design. The alternator had not yet been sourced at this point and so a certain degree of flexibility was required in the transmission design so as to allow for a range of diameters. Following are the mathematical calculations involved:

Types of Belts: Flat Belts, Vee-Belts (Wedge Belts is a type of vee belt that is usually used for micro-hydro applications).

Speed Ratio = 2.3:1(see, Table 3.2)

Design Power = (36.5)(1.18)(1.2) [Where, Service Factor = 1.18 & Duty Factor = 1.2]

= 51.7kW

Belt type selected: SPB Wedge Belt [From Fenner Belt Selection Envelopes]

Min. Pulley Diameter (d): 140mm [Selected from Fenner Wedge Belt Catalogue]

Rated Power/Belt = 7.09kW/Belt [From Fenner Wedge Belt Catalogue]

Number of Belts (N) = Design Power/Rated Power per Belt, N = 7

Larger Pulley Diameter: 2.3(140) = 322mm,

Approx. Center Distance = (D+d)/2, C = 231mm

Belt Length = $2C + \pi(D+d)/2 + (D-d)^2/4C$ =462+725.7+35.84=1.22m

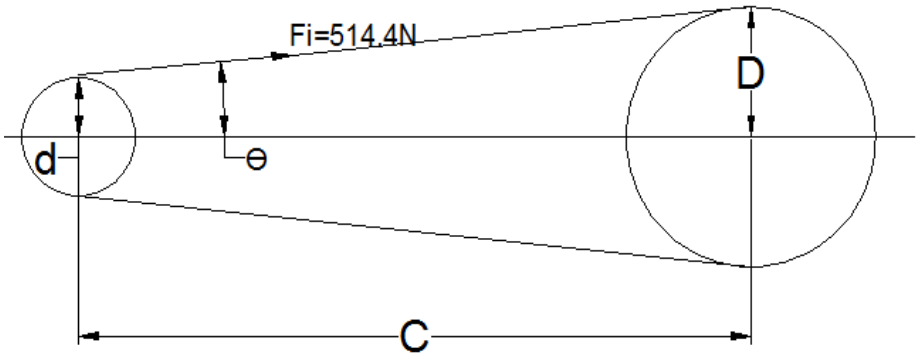

Figure C-1: Sketch of the pulley system

Appendix C: Pelton Wheel Instructions And Technical Description

(Source: Rainbow Micro Hydro Instruction Manual, Certified by: OFFICE OF ENERGY (NSW) Certificate of Suitability Number: 6273)

1. Correct alignment of the water jet is important with this design of the runner, both to achieve maximum efficiency and to prevent possible damage to the blade edge of the runner buckets. The nozzle must be adjusted so that the jet strikes the wheel tangentially.
2. If there is manufacturing defect in the alignment of the Pelton wheel, then there will be vibrations to the Pelton wheel which may result in fewer rotations or zero rotations.
3. Special care should be given to the manufacture of the frame so that it could not fall down during operation.
4. The Pelton wheel, shaft and Alternator should be held tightly in the frame so that there must be lesser vibrations as much as possible.
5. The design of the nozzle should be such that it could discharge the required amount of water without any failure with a high velocity. This velocity of jet would generate the force on the Pelton wheel will lastly rotate the conductor of the Alternator.
6. Care should be taken during the manufacturing process so that there should be no loss of materials which would result in more amount of investment.

Appendix D: Manufacturing Methods and Finance

S. N	Part Name	Activities	Workshop to be manufactured	Unit	Qty	Expected Unit Price (Birr)	Total Price (Birr)
1	Turbine Bucket	**Molding:** 3D Printing and then duplicating the 3D print via wax and/or wood mould	AAU, Art School, MOST	Pcs	2	4,000.00	8,000.00
		Casting: using the wax/wood mould casting will be done via sand casting and then surface finishing will be done using rotor grinding machine and CNC machines	Aniley Foundary Plc for Casting and TiGro Power & METEC, Hibret Industry for surface finishing works	Pcs	40	296.00	11,840.00
2	Turbine Flanges	Option 1: using plasma cutting machine to produce the plates. Option2: using Lathe machine or Option3 using CNC machine	TiGro Power, METEC Hibret Industry, METEC Metals Fabrication Industry, Lucy Metal Crafts Plc	Pcs	2	740.00	1,480.00
3	Turbine Bushing	the bushing in which the plates will fix will be manufactured using lathe machine	AAiT, Mechanical workshop, Lucy Metal Crafts Plc	Pcs	1	500.00	500.00
4	Turbine Shaft	using 60mm steel circular solid section 55mm shaft will be fabricated using lathe machine via turning as per the design to suit for 55mm bearing with housing which is a standard bearing on the market and the shaft keyway will be produced using shaper or milling machines	AAiT or Rediet or Nigsty or Tana or Abinet machine shops	Pcs	1	4,500.00	4,500.00
5	Bearing with Housing	Bearing with housing: to be purchased from market	Assembly could be done in AAiT, Mechanical	Pcs	2	800.00	1600.00

6	Bolts and Nut with Washer	Hub: to be purchased from market	Assembly could be done in AAiT, Mechanical	Pcs	19	12.00	228.00
7	Pulley	to be purchased from market	AAiT or Rediet or Nigsty or Tana or Abinet machine shops	Pcs	1	600.00	600.00
8	Belt			Pcs	2	150.00	300.00
9	Bearing with housing mounting buckets	to be purchased from market	Assembly could be done in AAiT, Mechanical workshop	Pcs	2	250.00	500.00
10	O-ring			Pcs	2	275.00	550.00
11	Casing	sheet metal	Assembly could be done in AAiT, Mechanical workshop	Pcs	3	1,500.00	4500.00
12		Angle Iron		Pcs	2	1,900.00	3800.00
13		Bolt and Nut with Washer		pcs	30	30	90.00
14		Flanges for distributor connection		pcs	2	230.00	460.00
15		Clear glass(to be purchased from market)	Assembly could be done in AAiT, Mechanical	m^2	2	500.00	1000.00
Total							39,948.00

Appendix E: Technical Drawings

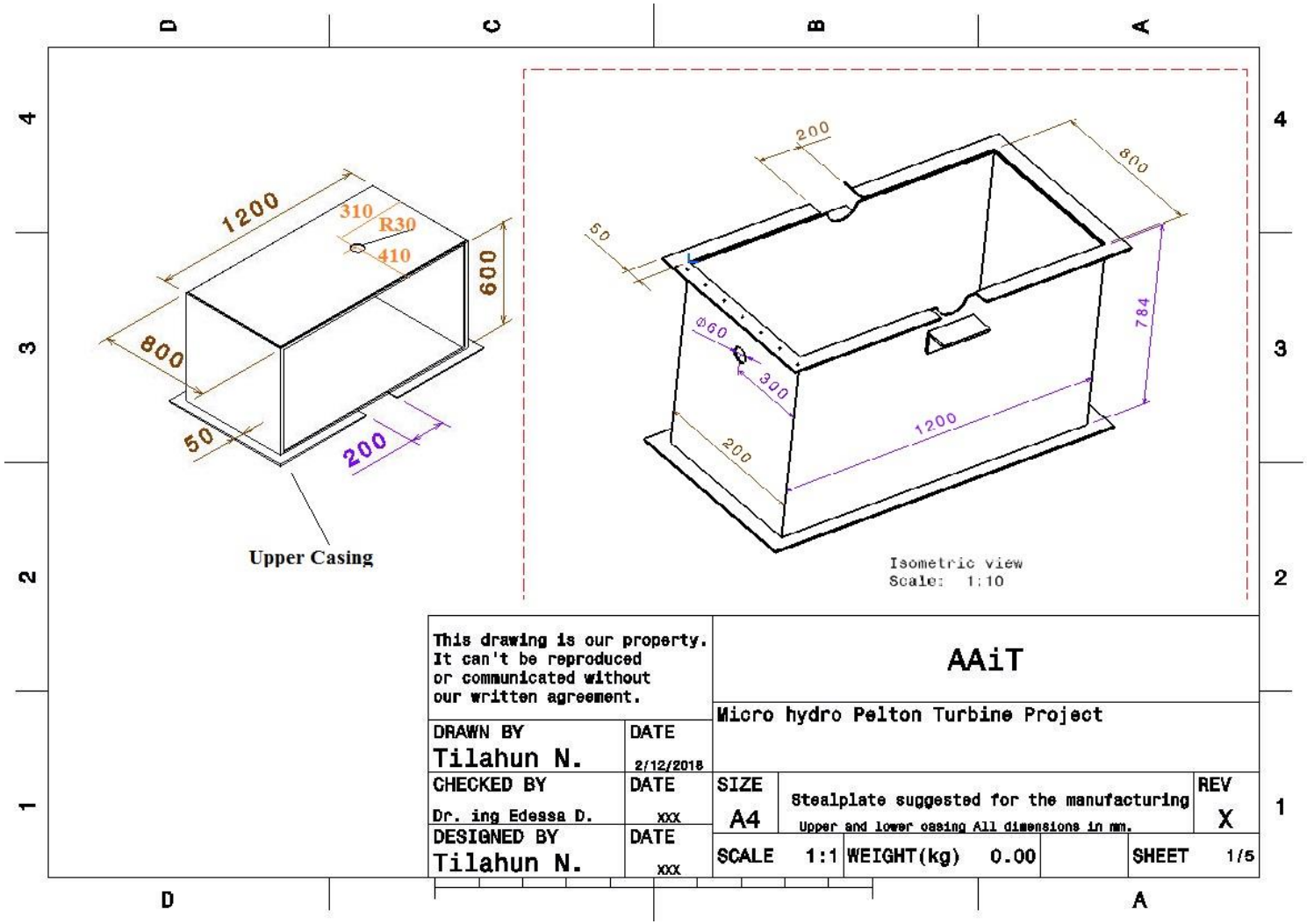

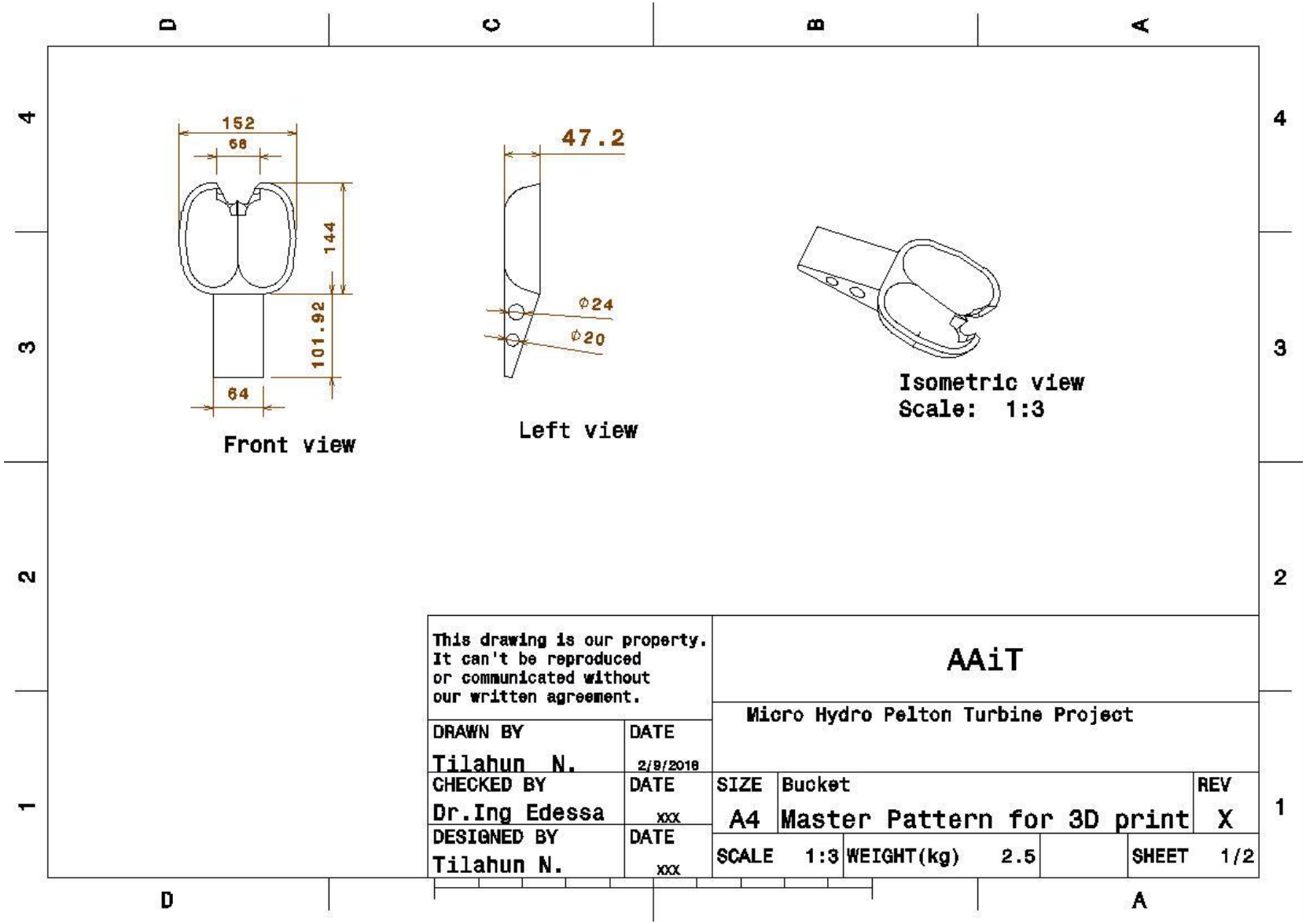
152
68
144
101.92
64
Front view
47.2
Φ24
Φ20
Left view
Isometric view
Scale: 1:3
This drawing is our property.
It can't be reproduced
or communicated without
our written agreement.
AAiT
Micro Hydro Pelton Turbine Project
DRAWN BY
Tilahun N.
DATE
2/9/2018
CHECKED BY
Dr.Ing Edessa
DATE
xxx
DESIGNED BY
Tilahun N.
DATE
xxx
SIZE
A4
Bucket
Master Pattern for 3D print
REV
X
SCALE 1:3
WEIGHT(kg) 2.5
SHEET 1/2

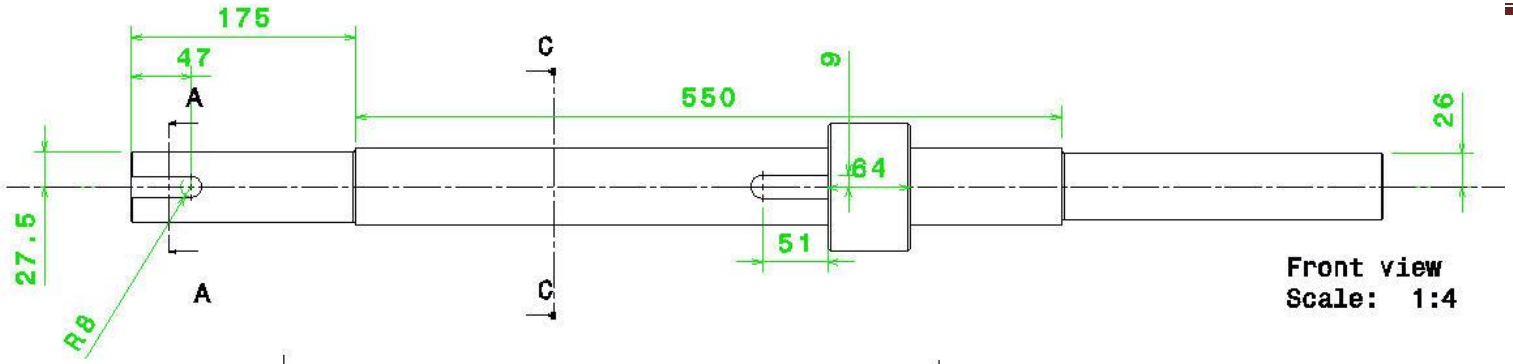

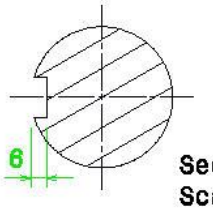

Section view A-A
Scale: 1:2

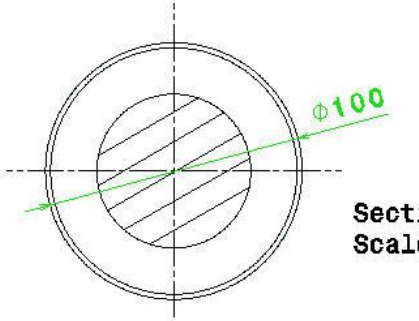

Section view C-C
Scale: 1:2

DESIGNED BY: Tilahun DATE: 2/9/2018 CHECKED BY: Dr. Edessa		Addis Ababa Institute of Technology	
size A4		Pelton Turbine Shaft made from mild steel	
SCALE	WEIGHT (kg) 2.81	All dimensions are in mm Part1	SHEET 1/3

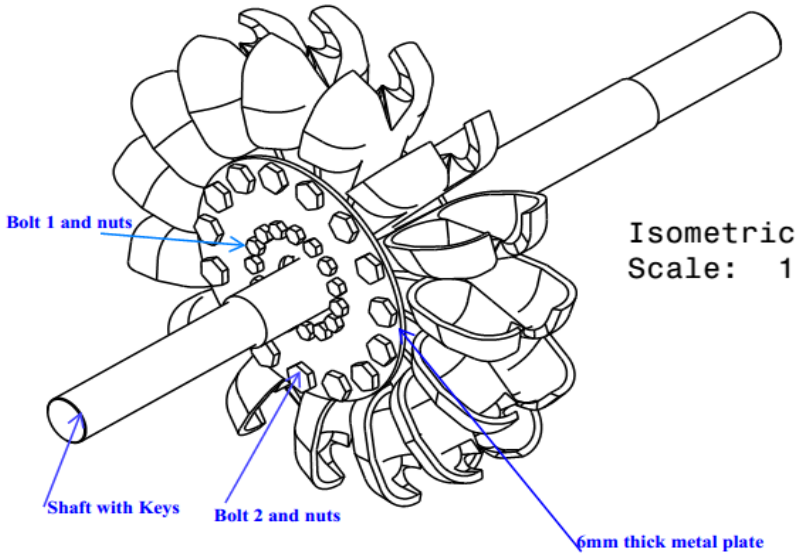

Isometric view
Scale: 1:6

Part List

Items	QTY	Descriptions
Bolt 1	15	M16
Bolt 2	15	M20
Shaft keys	3	Material: AISI 1006 HR 17X11, 60mm long
Buckets	15	grey cast iron: BS 1452 Grade 220 (7150kg/m3) or 260(7200kg/m3)
Circular Metal Plate	2	Made from 6mm thick

DRAWN BY Tilahun N.	DATE 2/9/2018	AAiT			
CHECKED BY Dr.Ing Edessa	DATE xxx	Micro Hydro Pelton Project			
DESIGNED BY Tilahun N.	DATE xxx	SIZE A4	Runner Product1	REV X	
		SCALE 1:6	WEIGHT(kg) 59.64		SHEET 1/4

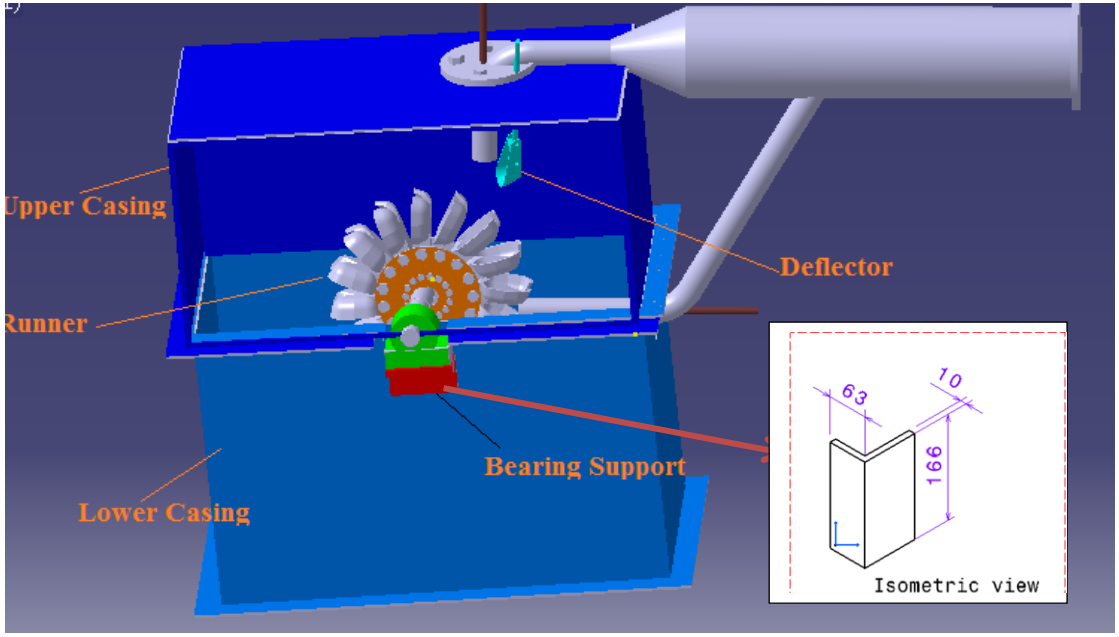

Figure. E1: Proposed Assembly for Pelton runner with casing.

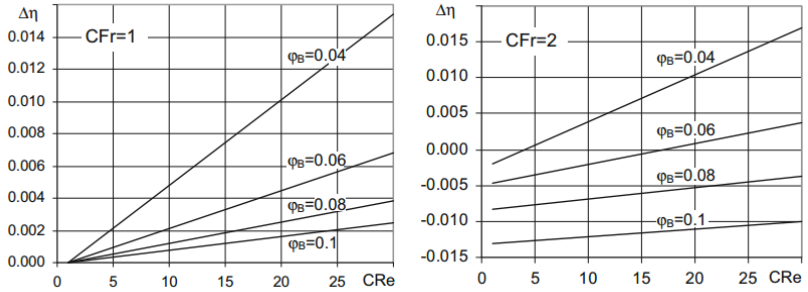

Figure. E2: Diagrams for scaling up the efficiencies from the model turbine to the prototype.

Appendix F: Pelton Turbine Characteristic Calculating Sheet (Sample datasheet used for Turbine Testing).

S.no	Parameters	Dimensions	1	2	3	4
1	Feed-Pressure	bar				
2	Spear Valve Position, δ	% of fully open	25%	50 %	75%	100 %
3	Speed, n	rpm				
4	Load on spring balance, W	kg				
5	Flow over Notch h'	mm				
	(h_0= 954.7 mm),h=h'-h_0	mm				
6	Orifice ΔP ΔP=9.81×12.55 ΔP(mmHg)	Kg/m.s^2				
7	Discharge ,Q $Q = \alpha A_d \sqrt{\frac{2\Delta P}{\rho}}$ Where, Flow coefficient -α=f(Re)=0.68, ρ=1000kg/m^3- water medium, orifice area, A_d =3.137×10^{-3} m^2 $\therefore Q = 9.54\times10^{-5}\sqrt{\Delta P}$	m^3/s				
8	P_{in}= γ Q H	W				
9	F=9.81N/kg×W	N				
10	ω=2πn/60	1/s				
11	T=F×R_d, moment arm, R_d=0.15m (brake radius)	Nm				
12	P_{out}, P=Tω	W				
13	η=P_{out}/P_{in}					

Note that from step 1 to step 7 are used to calibrate the v-notch with the help of the orifice installed in the penstock of Pelton turbine to determine the discharge. Final reading of V-notch at 25%, 50%, 75% and 100% of fully open taken for further analysis.